PRECIPITATION EFFECTS ON ATMOSPHERIC ELECTRON DENSITIES

A thesis submitted for the Degree of Master of Science of Rhodes University.

by

CHERYL YU-YIN HUANG

August, 1977.

ACKNOWLEDGEMENTS

My grateful thanks are due to the many people who offered help, encouragement and advice during the course of this project, in particular to:

Professor J.A. Gledhill, for his patient supervision and insight during the many difficult periods of this thesis.

Dr. P.D. Terry, for copious assistance with computation, and especially for allowing me the use of his subroutines.

The computer centre staff - Mr. M. Lawrie, Mr. M. Urry, Mr. A. Morrison, Mr. E. de Jager, Mr. M. Sha, Mr. H. Mager - for running of my programs and general help.

Dr. D.G. Torr, for discussions on boundary problems.

Dr. A. Gagliardini, for passing on to me a copy of the MSIS program.

My parents, for their constant sympathy and encouragement.

The staff and students of the Physics Department for helpful comments and suggestions.

Deon Delport and Vivian Huang, for painstaking checking of the final copy.

Daisy Turner, for her fine typing under rushed circumstances.

The CSIR, for financial support which made this thesis possible.

ABSTRACT

In this thesis the effects of precipitated electrons on electron densities in the upper atmosphere are investigated. A method for solving the continuity equation has been developed, and this has been used to calculate electron density profiles under various conditions: daytime equilibrium conditions, with and without additional ionization by precipitated electrons; and nighttime conditions, with and without precipitation. This preliminary study seems to show that certain effects may be attributable to precipitation, and that these effects may be significant at night.

TABLE OF CONTENTS

CHAPTER ONE

INTRODUCTION

CHAPTER TWO

THEORY

CHAPTER THREE

NUMERICAL METHODS

CHAPTER FOUR

COMPUTATIONS

CHAPTER FIVE

EQUILIBRIUM AND NIGHTTIME SOLUTIONS

CHAPTER SIX

NIGHTTIME PRECIPITATION EFFECTS

CHAPTER SEVEN

CONCLUSION

CHAPTER 1

INTRODUCTION

1.1 Background

Effects of precipitated particles on the upper atmosphere have long been regarded with interest. The origin of these particles lies in the magnetosphere, which lies at a few earth radii from the earth, and is the extension of the earth's geomagnetic field. Within the magnetosphere exist radiation belts (Van Allen and Frank, 1959) which contain charged particles. Two belts may be delineated: an inner one which contains fluxes of protons with energies of tens and hundreds of MeV; and an outer belt which consists mainly of electrons with energies ranging from tens of keV to a few MeV. Beyond the outer belt lies a region of auroral particles which are not held in stable orbits. For the purposes of this discussion, this region will be included in the outer radiation belt. The fluxes in the inner belt appear to be relatively stable, but those in the outer one are subject to variations which may be connected to magnetic disturbances.

Figure 1, below, reproduced from Gledhill (1975), gives a pictorial representation of the magnetosphere.

Within the radiation belts, the charged particles execute motions which may be divided into three main types. Numerical values quoted below are for a 1MeV particle at an altitude of 2000 km (Hess et al., 1965).

The motions are:

(1) Gyration around magnetic field lines with a period of 7×10^{-6}s for a proton and 4×10^{-3}s for an electron, and radii of 0,3 km and 10 km respectively.

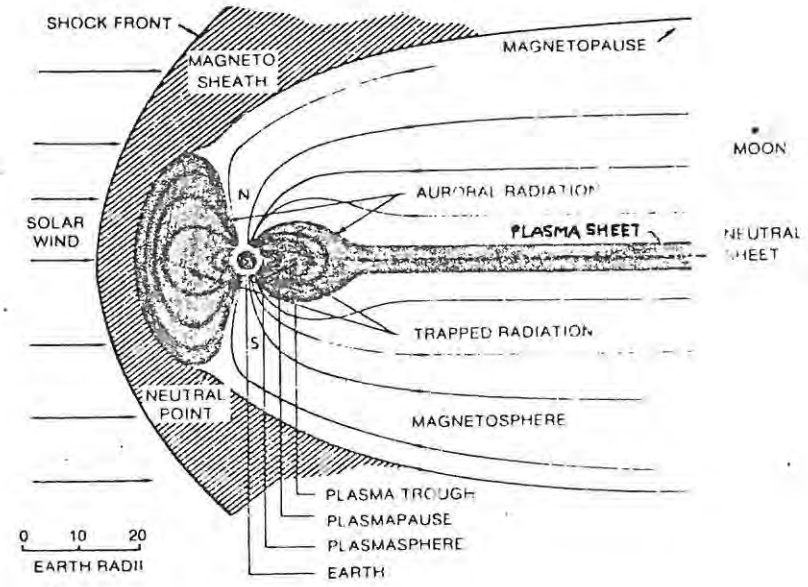

Figure 1. The earth's magnetosphere, from the equatorial plane. Dark shaded areas indicate trapped particles. Some typical field lines are shown.

(2) Bouncing between conjugate mirror points on opposite sides of the magnetic equator. As the particle moves towards the magnetic north or south pole, the increasing field strength causes it to be mirrored back along its path. The bounce period is 0,1s for electrons, 2s for protons.

(3) Longitudinal drift around the earth. Due to the curvature of the field lines around the earth, and the outward decrease in $|\underline{B}|$, there is a slow azimuthal drift. Electrons drift eastwards, with a period of 50 mins, and protons drift westwards with a period of 30 mins.

During these motions, the charged particle approaches the earth most closely at the mirror points. If these points are sufficiently low in the atmosphere, where the density of neutral atoms and molecules is relatively high, the particle

can interact with the atmosphere to produce a variety of effects, such as ionization, excitation, optical emission and heating. As a result of such collisions, the trajectories of light particles (e.g. electrons) may be considerably altered. If the pitch angle is decreased by a collision, the electron penetrates more deeply into the atmosphere, while an increase in pitch angle can lead to the electron being backscattered, and consequently entering the atmosphere at its conjugate mirror point at the other end of its path. The overall result is the removal of trapped electrons and production of aeronomic effects.

1.2 The South Atlantic Geomagnetic Anomaly

Since the earth's magnetic field is not symmetrical, the mirror heights in the northern and southern hemispheres are different, the magnetic intensity B being particularly low over the South Atlantic Ocean (Torr et al., 1975). Thus particles drifting across the South Atlantic region would have a high probability of being lost, and it might be expected that fluxes would be higher here than in any other area outside of the auroral zones. The actual extent of the South Atlantic Geomagnetic Anomaly is not clearly defined, but the map below, reproduced from Gledhill (1976), indicates its position as well as that of other anomalous areas.

1.3 Atmospheric Ionization and Excitation by Precipitated Electrons

As mentioned above, one of the effects of energetic electron precipitation is ionization. The electron undergoes inelastic collisions as it travels through the atmosphere, transferring energy to the atoms and molecules sufficient to create ion-electron pairs. The ionization rate profiles due to electron precipitation have been calculated for various types of energy

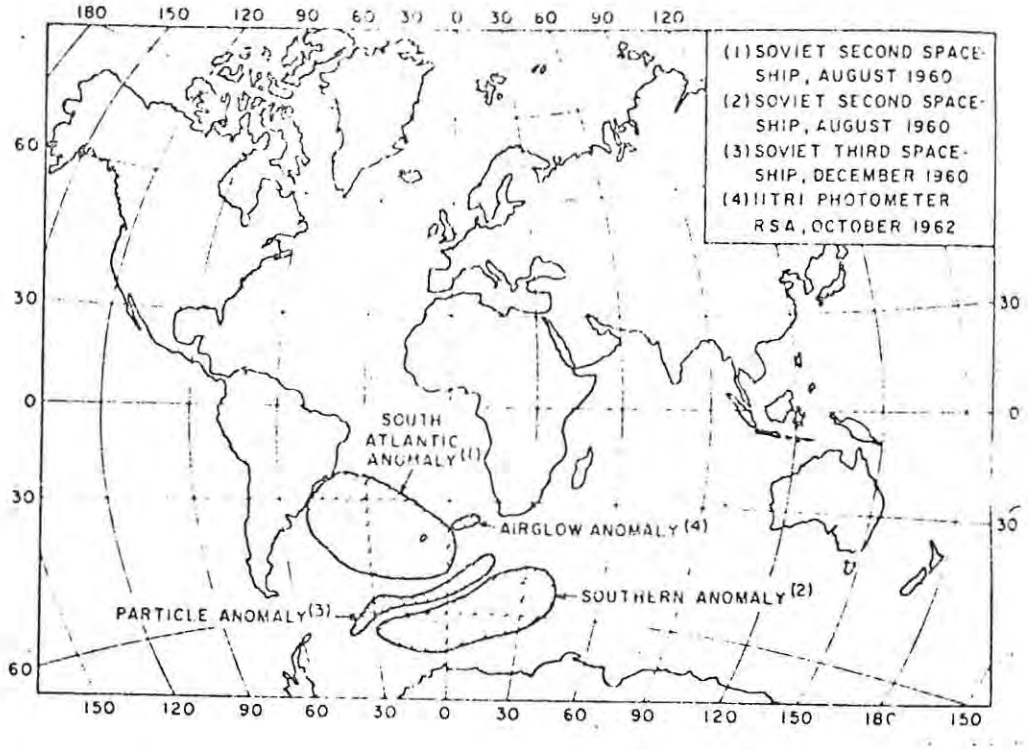

Figure 2. Anomalous regions in the South Atlantic

spectra and for both monodirectional and IDH (isotropic over the downward hemisphere) fluxes of electrons (Wulff and Gledhill, 1974; Heighway, 1973; Huang 1975). To find the effect of such ionization on the electron density in the atmosphere, these production rates must be included in the continuity equation for electrons. The present study is a preliminary investigation of the effect of a secondary ionization source on the electron density in the atmosphere under both daytime and nighttime conditions. As the ionization rate profiles peak low down in the atmosphere (from approximately 142 km for a 500 eV electron, to 91 km for a 27 keV electron) it would be expected that precipitation effects would be most noticeable in the E- and low F-regions, or lower. One would also expect that daytime effects would be more difficult to observe due to the large production rate due to photoionization. At night, however, when there is no other major source of ionization, precipitation should produce a noticeable change in electron density particularly

under disturbed magnetic conditions. This has been observed in the appearance of a spurious E-layer ("particle-E") of ionization on nighttime ionograms, which may be attributable to electron precipitation. It should be noted that the above applies to auroral precipitation as well as that over the Anomaly, so that the present work may be applicable, with some modifications, to higher latitudes.

Probably the best known evidence of particle precipitation are aurora, or airglow. In this case the precipitated electron transfers sufficient energy to the atom or molecule to excite it to a higher energy state. The excited particle then undergoes a transition to a lower state, emitting radiation. Examples of this are the red and green lines of atomic oxygen at 6300A^{o} and 5577A^{o} respectively. In addition, the ion created by a precipitated electron may be in an excited state, and can de-excite in the same way, e.g. the N_2^+ emission of radiation at 3914A^{o}.

The present work can be extended to calculate emission rates of such auroral radiation; this is particularly simple in the case of the 3914A^{o} line (Stolarski, 1968; Banks et al., 1974). This would provide useful information, since measurements of airglow intensities could then be interpreted to give values of the primary auroral electron flux. Using ionosonde and airglow data collected by the Rhodes team at SANAE, the intensity of the 3914A^{o} line was calculated. The results appear to be promising, although this work is still in its initial stages (Fisher et al., 1977).

In the following chapters a description of the theory and computations are given. A suitable daytime profile for equilibrium conditions is obtained, and the effect of a fairly large flux of energetic electrons on this is examined. A nighttime ionosphere is simulated, and various fluxes of electrons with a range of energies are added. The resultant profiles are shown and discussed.

There are two points which should be stressed at the outset:

(1) The calculations are approximate in nature, as order of magnitude effects were sought. Thus simplicity and speed were the main requirements of the methods used. In order to extract more precise information, various refinements will be needed. These are discussed in the final chapter.

(2) There seems to be a remarkable lack of reliable data of electron precipitation over the South Atlantic. The information received from satellites is sometimes suspect because of unusual geomagnetic conditions, experimental error (such as lack of correction for the effects of energetic and backscattered electrons), etc. Until more accurate data are obtained, theoretical predictions must remain largely speculative.

CHAPTER 2

THEORY

2.1 Introduction

In order to study the dynamical behaviour of electron densities in the atmosphere, the time-dependent continuity equation for electrons must be solved. This equation, in simplified form, describes the time variation in electron density due to chemical reactions (photoionization and loss processes), transport of ionization and possible additional ionization by precipitated energetic electrons.

The equation is written:

$$\frac{\partial N}{\partial t} = Q - L - \nabla.(N\underline{V}) \qquad \text{(Rishbeth and Garriott, 1969, Chapter 4)}$$

where N = electron density (number of electrons per cubic centimetre)

Q = production rate (due to photoionization, precipitated particles or both)

L = loss of electrons by chemical recombination

$\nabla.(N\underline{V})$ = transport term

V = velocity of electrons

The effects of neutral gas motions have been excluded because of the complexity of the resultant equations. Winds are established through solar heating, Joule dissipation and ion convection at high latitudes. In addition, the winds are themselves modified by the ionosphere resulting in a high degree of coupling between densities, temperatures and winds. Their inclusion leads to a system of coupled non-linear partial differential equations, considerably more difficult to solve satisfactorily than the continuity equation alone. The importance of various terms, such as the acceleration of the wind, is not well known (Rüster, 1971); while boundary conditions which depend on a knowledge of vertical

and horizontal gas motions are somewhat arbitrary (Stubbe, 1970). Consequently it was felt that as a first approximation, the neutral gas would be assumed to be at rest.

2.2 Chemical Reactions

Chemical processes are dominant in the lower part of the atmosphere (E-region), diffusion being significant in the F-region. The types of reactions considered are those producing or removing ionization. The main source of electron production during the day is photoionization, where solar extreme ultraviolet and X-ray radiation are absorbed by the atmosphere. The consequent reactions are, in general, temperature dependent, their rate coefficients falling off at higher altitudes as temperature increases. The reactions may be divided into three main categories: production (photoionization), ion-atom/molecule exchange, and dissociative recombination. The most important reactions for the range of heights under study are listed below.

Production

$$O_2 + h\nu \rightarrow O_2^+ + e$$

$$N_2 + h\nu \rightarrow N_2^+ + e$$

$$O + h\nu \rightarrow O^+ + e$$

Ion-Atom Exchange

$$O^+ + N_2 \xrightarrow{k_1} NO^+ + N \qquad \text{-----} \qquad (1)$$

$$O^+ + O_2 \xrightarrow{k_2} O_2^+ + O \qquad \text{-----} \qquad (2)$$

$$N_2^+ + O \xrightarrow{k_3} NO^+ + N \qquad \text{-----} \qquad (3)$$

Dissociative Recombination

$$NO^+ + e \xrightarrow{\alpha_1} N + O \qquad \text{-----} \qquad (4)$$

$$O_2^+ + e \xrightarrow{\alpha_2} O + O \qquad \text{-----} \qquad (5)$$

$$N_2^+ + e \xrightarrow{\alpha_3} N + N \qquad \text{-----} \qquad (6)$$

The rate coefficients of these reactions are given in Table 1.

Table 1. Reaction Rates

Reaction	Rate Coefficient ($cm^3 s^{-1}$)	Reference
k_1	$3,6 \times 10^{-10} T^{-1,0}$ ($T<750$ K)	McFarland et al., 1973
k_2	$2,0 \times 10^{-10} T^{-0,4}$	McFarland et al., 1973
k_3	$1,7 \times 10^{-9} T^{-0,4} - 3,6 \times 10^{-11} T^{-0,2}$	McFarland et al., 1974b
α_1	$1,4 \times 10^{-4} T_e^{-1,0}$	Biondi, 1969
α_2	$3,8 \times 10^{-6} T_e^{-0,5}$	Biondi, 1967
α_3	$2,2 \times 10^{-6} T_e^{-0,3} T_i^{-0,02}$	Biondi, 1969

T = neutral gas temperature

T_e = electron temperature

T_i = ion temperature

Various other reactions are sometimes considered by other authors (Heroux, 1975; Stubbe, 1970; Rüster, 1971). These include:

$$N_2 + O_2 \xrightarrow{\lambda_1} NO^+ + NO \qquad \text{-----} \qquad (7)$$

$$O_2^+ + N_2 \xrightarrow{\lambda_2} NO^+ + NO \qquad \text{-----} \qquad (8)$$

$$O^+ + NO \xrightarrow{\lambda_3} NO^+ + O \qquad \text{-----} \qquad (9)$$

$$N_2^+ + NO \xrightarrow{\lambda_4} NO^+ + N_2 \qquad \text{-----} \qquad (10)$$

$$O_2^+ + NO \xrightarrow{\lambda_5} NO^+ + O_2 \qquad \text{-----} \qquad (11)$$

$$N_2^+ + O \xrightarrow{\lambda_6} O^+ + N_2 \qquad \text{-----} \qquad (12)$$

$$N_2^+ + O_2 \xrightarrow{\lambda_7} O_2^+ + N_2 \qquad \text{-----} \qquad (13)$$

The rate coefficients for these reactions are shown in Table 2.

Table 2. Additional Reaction Rates

Reaction	Rate Coefficient ($cm^3 s^{-1}$)	Reference
λ_1	1×10^{-14}	Donahue, 1966
λ_2	1×10^{-15}	Ferguson et al.,1965
λ_3	$2{,}1 \times 10^{-17} T^{1,6}$	McFarland et al.,1974a
λ_4	$3{,}3 \times 10^{-10}$	Fehsenfeld et al., 1970
λ_5	$2{,}1 \times 10^{-17} T^{-1,6}$	McFarland et al., 1974a
λ_6	$3{,}6 \times 10^{-11} T^{-0,2}$	McFarland et al., 1974b
λ_7	$4{,}8 \times 10^{-9} T^{-0,8}$	McFarland et al., 1973

Reactions (7) and (8) which produce NO are both extremely slow, and consequently are disregarded. Reactions (9), (10) and (11) which involve NO are also omitted. As (12) and (13) compete with (3) but NO^+ is produced by the latter, only this is included. In the expression for the electron loss rate (see later) NO^+ is the most important constituent due to the high value of α_3, thus reaction (3) is important. Inclusion of all these reactions would probably lead to greater accuracy in the electron density calculations, particularly in the E-region, but the first system (1) - (6)

was regarded as sufficiently comprehensive for a simple approach.

2.3 Production by Photoionization

In order to calculate the production rate, the solar spectrum was divided into twelve wavelength bands, ranging from 1026A^{o} (Lyman β) to 31A^{o} (X-Rays). The neutral species considered were O_2, N_2 and O. The upper limit of the atmosphere was taken to be 600 km, so that H and He are excluded.

The production term in the continuity equation is

$$Q = Q(O_2^+) + Q(N_2^+) + Q(O^+)$$

and the production of each species, j is written

$$Q_j = \sum_{\lambda} q_j = n_j \sum_{\lambda} \sigma_I^{\,j}(\lambda)\phi_\infty(\lambda)e^{-\tau(\lambda)}$$ (Banks and Kockarts, 1973b, p.108)

where Q_j = total production rate of species j.

q_j = production rate of species j for a particular wavelength

n_j = number density of neutral species

$\sigma_I^{\,j}(\lambda)$ = wavelength-dependent photoionization cross-section of neutral species

$\phi_\infty(\lambda)$ = solar radiation flux for a particular wavelength

$\tau(\lambda)$ = optical depth for a particular wavelength

The product of the photoionization cross-section and the solar radiation flux may be written as the ionization rate coefficient, $I_j(\lambda)$.

The optical depth τ may be expressed as

$$\tau = \sec\chi \sum_j n_j H_j \sigma_a^{\,j}(\lambda)$$ (Banks and Kockarts, 1973b, p.106)

where χ = solar zenith angle

H_j = scale height of neutral species, j.

$\sigma_a^j(\lambda)$ = wavelength-dependent photoabsorption cross-section of neutral species.

The above formulation of τ is valid for all except large values of χ ($\chi < 60^o$).

The scale height of species j is defined thus:

$$H_j = \frac{kT}{m_j g} \quad \text{(Rishbeth and Garriott, 1969, p.5)}$$

where k = Boltzmann's constant

T = neutral gas temperature

m_j = mass of neutral species j.

g = acceleration due to gravity.

$= 980{,}6/(1 + (1{,}573 \times 10^{-4} z))^2$ (z = altitude in km)

(Banks and Kockarts, 1973a, p.9)

The photoabsorption cross-sections and ionization rate coefficients given in Table 2 are taken from Banks and Kockarts (1973a, Chapters 6 and 7), and are for high solar activity. The number of photons in the spectral ranges is of the order of 1×10^{10} photons $cm^{-2}s^{-1}$, except for the three bands from $80A^o$ to $31A^o$, where the photon flux is lower. This is justified by analysis of the solar spectrum.

Table 3. Absorption cross-sections and ionization rate coefficients

Wave-lengths	O_2		N_2		O	
(A^o)	$\sigma_a(\lambda)$ (cm^2)	$I(\lambda)$ (s^{-1})	$\sigma_a(\lambda)$ (cm^2)	$I(\lambda)$ (s^{-1})	$\sigma_a(\lambda)$ (cm^2)	$I(\lambda)$ (s^{-1})
1026	$1,55 \times 10^{-18}$	5×10^{-9}				
977	$4,0 \times 10^{-18}$	$1,1 \times 10^{-8}$				
910-796	$7,5 \times 10^{-18}$	$5,7 \times 10^{-8}$			3×10^{-18}	$4,5 \times 10^{-8}$
796-732	2×10^{-17}	$1,5 \times 10^{-8}$	2×10^{-17}	$1,5 \times 10^{-8}$	3×10^{-18}	$1,5 \times 10^{-8}$
732-665	$2,0 \times 10^{-17}$	$1,5 \times 10^{-8}$	$2,3 \times 10^{-17}$	$1,6 \times 10^{-8}$	8×10^{-18}	$1,5 \times 10^{-8}$
665-375	$2,5 \times 10^{-17}$	2×10^{-7}	$2,3 \times 10^{-17}$	$1,9 \times 10^{-7}$	$1,2 \times 10^{-17}$	$8,7 \times 10^{-8}$
375-275	$1,7 \times 10^{-17}$	$2,3 \times 10^{-7}$	$1,4 \times 10^{-17}$	$1,9 \times 10^{-7}$	$8,0 \times 10^{-18}$	$1,1 \times 10^{-7}$
275-150	$7,5 \times 10^{-18}$	$1,0 \times 10^{-7}$	5×10^{-18}	7×10^{-8}	$3,8 \times 10^{-18}$	$5,2 \times 10^{-8}$
150-80	$3,5 \times 10^{-18}$	$9,0 \times 10^{-8}$	$2,2 \times 10^{-18}$	$5,5 \times 10^{-9}$	$1,8 \times 10^{-18}$	$4,4 \times 10^{-9}$
80-60	$9,28 \times 10^{-19}$	$4,87 \times 10^{-10}$	$5,45 \times 10^{-19}$	$2,86 \times 10^{-10}$	$4,64 \times 10^{-19}$	$2,44 \times 10^{-10}$
60-41	$4,40 \times 10^{-19}$	$2,20 \times 10^{-10}$	$2,35 \times 10^{-19}$	$1,20 \times 10^{-10}$	$2,0 \times 10^{-19}$	$1,0 \times 10^{-10}$
41-31	$1,64 \times 10^{-19}$	$2,0 \times 10^{-11}$	$9,67 \times 10^{-20}$	$1,18 \times 10^{-11}$	$0,82 \times 10^{-19}$	$1,0 \times 10^{-11}$

2.4 Production by Precipitated Particles

The production of electron-ion pairs by collisions between precipitated electrons from the magnetosphere and molecules in the atmosphere is considered. The electrons are assumed to be isotropically distributed over the downward hemisphere (IDH), and with a spectrum of the type

$$J_{>E} = J_0 \exp(-E/E_0)$$

where $J_{>E}$ = total flux of electrons with energies greater than E

J_0 = total flux of electrons with energies greater than zero

E = any selected energy of the incoming electrons

E_0 = characteristic or e-folding energy, i.e. $\frac{1}{e}$ of the total flux of electrons have energies greater than E_0. It can be shown (Wulff, 1972) that E_0 is the average energy of electrons with spectra of this type.

Scaled Penetration Function

The amount of energy lost by incoming electrons at any stage of their entire range is dependent on the fraction of the range covered (Grün, 1957). This functional dependence is expressed in Grün's "lambda function" $\lambda(z/r_p)$, where

z = atmospheric depth from upper limit of ionosphere to height h

r_p = practical range covered by electron before giving up all its energy in collisions

$$z = \int_{h}^{h_0} D(h')dh'$$

where h'= dummy height variable

$D(h')$ = atmospheric density at height h'

h_0 = height of upper limit of ionosphere

h = height under consideration

z is measured in gm cm^{-2}.

The practical range of the electron, r_p, is related to its initial energy, E, by the formula due to Gledhill (1973):

$$y = -5{,}100 + 1{,}358x + 0{,}215x^2 - 0{,}043x^3$$

where $y = \log_{10} r_p$

$x = \log_{10} E$

Only low-energy electrons (E<100keV) are considered, for which the above expression applies.

The lambda function can be scaled to remove most of its energy dependence. This was done by Berger et al (1970) as follows:

$$A(z/r_p) = \lambda(z/r_p).r_p/E$$

The resultant scaled penetration function, $A(z/r_p)$ shows very little energy dependence (at most 5%) and may be averaged to obtain a single curve applicable for all energies. Graphs of $A(z/r_p)$ and $\lambda(z/r_p)$ are shown in Heighway (1973).

$A(z/r_p)$ is represented by the following expression due to Heighway (1973)

$$y = 1,212 \exp(-2,228x^3) + 0,0776 \exp(-37,83x^2)$$

where $y = A(z/r_p)$

$x = z/r_p$

Ionization Rate

The energy deposition rate per unit flux is defined as (Berger et al, 1970)

$$E_h/F = D(h)\lambda(z/r_p)E/r_p$$

where E_h = energy deposited at height h

F = IDH flux for a given energy interval ΔE.

All other symbols as previously defined.

If the energy used per ion-electron pair produced is 0,035 keV (Dalgarno and Griffing, 1958; Rees, 1963), then

$$q/F = D(h)\ \lambda(z/r_p)E/0,035r_p = E_h/0,035 \text{ ion-electron pairs } el^{-1}cm^{-1}$$

where q = ion-electron pairs produced per unit volume per unit time, for a given energy interval, ΔE.

The ionization rate Q_h at a given height is obtained by integrating over the energy spectrum of the incoming electrons (Wulff, 1972)

$$Q_h = \sum_E \left(\frac{q}{F} \frac{\Delta E}{E_0} \pi J_0 \exp(-E/E_0)\right)$$

and $$Q_h/\pi J_0 = \sum_E \left(\frac{q}{F} \cdot \frac{\Delta E}{E_0} \exp(-E/E_0)\right)$$

is the ionization rate per unit integral IDH flux.

The numerical integration is carried out over an energy range $0{,}1\text{keV} \leq E \leq 10E_0$, and the energy interval ΔE is E/100, the width of the interval thus increasing with increasing energy.

To find the actual ionization rate of each of the neutral species O_2, N_2, O, the total production rate Q is divided into rates proportional to the density of the neutral species, thus giving values of $Q(O_2^+)$, $Q(N_2^+)$ and $Q(O^+)$.

2.5 Loss due to Chemical Reactions

From the set of equations for the photochemical reactions given in 2.1, the loss term is written:

$$L = [\alpha_1 n(NO^+) + \alpha_2 n(O_2^+) + \alpha_3 n(N_2^+)]N$$

The time variation in the ion densities can be written simply (ignoring diffusion effects) as:

$$\frac{\partial n(O^+)}{\partial t} = Q(O^+) - k_1 n(O^+) n(N_2) - k_2 n(O^+) n(O_2) \qquad \text{-----} \quad (1)$$

$$\frac{\partial n(O_2^+)}{\partial t} = Q(O_2^+) + k_2 n(O^+) n(O_2) - \alpha_2 n(O_2^+) N \qquad \text{-----} \quad (2)$$

$$\frac{\partial n(N_2^+)}{\partial t} = Q(N_2^+) - k_3 n(N_2^+) n(O) - \alpha_3 n(N_2^+) N \qquad \text{-----} \quad (3)$$

$$\frac{\partial n(NO^+)}{\partial t} = k_1 n(O^+) n(N_2) + k_3 n(N_2^+) n(O) - \alpha_1 n(NO^+) N \qquad \text{-----} \quad (4)$$

Eqn. (1) is particularly affected by the omission of a transport term. However, where diffusion is of importance (above 200 km, approximately, in this treatment), the charge-balance equation is used to find $n(O^+)$, i.e.

$$N = n(O^+) + n(O_2^+) + n(N_2^+) + n(NO^+),$$

hence; $$n(O^+) = N - n(O_2^+) - n(N_2^+) - n(NO^+) \qquad \text{-----} \quad (5)$$

2.6 Transport by Diffusion

The derivation of the expression for transport is given in Appendix A. The result only is quoted here.

$$\nabla\cdot(N\underline{V}) = -2D\sin^2 I \frac{\partial^2 N}{\partial h^2} - D\sin^2 I \left(\frac{5}{T}\frac{\partial T}{\partial h} + \frac{3}{H}\right)\frac{\partial N}{\partial h} - D\sin^2 I \left(\frac{7}{2HT}\frac{\partial T}{\partial h} + \frac{1}{T^2}\left(\frac{\partial T}{\partial h}\right)^2 + \frac{2}{T}\frac{\partial^2 T}{\partial h^2} - \frac{1}{H^2}\frac{\partial H}{\partial h} + \frac{1}{H^2}\right) N$$

The meaning of the symbols is given in Appendix A.

2.7 Method of Solution

The Jacchia (1971) model atmosphere is used to give temperatures and densities of neutral species from 120 km to 600 km. The particular model chosen has a 700 K exospheric temperature, as the main interest was in nighttime effects. The

geographic position for which the equations were solved was $30^{o}S, 35^{o}W$, i.e. the geomagnetic dip angle I, was - 40^{o}.

The techniques used to solve the equations are discussed fully in the following chapter. Briefly, a finite-difference method is used for the continuity equation itself, while the ion density equations are solved by linear segments integration. Initial values must be supplied to start the integration process.

Initial Values

Using eqn (5), $n(0^+)$ can be eliminated in (1) - (4), giving

$$\frac{\partial n(O_2^+)}{\partial t} = Q(O_2^+) + k_2 n(O_2)\left[N - n(O_2^+) - n(N_2^+) - n(NO^+)\right] - \alpha_2 n(O_2^+) N \quad \text{-----} \quad (6)$$

$$\frac{\partial n(N_2^+)}{\partial t} = Q(N_2^+) - k_3 n(N_2^+) n(O) - \alpha_3 n(N_2^+) N \quad \text{-----} \quad (7)$$

$$\frac{\partial n(NO^+)}{\partial t} = k_1 n(N_2)\left[N - n(O_2^+) - n(N_2^+) - n(NO^+)\right] + k_3 n(N_2^+) n(O) - \alpha_1 n(NO^+) N \quad \text{-----} \quad (8)$$

For an equilibrium solution, each of the equations (6)-(8) is set equal to zero.

$$n(O_2^+) = \frac{Q(O_2^+) + k_2 n(O_2) n(O^+)}{\alpha_2 N} \quad \text{-----} \quad (9)$$

$$n(NO^+) = \frac{k_1 n(O^+) n(N_2) + k_3 n(N_2^+) n(O)}{\alpha_1 N} \qquad \text{-----} \quad (10)$$

$$n(N_2^+) = \frac{Q(N_2^+)}{\alpha_3 N + k_3 n(O)} \qquad \text{-----} \quad (11)$$

Neglecting diffusion, the steady-state continuity equation becomes

$$Q - L = 0$$

Substituting for L from (9)-(11) yields a cubic in N of the form $AN^3 + BN^2 + CN + D = 0$ ----- (12)

where $A = -\alpha_1\alpha_2\alpha_3(k_1 n(N_2) + k_2 n(O_2))$

$$B = \alpha_1\alpha_2\alpha_3 Q(O^+) - \alpha_1\alpha_2 k_3 n(O)(k_1 n(N_2) + k_2 n(O_2))$$

$$C = Q(\alpha_1\alpha_3 k_2 n(O_2) + \alpha_2\alpha_3 k_1 n(N_2) + \alpha_1\alpha_2 k_3 n(O))$$

$$-Q(N_2^+)(\alpha_1\alpha_3 k_2 n(O_2) + \alpha_2\alpha_3 k_1 n(N_2) + \alpha_1\alpha_2 k_3 n(O))$$

$$-Q(O_2^+)(\alpha_2\alpha_3 k_1 n(N_2) + \alpha_1\alpha_2 k_3 n(O) - \alpha_1\alpha_3 k_1 n(N_2))$$

$$D = \alpha_1 k_2 k_3 n(O) n(O_2) Q + \alpha_2 k_1 k_3 n(O) n(N_2) Q$$

$$-\alpha_1 k_2 k_3 n(O) n(O_2) Q(N_2^+) + \alpha_1 k_1 k_3 n(N_2) n(O) Q(O_2^+)$$

$$+\alpha_2 k_2 k_3 n(O_2) n(O) Q(N_2^+) - \alpha_2 k_1 k_3 n(O) n(N_2) Q(O_2^+)$$

Substituting in (12) and solving, values of N are obtained which are then used to solve (9)-(11), yielding steady-state initial values of the ion species. The values of N obtained from (12) are not valid for heights where diffusion is of importance.

To obtain initial values of N, the solution to (12) is used up to 145 km. Above this, values are taken from Stubbe (1970) and smoothly joined.

Boundary Conditions

Boundary conditions are required at the lower and upper limits of the atmosphere. The lower boundary condition is simply

$$N|_{120km} = \text{constant}$$

When an equilibrium solution is required, this constant is the initial value found from (12), since (12) is a steady-state solution to the continuity equation with no diffusion. The change in this boundary condition under different circumstances is discussed in Chapter 4.

A number of different boundary conditions may be used for the upper limit : specification of electron velocity, of vertical ion fluxes, of electron density gradients, etc. (Herman and Chandra, 1969; Schunk and Walker, 1970; Stubbe, 1970). The boundary condition which was used was suggested by Torr (1976).

At the upper limit, it is assumed that production=loss=zero. The continuity equation then becomes

$$\frac{\partial N_j}{\partial t} = - \nabla \cdot (N_j V_j) \qquad \text{-----} \qquad (13)$$

where j = upper boundary height.

Integrating (13) from the upper boundary to infinity gives

$$\int_{h_j}^{\infty} \frac{\partial N_j}{\partial t} \, dh = - [\phi_\infty - \phi_{h_j}] \qquad \text{-----} \qquad (14)$$

where ϕ_∞ = flux at infinity

ϕ_{h_j} = flux at the upper boundary = $N_j V_j$

Also, assuming that $N = N_0 e^{-h/H(N)}$ at this height, where

$H(N)$ = plasma scale height,

$$\int_{h_j}^{\infty} \frac{\partial N_j}{\partial t}\, dh = \frac{\partial}{\partial t} \int_{h_j}^{\infty} N_j\, dh = \frac{\partial}{\partial t}\,(N_j H(N)) \qquad \text{-----} \qquad (15)$$

Using (14) and (15), $\frac{\partial}{\partial t}\,(N_j H(N)) = -\left[\phi_\infty - \phi_{h_j}\right]$

$$= -\left[\phi_\infty - N_j V_j\right]$$

$$V_j = -V_D = -D\sin^2 I\left[\frac{2}{NT}\,\frac{\partial}{\partial h}\,(NT) + \frac{1}{H(0)}\right] \quad \text{(from eqn (22), App. A)}$$

$$= -D\sin^2 I\left[\frac{2}{T}\,\frac{\partial T}{\partial h} + \frac{2}{N}\,\frac{\partial N}{\partial h} + \frac{1}{H(0)}\right]$$

Hence, at the upper boundary,

$$\frac{\partial}{\partial t}(N_j H(N)) = -\left[\phi_\infty + N_j D\sin^2 I\left\{\frac{2}{T}\,\frac{\partial T}{\partial h} + \frac{2}{N_j}\,\frac{\partial N_j}{\partial h} + \frac{1}{H(0)}\right\}\right]$$

This is the condition used at 600 km.

The value of ϕ_∞ used was -3×10^8 els $cm^{-2}s^{-1}$ (Eccles et al., 1973; Banks and Kockarts, 1973b, p.184). This figure is somewhat arbitrary, but as seen in Banks and Kockarts, the effect of variations in this value is not great. A downward drift from the plasmasphere was chosen rather than an upward one because of our main interest, viz. the nighttime ionosphere. A full discussion of vertical fluxes can be found in Evans (1975), and in Banks and Kockarts (1973b, Chapter 20).

CHAPTER 3

NUMERICAL METHODS

3.1 Finite Difference Techniques

In order to solve the equations numerically, they must be written in a form suitable for computation. In the finite-difference approximation some or all of the derivatives are replaced by numerical differences, e.g. $\frac{\partial N}{\partial t}$ can be written as

$\frac{\Delta N}{\Delta t}$, which becomes $\frac{N^{j+1} - N^{j}}{\Delta t}$, ----- (1)

where N^{j} = electron density at time t_j

Δt = time interval between t_{j+1} and t_j.

Similarly $\frac{\partial N}{\partial h}$ becomes $\frac{N_{i+1} - N_{i-1}}{2\Delta h}$ ----- (2)

where N_i = electron density at height h_i.

Δh = height interval between h_{i+1} and h_i.

It should be noted that in (2) the finite-difference ratio is an approximation to the derivative at the midpoint of the interval h_{i-1} to h_{i+1}, while in (1) the approximation relates to the derivative at the beginning of the interval over which the difference is taken. It is also assumed in (2) that the height interval between h_{i+1} and h_i is equal to that between h_i and h_{i-1}, i.e. Δh is a constant with height.

To find an expression for $\frac{\partial^2 N}{\partial h^2}$, a second-order equation of the form

$$N = Ah^2 + Bh + C \quad (h=\text{height};\ A,B,C = \text{constants}) \qquad \text{-----} \quad (3)$$

is fitted to each set of three points: N_{i-1}, N_i, N_{i+1}. The value of $\frac{\partial^2 N}{\partial h^2}$ from (3) is 2A and this is solved for in terms of the N_i, giving

$$\frac{\partial^2 N}{\partial h^2} = \frac{N_{i+1} - 2N_i + N_{i-1}}{(\Delta h)^2} \qquad \text{-----} \quad (4a)$$

This derivation is explained in further detail later in this chapter. The expression for $\frac{\partial^2 N}{\partial h^2}$ as given by (4a) can also be found by expanding N_{i+1} and N_{i-1} in Taylor series and ignoring second-order terms in (Δh) and higher. This is done in Crank (1956).

The approximations (1), (2) and (4a) can be used in different ways, depending on the method to be used.

3.2 The Crank-Nicolson Method

As has been noted above, (1) gives a forward difference approximation to the derivative, while (2) gives a central difference. The expression $\frac{N^{j+1} - N^j}{\Delta t}$ may be regarded as a central difference, however, if one assumes it to correspond to the midpoint of the time interval, Δt. Thus a central difference approximation to $\frac{\partial^2 N}{\partial h^2}$ is found by averaging the difference quotients at the beginning and end of the time interval.

$$\frac{\partial^2 N}{\partial h^2} = \tfrac{1}{2}\left[\frac{N_{i+1}^{j+1} - 2N_i^{j+1} + N_{i-1}^{j+1}}{(\Delta h)^2} + \frac{N_{i+1}^{j} - 2N_i^{j} + N_{i-1}^{j}}{(\Delta h)^2}\right]$$

$$\text{-----} \quad (4b)$$

where N_i^j = electron density at time t_j, height h_i. (Gerald, 1970, Chapter 10; Crank, 1956, pp.189-191).

This particular formulation was chosen for its stability and computing speed. A full discussion of convergence, error analysis and stability can be found in Gerald (1970), Chapter 10.

In (4a) and (4b), the height interval is again assumed to be constant, i.e.

$$h_{i+1} - h_i = \Delta h = h_i - h_{i-1}$$

3.3 The Continuity Equation in Finite Difference Form

The continuity equation may be written

$$\frac{\partial N}{\partial t} = X \frac{\partial^2 N}{\partial h^2} + Y \frac{\partial N}{\partial h} + ZN + C$$

where $X = 2D\sin^2 I$

$$Y = D\sin^2 I \left(\frac{5}{T}\frac{\partial T}{\partial h} + \frac{3}{H}\right)$$

$$Z = D\sin^2 I \left(\frac{7}{2HT}\frac{\partial T}{\partial h} + \frac{1}{T^2}\left(\frac{\partial T}{\partial h}\right)^2 + \frac{2}{T}\frac{\partial^2 T}{\partial h^2} - \frac{1}{H^2}\frac{\partial H}{\partial h} + \frac{1}{H^2}\right)$$

$$- \left(\alpha_1 n(NO^+) + \alpha_2 n(O_2^+) + \alpha_3 n(N_2^+)\right)$$

$C = Q$ (see previous chapter)

This becomes, using (1), (2) and (4b),

$$\frac{N_i^{j+1} - N_i^j}{\Delta t} = \frac{X}{2}\left(\frac{N_{i+1}^{j+1} - 2N_i^{j+1} + N_{i-1}^{j+1}}{(\Delta h)^2} + \frac{N_{i+1}^j - 2N_i^j + N_{i-1}^j}{(\Delta h)^2}\right)$$

$$+ Y\left(\frac{N_{i+1}^j - N_{i-1}^j}{2\Delta h}\right) + ZN_i^j + C \qquad \text{-----} \quad (5)$$

which can be rearranged thus:

$$\frac{N_i^{j+1}}{\Delta t} - \frac{X}{2}\left(\frac{N_{i+1}^{j+1} - 2N_i^{j+1} + N_{i-1}^{j+1}}{(\Delta h)^2}\right) = \frac{N_i^j}{\Delta t} + \frac{X}{2}\left(\frac{N_{i+1}^j - 2N_i^j + N_{i-1}^j}{(\Delta h)^2}\right)$$

$$+ Y\left(\frac{N_{i+1}^j - N_{i-1}^j}{2\Delta h}\right) + ZN_i^j + C \qquad \text{-----} \qquad (6)$$

In order to begin the integration process, initial values of N_i^j at some time t_o, and for all heights must be supplied. Consequent N(h) profiles are then found by solving (6). It should be noted that the electron density at any height h_i cannot be found explicitly from a single equation, since N_i^{j+1} is coupled to both N_{i+1}^{j+1} and N_{i-1}^{j+1}, i.e. to the electron densities at adjoining heights as well as to the electron densities of the previous profile, the N_i^j. This may be schematically represented as follows:

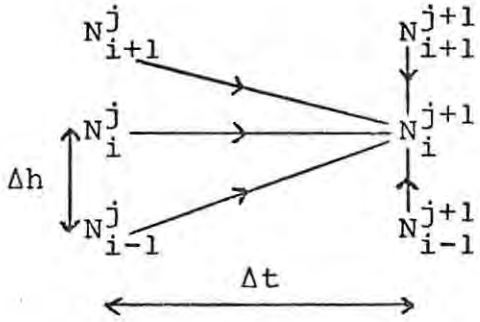

Thus N_i^{j+1} is dependent on all its neighbours on the height versus time grid, excepting those of the next time step N_i^{j+2}. The Crank-Nicolson method is also termed an implicit method because of this coupling. The formulation (6) leads to a system of linear equations, one for each of the n heights in the atmosphere, which must be solved simultaneously. These equations are of the form

$$a_{k\,i-1}\ N_{i-1} + a_{k\,i}\ N_i + a_{k\,i+1}\ N_{i+1} = R_i \quad \text{-----} \quad (7)$$

where k, i run from 1 to n.

As can be seen from (7), there are (n+2) unknowns in the system because of the inclusion of the N_{i-1}, N_{i+1} terms. The extra equations needed are supplied by boundary conditions at the lower and upper limits of the atmosphere.

The system of equations can be expanded as shown below

$$\begin{bmatrix} a_{11} & a_{12} & 0 & 0 & 0 & \cdots & & \\ a_{21} & a_{22} & a_{23} & 0 & 0 & \cdots & & \\ 0 & a_{32} & a_{33} & a_{34} & 0 & \cdots & & \\ \vdots & & & & & & & \\ & \cdots\cdots\cdots & & a_{n-1\,n-2} & a_{n-1\,n-1} & a_{n-1\,n} & & \\ & \cdots\cdots\cdots & & 0 & a_{n\,n-1} & a_{n\,n} & & \end{bmatrix} \begin{bmatrix} N_1^{j+1} \\ N_2^{j+1} \\ N_3^{j+1} \\ \vdots \\ N_{n-1}^{j+1} \\ N_n^{j+1} \end{bmatrix} = \begin{bmatrix} R_1 \\ R_2 \\ R_3 \\ \vdots \\ R_{n-1} \\ R_n \end{bmatrix}$$

----- (8)

where the column vector R_i is the right-hand side of (6). All the terms in the matrix a_{ii} are constants for a fixed time interval Δt and model atmosphere. The column vector R_i, however, changes with each new N(h) profile calculated, as can be seen from (6). Thus the process of integration consists of

(1) Evaluation of the matrix elements a_{ii}.

(2) Evaluation of the right-hand side of (6), the column vector R_i.

(3) Solution of the system (8), yielding values of electron density advanced in time by Δt, i.e. $N_i^{t_o+\Delta t}$.

(4) Re-evaluation of R_i using these new electron densities.

(5) Solution of system (8) with a new R_i, to give a new profile at time $t_o+2\Delta t$.

The process is continued as long as may be required. Each time the equations are solved, the solution advances by Δt. The method is shown schematically later in this chapter.

As the integration process is an iterative one it is important that the algorithm used to solve the linear equations be stable, and with minimal rounding errors. This particular method was tested using a number of different routines for solving linear equations, as well as in double and single precision mode. The solutions showed no variation to within four significant figures. As the system is tridiagonal computation is relatively fast (less than 1 second of processor time per integration, with 53 equations).

3.4 Boundary Conditions

As discussed in Chapter 2, the two boundary conditions are:

$$N\big|_{120\ km} = \text{constant}$$

$$\frac{\partial}{\partial t}\,(N_i H(N)) = -\left[\phi_\infty + N_i D \sin^2 I\ \left(\frac{2}{T}\frac{\partial T}{\partial h} + \frac{2}{N_i}\frac{\partial N_i}{\partial h} + \frac{1}{H(O)}\right)\right]$$

This latter equation in finite difference form, becomes

$$H(N)\ \left[\frac{N_i^{j+1} - N_i^j}{\Delta t}\right] = -\left[\phi_\infty + N_i D \sin^2 I\ \left(\frac{2}{T}\frac{\partial T}{\partial h} + \frac{2}{N_i}\left[\frac{N_i^j - N_{i-1}^j}{\Delta h}\right] + \frac{1}{H(O)}\right)\right] \qquad \text{-----} \quad (9)$$

where the $\frac{\partial N}{\partial h}$ term has been backward differenced to $\frac{N_i^j - N_{i-1}^j}{\Delta h}$.

Note that the use of this type of boundary condition (derivative boundary condition) decouples the unknown electron densities at adjacent heights. The N_i^{j+1} can be found explicitly at the upper limit.

3.5 Changes in Height Interval

The expressions for $\frac{\partial N}{\partial h}$ and $\frac{\partial^2 N}{\partial h^2}$ as given in (2), (3) are valid only if Δh is constant. If this condition is not met, new expressions must be found.

It is assumed that a cubic spline can be fitted to the electron density profile.

$$N = Ah^2 + Bh + C \qquad \text{-----} \qquad (10)$$

From (10), $\frac{\partial^2 N}{\partial h^2} = 2A$

To find the value of A, the following system of equations must be solved:

$$\begin{aligned} Ah_{i-1}^2 + Bh_{i-1} + C &= N_{i-1} \\ Ah_i^2 + Bh_i + C &= N_i \qquad \text{-----} \qquad (11) \\ Ah_{i+1}^2 + Bh_{i+1} + C &= N_{i+1} \end{aligned}$$

This system of equations can be written in matrix form as

$$\begin{bmatrix} h_{i-1}^2 & h_{i-1} & 1 \\ h_i^2 & h_i & 1 \\ h_{i+1}^2 & h_{i+1} & 1 \end{bmatrix} \begin{bmatrix} A \\ B \\ C \end{bmatrix} = \begin{bmatrix} N_{i-1} \\ N_i \\ N_{i+1} \end{bmatrix}$$

and, from Kraut (1967, pp.30-31), A can be found by using Cramer's rule.

$$A = \frac{\begin{vmatrix} N_{i-1} & h_{i-1} & 1 \\ N_i & h_i & 1 \\ N_{i+1} & h_{i+1} & 1 \end{vmatrix}}{\begin{vmatrix} h_{i-1}^2 & h_{i-1} & 1 \\ h_i^2 & h_i & 1 \\ h_{i+1}^2 & h_{i+1} & 1 \end{vmatrix}}$$

$$A = \frac{\begin{vmatrix} N_i - N_{i-1} & h_i - h_{i-1} \\ N_{i+1} - N_{i-1} & h_{i+1} - h_{i-1} \end{vmatrix}}{\begin{vmatrix} h_i^2 - h_{i-1}^2 & h_i - h_{i-1} \\ h_{i+1}^2 - h_{i-1}^2 & h_{i+1} - h_{i-1} \end{vmatrix}} \quad \text{-----} \quad (12)$$

If $h_{i+1} - h_i = \Delta h = h_i - h_{i-1}$, eqn (12) reduces to

$$A = \frac{N_{i+1} - 2N_i + N_{i-1}}{2(\Delta h)^2}$$

which is the expression used previously. If Δh is not constant, eqn (12) must be solved explicitly.

The expression for $\frac{\partial N}{\partial h}$ becomes $\frac{N_{i+1} - N_{i-1}}{h_{i+1} - h_{i-1}}$

Such a change in Δh takes place at 160 km in the Jacchia (1971) model atmosphere, where the height interval increases from 5 km to 10 km.

3.6 Ion Densities

The loss rate term in the continuity equation is dependent on the ionic species, O_2^+, O^+, N_2^+, NO^+ as discussed in Chapter 2. To solve the first-order differential equations expressing the time variation in the ion densities, a linear segments integration process is used. This has the advantage of speed and simplicity, and as the time interval Δt is small (1 second), should not be too inaccurate. A more sophisticated routine, written by Gear (1971), Chapter 9, was used at first but was found to be prohibitively time- and core-consuming.

Equations (2) - (4) of Chapter 2 become, in linearised form,

$$n(NO^+)^{j+1} = n(NO^+)^j + \Delta t \left(k_1 n(O^+)^j n(N_2) + k_3 n(N_2^+)^j n(O) - \alpha_1 n(NO^+)^j N^j\right) \quad \text{-----} \quad (13)$$

$$n(O_2^+)^{j+1} = n(O_2^+)^j + \Delta t(Q(O_2^+) + k_2 n(O^+)^j n(O_2) - \alpha_2 n(O_2^+)^j N^j) \quad \text{-----} \quad (14)$$

$$n(N_2^+)^{j+1} = n(N_2^+)^j + \Delta t(Q(N_2^+) - k_3 n(N_2^+)^j n(O) - \alpha_3 n(N_2^+)^j N^j) \quad \text{-----} \quad (15)$$

At heights where diffusion can be ignored, the $n(O^+)$ equation is

$$n(O^+)^{j+1} = n(O^+)^j + \Delta t(Q(O^+) - k_1 n(O^+)^j n(N_2) - k_2 n(O^+)^j n(O_2)) \quad \text{-----} \quad (16)$$

This applies up to 200 km in the particular model atmosphere used. At greater altitudes, the charge balance equation is used instead.

$$n(O^+)^{j+1} = N^j - n(O_2^+)^j - n(N_2^+)^j - n(NO^+)^j \quad \text{-----} \quad (17)$$

The expression for the loss rate is incorporated into the column vector R_i, as mentioned in 3.2. Thus the ion density equations (13) - (17) are solved before evaluating R_i, using the electron densities as they are calculated. The process is shown below.

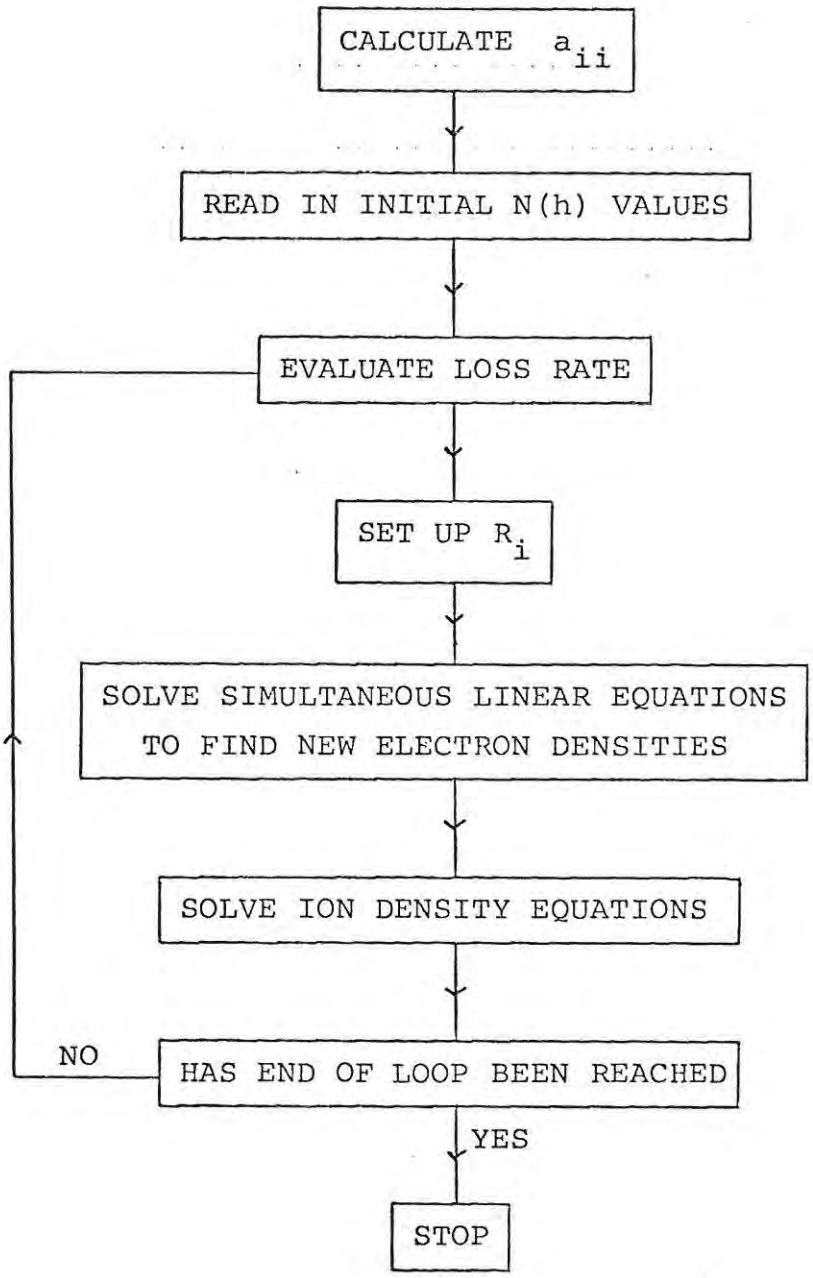
CALCULATE a_{ii}
READ IN INITIAL N(h) VALUES
EVALUATE LOSS RATE
SET UP R_i
SOLVE SIMULTANEOUS LINEAR EQUATIONS TO FIND NEW ELECTRON DENSITIES
SOLVE ION DENSITY EQUATIONS
NO
HAS END OF LOOP BEEN REACHED
YES
STOP

CHAPTER 4

COMPUTATIONS

4.1 Introduction

The program that solves the continuity equation is extremely time-consuming. In order to economize on time and core, the computation was broken up into a series of smaller programs which calculate various quantities which can be stored on disc, rather than be recalculated each time the program is run; and a main program which actually solves the continuity equation.

In this chapter the model atmosphere and subsidiary programs are briefly discussed. The conditions for which solutions to the continuity equation are sought are specified, and a typical program is described in some detail. Finally some mention is made of the program which calculates the production rate due to precipitated electrons.

4.2 The Model Atmosphere

The Jacchia (1971) model atmosphere is used, giving values of atmospheric temperatures and composition as functions of height and exospheric temperature, for heights from 120 km to 600 km. The particular model chosen has an exospheric temperature of 700 K (Thuillier et al., 1977). Between 400 km and 600 km, the model atmosphere values are quoted at 20 km intervals. As this was felt to be too large a height interval, an interpolation program was written to find values at 10 km intervals. Between 120 km and 160 km the height step is 5 km; thereafter it changes to 10 km. This was taken into account throughout (see previous chapter, section 3.5). Alternative model atmospheres are discussed in the final chapter.

4.3 Preliminary Data

The program INIT is used to calculate the following:

(1) Scale heights of neutral constituents 0, 0_2, N_2 as functions of height according to the formula $H_j = \frac{kT}{m_j g}$ (see Chapter 2).

(2) Optical depths and hence production rates due to photoionization.

(3) Initial values of N (no diffusion) (Eqn (12), Chapter 2).

(4) Initial values of ion densities (Eqns (9)-(11), Chapter 2).

Values of $Q(0^+)$, $Q(0_2^+)$, $Q(N_2^+)$, $n(0_2^+)$, $n(NO^+)$, $n(N_2^+)$ and $n(0^+)$ are filed on discfile ARCHDATAO2 for further use. A listing and flow-chart of the program are given in Appendix B.

Various other small programs are used to find $\frac{\partial H}{\partial h}$, $\frac{\partial T}{\partial h}$ and $\frac{\partial^2 T}{\partial h^2}$ by fitting cubic splines to the T(h) (as given in the model atmosphere) and H(h) (as found by INIT) profiles and hence finding first and second derivations. The cubic spline fitting routine (Subroutine Splinepolyfit) ensures continuity of the fitted polynomial $P_i(h)$, its slope $P_i'(h)$ and its curvature $P_i''(h)$. The coefficients of N, $\frac{\partial N}{\partial h}$ and $\frac{\partial^2 N}{\partial h^2}$ of eqn (23), Appendix A, were then calculated and filed on ARCHDATAO2. The values of the reaction rate coefficients k_1, k_2, k_3 α_1, α_2, α_3 and the tridiagonal matrix of Chapter 3, eqn (8) were also filed on disc.

4.4 The Continuity Equation Programs

Solutions to the continuity equation were sought for the following conditions: daytime equilibrium conditions, with and without precipitation fluxes; and nighttime conditions, with and without precipitation. As the main routine used is virtually the same in all cases, only one will be described in detail, viz. the program to find a daytime steady-state solution with no electron precipitation.

The program may be summarised as follows:

(a) Call up data from ARCHDATAO2.

(b) Enter loop: evaluate loss rate.

(c) Calculate vector R (see Chapter 3, eqn (8)).

(d) Solve tridiagonal set of linear equations, using Subroutine Tridiag.

(e) Solve ion density equations by linear segments integration.

(f) Check for instabilities in the electron density at 600 km.

(g) Check for instabilities in the ion densities.

(h) Print results.

(i) End of loop: write electron and ion densities back to ARCHDATAO2 for next run.

A number of points about the program should be noted:

(1) The time interval Δt is kept constant at 1 second throughout. This small interval was found to be necessary because of the effects of diffusion at heights above 400 km, where the diffusion coefficients are very large. With a smaller height interval at high altitudes, it should be possible to increase Δt.

(2) The diagonal elements of the tridiagonal matrix are destroyed by the matrix subroutine (Tridiag). Thus they must be recalled from disc on every integration.

(3) The linear segments integration routine used to solve the ion density equations must be checked for improbable results due to the inherent instabilities in the equations. As the ion densities are, in this case, of secondary importance, being used only to calculate the loss rate for electrons, it was felt that the increase in time that would result from a more sophisticated routine was not warranted.

(4) The electron density at 600 km is checked for numerical instabilities. If $N|_{600\ km}$ exceeds the value at 590 km, a least squares routine is called which fits an exponential curve to the electron densities at 570,580 and 590 km, then extrapolates to find the expected value at 600 km.

(5) As the whole program works on an iterative basis, the final values of electron and ion densities are written back onto disc to continue the process on the following run of the program.

(6) The boundary condition at 120 km for the steady-state solution is simply that $N|_{120\ km}$ = constant. This, however, changes for the nighttime solution, and is discussed below.

The above routine was used for the following:

(1) Equilibrium solution. The initial N(h) profile (see Fig. 1, Chapter 5) was used as input data, while production and transport terms were kept constant. The program was allowed to run until a steady-state solution had been found. This solution was tested for stability by using different input profiles and comparing the result with the original solution.

(2) Equilibrium solution with additional production by precipitated particles. The production due to a flux of 3×10^7 els cm^{-2} s^{-1} with characteristic energy 2,5 keV was included as a second ionization source, and another steady-state solution was found which was compared with (1).

(3) Nighttime solution. The equilibrium solution found under (1) was used as input data. The production rate due to photoionization was reduced by 0,1% on each step; thus after 1000 seconds, Q was zero. The lower boundary condition was adjusted so that on each step the electron density at 120 km was reduced as follows:

$$N\Big|_{120\ km}^{t_o+\Delta t} = 0{,}99\ N\Big|_{120\ km}^{t_o}$$

This is a somewhat arbitrary means of adjusting the lower value, but as the continuity equation is virtually a simple linear differential equation at this height, diffusion being negligible, the electron density is independent of neighbouring values. Thus a change in the value at 120 km does not affect any other part of the profile.

Once the production rate is zero, the integration process is allowed to continue with only loss and diffusion terms in the equation, and thus a nighttime ionosphere is simulated.

(4) Nighttime conditions with precipitation. The effects of precipitated electrons were then investigated, with fluxes ranging from $1{,}1 \times 10^4$ els cm^{-2} s^{-1} to 3×10^8 els cm^{-2} s^{-1}, and characteristic energies varying between 0,5 keV and 15 keV providing additional ionization. A nighttime profile from (3) was used as input data, and the production term Q was due to precipitation only.

A flow-chart, listing and sample output of the main routine are given in Appendix B.

To produce the various solutions for different conditions, the production rate must be adjusted accordingly, together with the lower boundary value.

4.5 Production by Precipitated Electrons

The program IONS calculates the ionization rate profile for precipitated electrons. The characteristic energy of the incoming electron flux, and the exospheric temperature of the model atmosphere are specified in the input. The resultant profile is for a unit integral IDH flux of electrons with an exponential energy spectrum. Since the profile applies to a unit flux of electrons, the profile for any other flux is obtained by multiplying the original values by the required flux (see Chapter 2, section 2.3). A flow-chart and listing of this program are given in Appendix B. This program is also used to produce a "normalized" ionization rate profile (Wagstaff et al., 1976).

Details of file handling, which accesses the file directly rather than serially, can be found in the ICL computer manual (1976), Chapter 5. The specifications for most of the scientific subroutines are due to Terry (1976).

CHAPTER 5

EQUILIBRIUM AND NIGHTTIME SOLUTIONS

5.1 Initial Values

As mentioned in Chapter 2, the initial values of electron and ion densities are found by solving the continuity equation under steady-state conditions with no diffusion. This leads to a cubic equation in N, of the form

$$AN^3 + BN^2 + CN + D = 0 \qquad \text{-----} \qquad (1)$$

A, B, C, D are defined in Chapter 2, section 2.6. The values of N obtained by solving (1) are valid only at heights where diffusion may be ignored. This was assumed to be at 145 km, and values of electron density above this were taken from Stubbe (1970). The ion densities are obtained by substituting the values of N obtained from (1) into eqns (9)-(11) of Chapter 2. The starting profile is shown in Figure 1, together with part of the solution to (1).

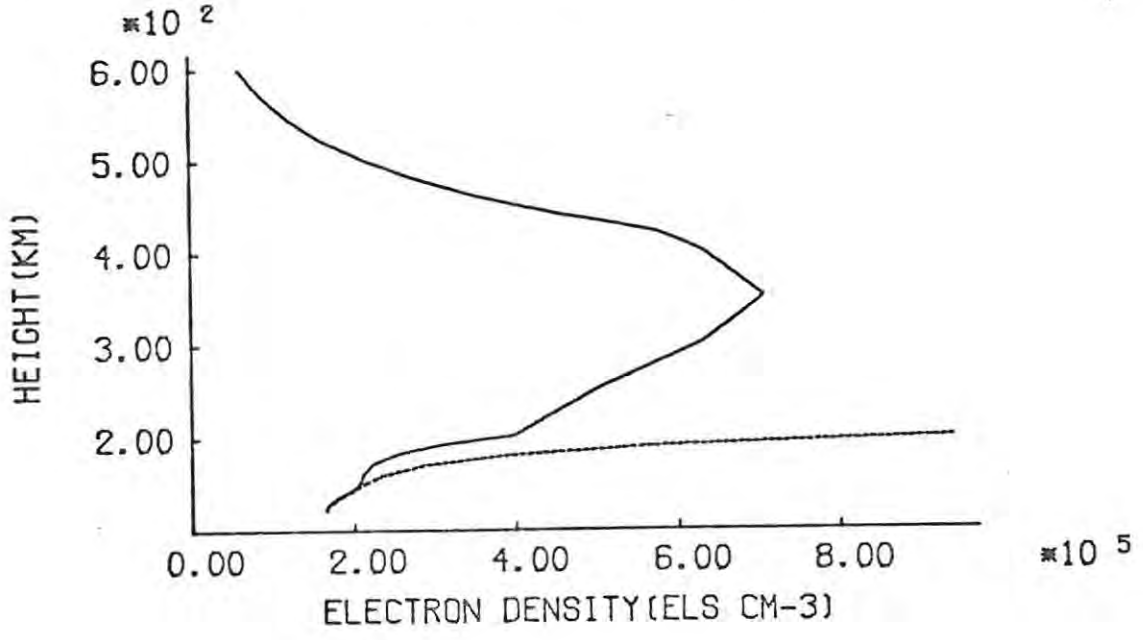

Figure 1. Initial values of electron density.

5.2 An Equilibrium Solution

It is a well-known fact that the ionosphere is relatively stable for a time around noon (Rishbeth and Garriott, 1969, pp 151-155), in that the time variation in N is small compared with other terms in the continuity equation. The initial N(h) profile of Figure 1 was put into the program NEQM, which solves the continuity equation, keeping production and transport terms constant. After 8000 seconds, the profile shown in Figure 2 was obtained. Some values of N from eqn (1) are also shown for comparison.

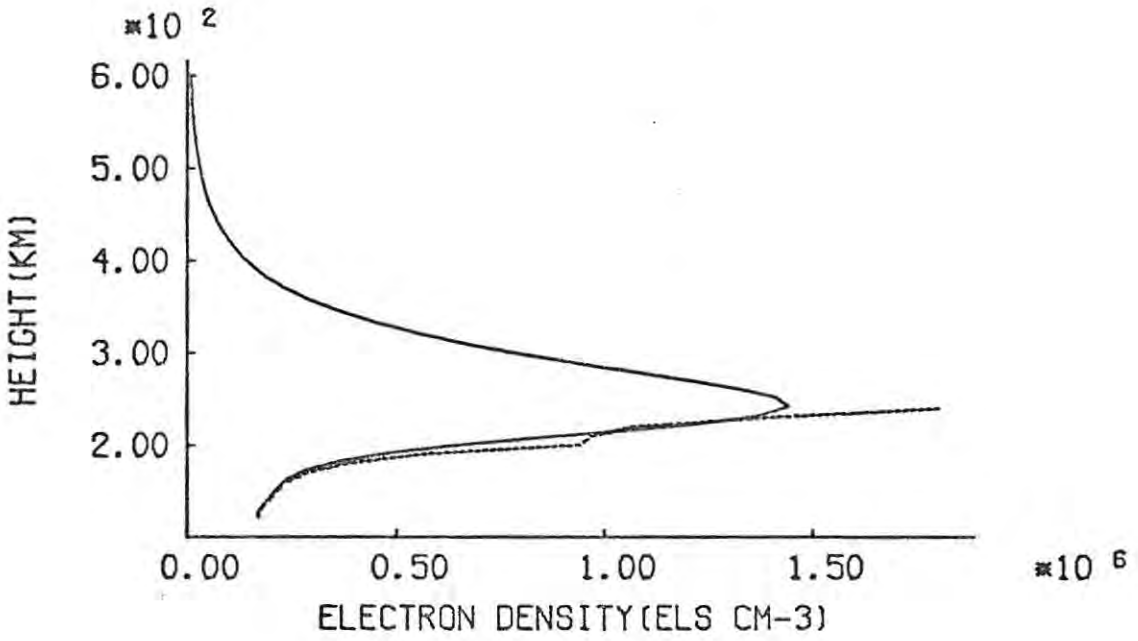

Figure 2. An equilibrium solution to the continuity equation corresponding to $\chi = 0^{o}$.

It should be noted that the point of inflection at approximately 200 km on the profile from (1) is due to computational rather than physical reasons. At this point the equation changes from being essentially a quadratic (since A is very much less than the other coefficients) to a full cubic. Thus the solution shows a slight disjointedness at the transition.

It can also be seen that diffusion is of importance only around 230 km and above, since the solution to (1), which is for a steady-state condition with no diffusion, agrees fairly well with the final solution up to this height. This indicates that below the peak, at least, the assumption of a steady-state is valid.

The equilibrium solution shows an F2 peak at 240 km, with an electron density of $1{,}445 \times 10^{6}$ els cm^{-3}. This is in approximate agreement with other authors (Briggs and Rishbeth, 1961; Stubbe, 1970; Rishbeth and Garriott, 1969, p 82), with allowances made for different conditions (model atmosphere, solar zenith angle, geomagnetic dip angle, solar activity, etc.). There is no other peak, but this may be due to the fact that $\chi = 0^{o}$, and that the lower limit is set at 120 km. The production rate shows a slight rise at 120 km. The values of Q from 140 km (height of maximum production rate) to 120 km are listed below in Table 1.

Table 1. Production rates below 140 km

Ht(km)	Production Rate ($cm^{-3}s^{-1}$)
140	$7{,}484 \times 10^{3}$
135	$7{,}405 \times 10^{3}$
130	$7{,}128 \times 10^{3}$
125	$6{,}942 \times 10^{3}$
120	$7{,}016 \times 10^{3}$

This seems to indicate that if the lower limit were reset at some lower altitude, an E-layer could be produced below 120 km. This is discussed in the final chapter.

5.3 Tests for Steady-State Condition

In order to test whether this profile (Figure 2) was indeed a steady-state solution, two further solutions were obtained by using initial N(h) profiles 10% higher and lower, respec-

tively, than that shown in Figure 1, as initial input data. These two solutions are shown below, together with the previous equilibrium solution (Figure 2).

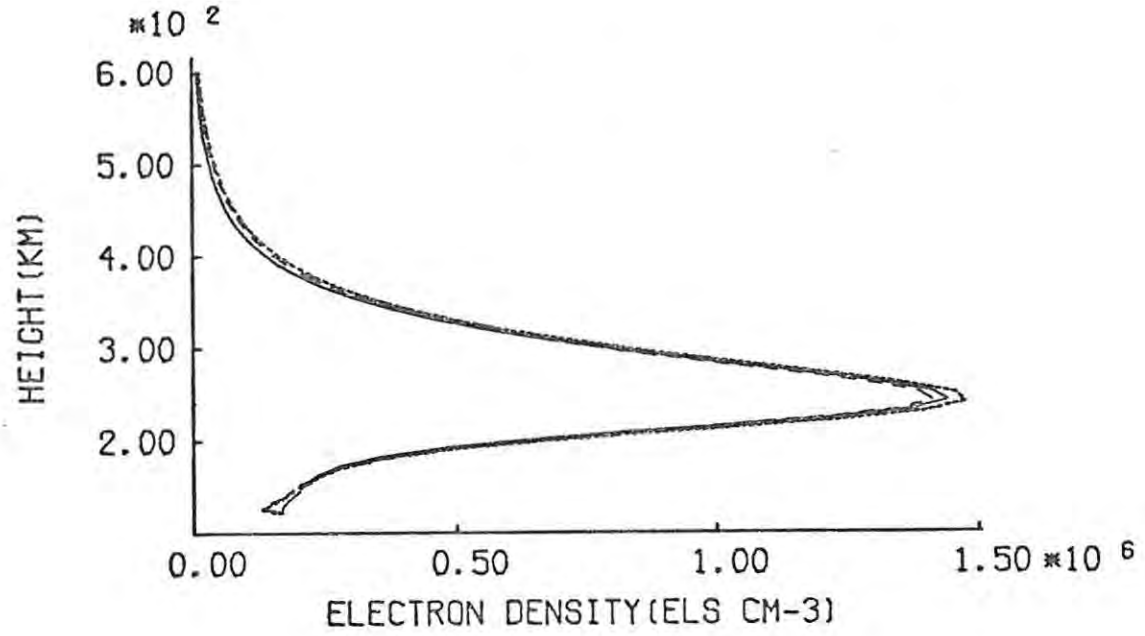

Figure 3. Comparison of final solution curves

It can be seen that the maximum variation occurs at the peak, where the profile obtained by using higher N(h) starting values has an electron density maximum of $1{,}475 \times 10^{-6}$ els cm^{-3}, while that found by using lower N(h) values gives a maximum of $1{,}413 \times 10^{6}$ els cm^{-3}. This represents a spread of approximately 2% on either side of the original solution, indicating that the steady-state solution found is acceptable, as such a small fluctuation is unlikely to be significant.

Figures 4(a)-(h) show the variation in electron density at specific heights with time, starting at t=0 with the original profile. Figures 4(a), (b) and (c) all show a maximum value as the original peak at 350 km "moves" down to its final value at 240 km.

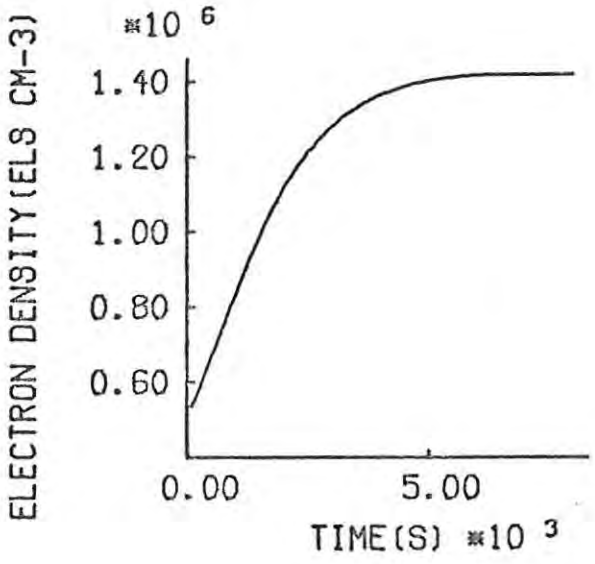

(a) N at 250 km.

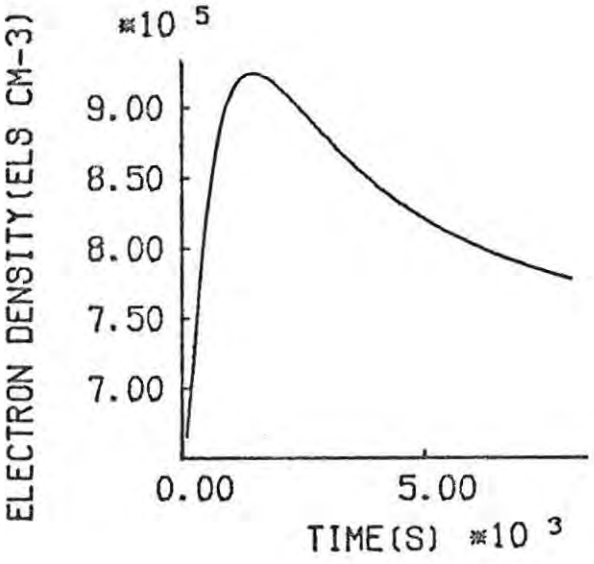

(b) N at 300 km.

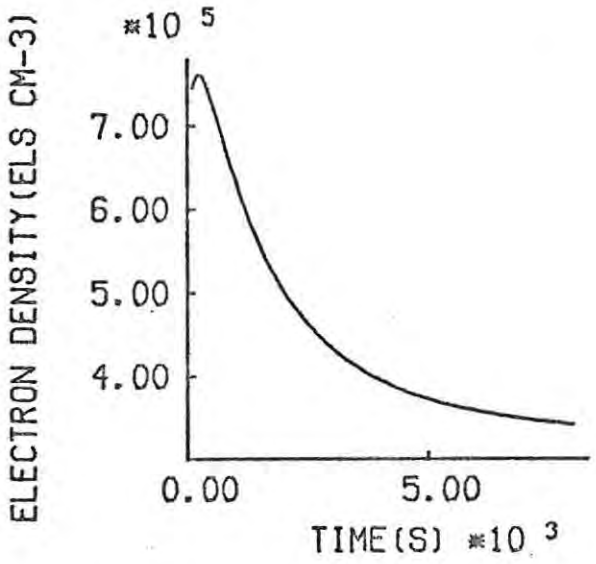

(c) N at 350 km.

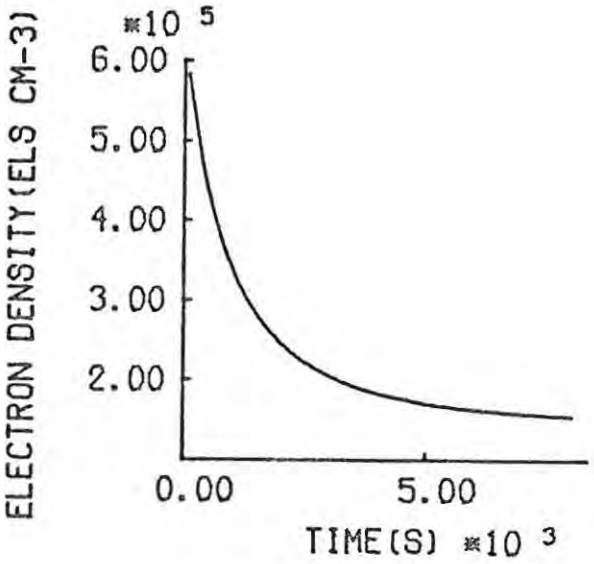

(d) N at 400 km.

Figure 4. Variation in electron density with time at specific heights.

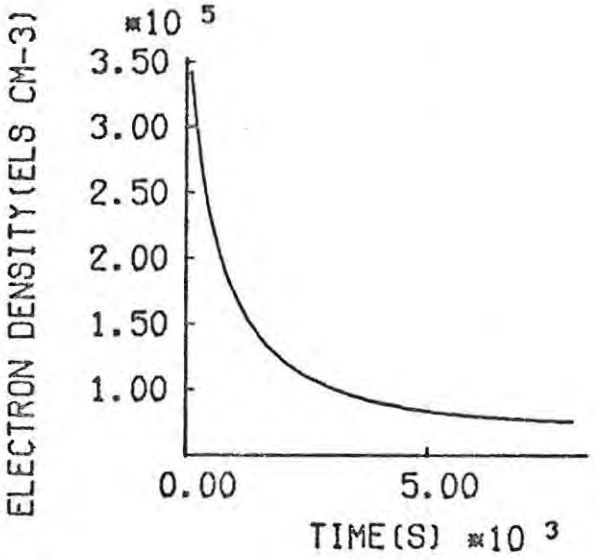

(e) N at 450 km.

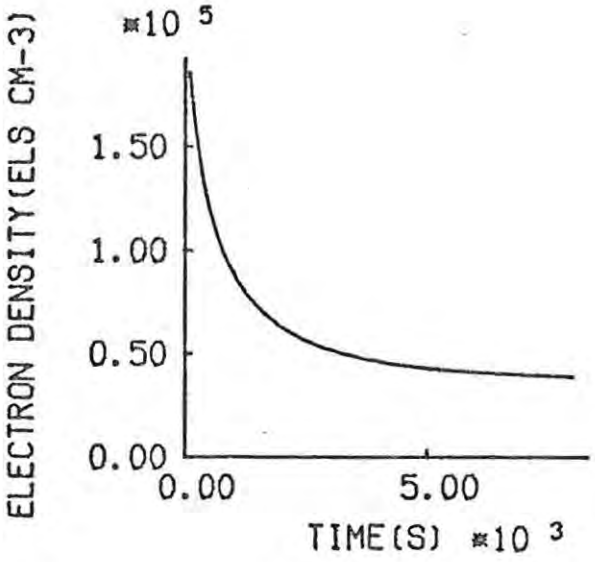

(f) N at 500 km.

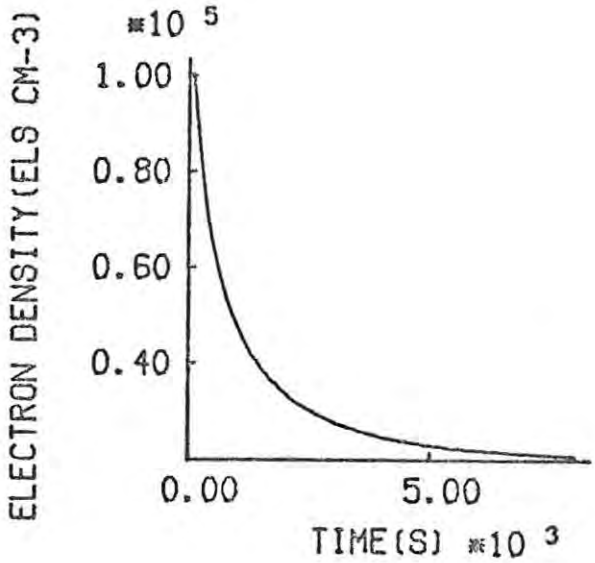

(g) N at 550 km.

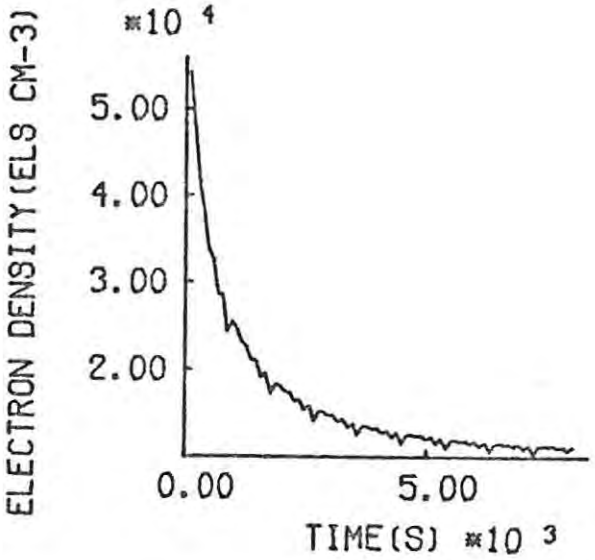

(h) N at 600 km.

Figure 4. Variation in electron density with time at specific heights.

5.4 Daytime Precipitation Effects

It would be expected that electrons with "soft" energy spectra would cause the maximum effect on ionospheric densities (Arnoldy et al., 1975), since such electrons produce peak ionization in the E- and low F-regions, where electron density is relatively low. Thus a characteristic energy of 2,5 keV was chosen, and a flux of 3×10^{7} els cm^{-2} s^{-1}. This represents a very large electron energy flux compared with those observed at present (Gledhill, 1977). The production rate due to such precipitation was included as a second ionization source in the continuity equation. The result is shown below.

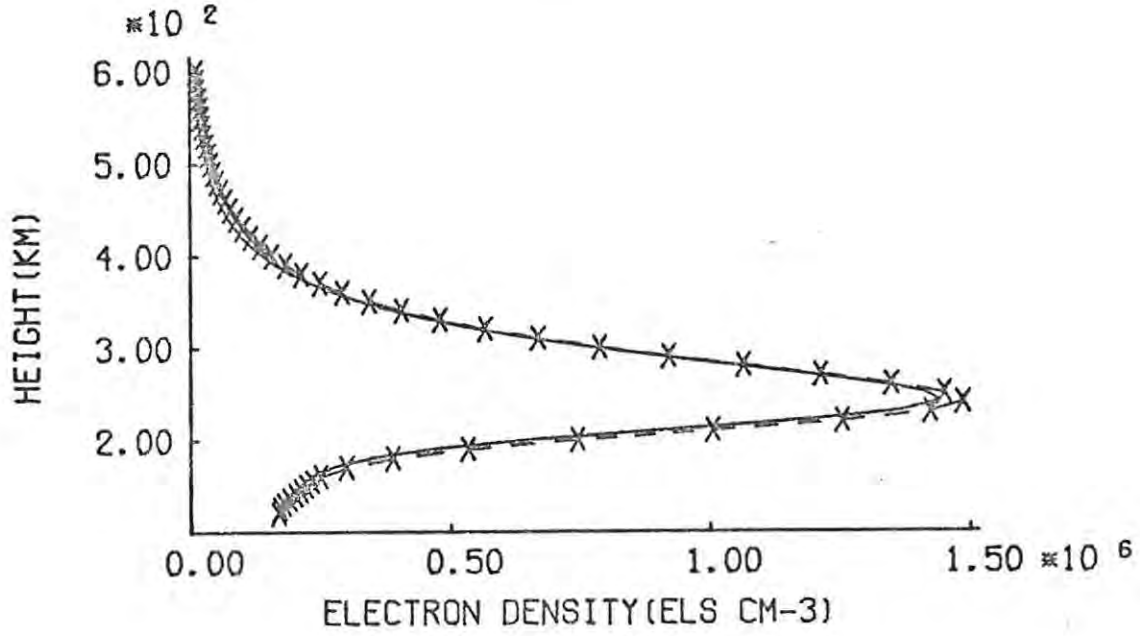

Figure 5. Equilibrium solution with and without precipitation.

It can be seen that there is no significant change in the E- or low F-regions. The maximum enhancement occurs at the peak, where the electron density rises to

1,486 x 10^6els cm^{-3} after 1000 seconds. This difference represents a variation of 2,8% of the original density. Irregularities in electron density are almost always present in the F-region, the frequency of occurrence increasing diurnally at noon, and in proportion to the electron density (Titheridge, 1968). Such fluctuations can be caused by ionospheric winds, electric fields, magnetic disturbances, hydromagnetic waves, changes in heat flux conducted from the protonosphere to the ionosphere, as well as auroral precipitation (Dixon and Forsyth, 1970; Dyson, 1969; Jones and Rishbeth, 1971). Large-scale variations in electron density due to magnetic storms for example, can be as much as 38% in mid-latitudes (Jones and Rishbeth, 1971). Small changes in heat flux could produce a variation of 5% or more (Dyson, 1969). Weak fluctuations which are usually present can cause variations of 4 x 10^6 to 2 x 10^7 els cm^{-3} (Titheridge, 1971). Evidence of such irregularities is seen in scintillation of satellite signals and spread-F traces on ionograms (Titheridge, 1968; Frihagen and Jacobsen, 1971). In view of this, it seems highly unlikely that a variation of 2,8% could be conclusively attributed to precipitation.

Thus, even with a large electron energy flux, one would not expect to see marked changes in electron densities under normal daytime conditions. This is probably due to the very much larger production rate due to photoionization (see Figures 1-5 of Chapter 6).

5.5 Nighttime Solution

As precipitation effects are not expected to be significant during the day, possible night effects were of interest. In order to produce a nighttime N(h) profile the following procedure was followed:

(1) The steady-state solution of Figure 2 was used as a starting profile.

(2) For 1000 seconds the production rate, Q, was reduced by 0,1% on each step.

(3) With Q=0, the integration process was allowed to continue for a further 4000 seconds.

The results are shown below in Figure 6, where the profiles are drawn after each 1000 seconds.

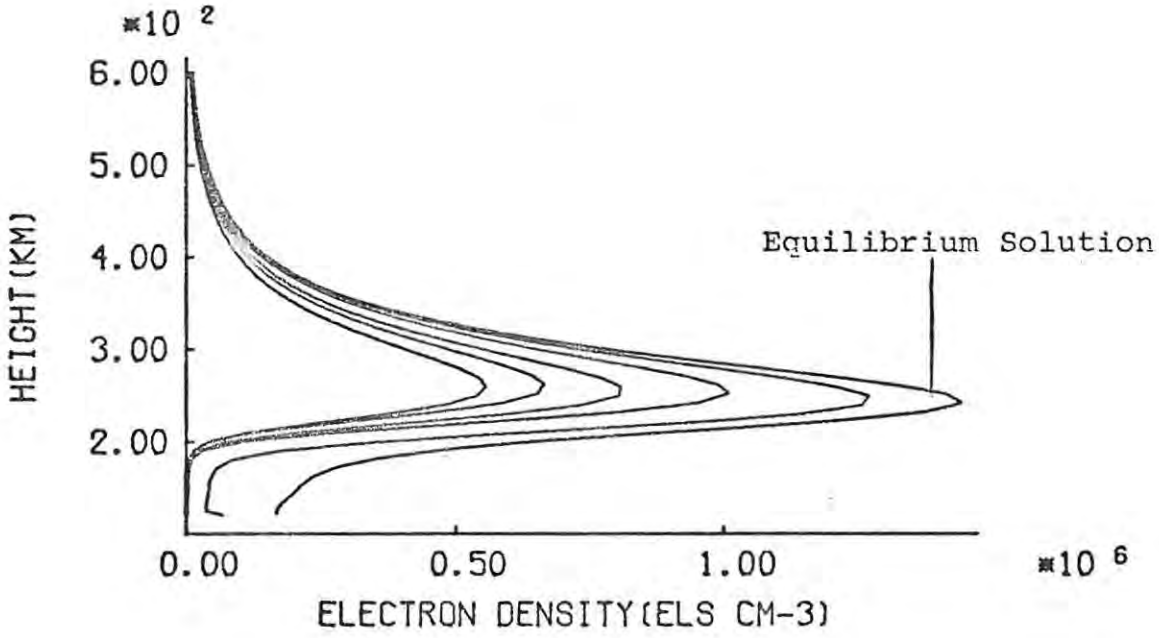

Figure 6. Equilibrium and nighttime solutions

After 5000 seconds in all, the height of maximum electron density has risen to 260 km, and the value at this height is $5,578 \times 10^5$ els cm^{-3}, compared to a peak of $1,445 \times 10^6$ els cm^{-3} at 240 km originally. As would be expected in this simple model the part of the ionosphere where electron decay is most marked is in the high E- and low F-regions.

The continuity equation for this situation where diffusion

and production terms can be neglected, may be written

$$\frac{dN}{dt} = - \alpha N^2 \qquad \text{-----} \quad (1) \quad \text{(Arnoldy et al., 1975)}$$

where α = recombination coefficient ($cm^3\ s^{-1}$).

Integrating (1), one obtains

$$\int_{N_o}^{N} \frac{dN}{N^2} = - \int_{t_o}^{t} \alpha\ dt$$

Hence $\alpha = \frac{1}{t - t_o} \left(\frac{1}{N} - \frac{1}{N_o}\right)$.

Using this, values of α were calculated from the profiles shown in Figure 6 for various heights in the ionosphere, and after different times. The results are listed in Table 2. Values quoted by Jesperson et al., (1969) and Arnoldy et al., (1975) are listed in Table 3 for comparison.

It is obvious that the recombination rate is far too high below 170 km, particularly around 125-140 km. The reasons are probably due to the following:

(a) The way in which the nighttime ionosphere is simulated. As the model atmosphere is kept constant, values of the neutral densities, temperatures and hence reaction rates, are higher than they would be in a nighttime atmosphere where the exospheric temperature would be falling.

(b) The reduction of the production rates. In this simple model, the production rate is reduced from its noon maximum to zero in 1000 seconds, a far shorter time than in the real case. This may give rise to unrealistic values of electron density, particularly about the production peak at 140 km.

Table 2. α as a function of height and time

Ht (km)	$\alpha(cm^3s^{-1})$ after 1500s	$\alpha(cm^3s^{-1})$ after 2000s	$\alpha(cm^3s^{-1})$ after 2500s	$\alpha(cm^3s^{-1})$ after 3000s	$\alpha(cm^3s^{-1})$ after 3500s	$\alpha(cm^3s^{-1})$ after 4000s	$\alpha(cm^3s^{-1})$ after 4500s	$\alpha(cm^3s^{-1})$ after 5000s
125	$3,448x10^{-7}$	$1,613x10^{-6}$	$1,020x10^{-5}$	$2,922x10^{-5}$	$5,608x10^{-5}$	$1,988x10^{-3}$	$2,176x10^{-4}$	$4,140x10^{-4}$
130	$3,104x10^{-7}$	$1,107x10^{-6}$	$8,097x10^{-6}$	$1,018x10^{-4}$	$1,430x10^{-3}$	$1,028x10^{-2}$	$3,122x10^{-2}$	$6,806x10^{-2}$
140	$2,436x10^{-7}$	$4,388x10^{-7}$	$1,168x10^{-6}$	$4,055x10^{-6}$	$1,734x10^{-5}$	$8,544x10^{-5}$	$4,352x10^{-4}$	$2,028x10^{-3}$
150	$2,097x10^{-7}$	$2,790x10^{-7}$	$4,760x10^{-7}$	$9,514x10^{-7}$	$2,123x10^{-6}$	$5,056x10^{-6}$	$1,220x10^{-5}$	$2,786x10^{-5}$
160	$1,817x10^{-7}$	$1,984x10^{-7}$	$2,502x10^{-7}$	$3,438x10^{-7}$	$4,924x10^{-7}$	$7,082x10^{-7}$	$9,900x10^{-7}$	$1,310x10^{-6}$
170	$1,440x10^{-7}$	$1,408x10^{-7}$	$1,282x10^{-7}$	$1,192x10^{-7}$	$1,166x10^{-7}$	$1,186x10^{-7}$	$1,232x10^{-7}$	$1,290x10^{-7}$
180	$7,326x10^{-8}$	$7,634x10^{-8}$	$6,064x10^{-8}$	$4,820x10^{-8}$	$4,020x10^{-8}$	$3,440x10^{-8}$	$3,100x10^{-8}$	$2,840x10^{-8}$
190	$2,051x10^{-8}$	$2,494x10^{-8}$	$2,246x10^{-8}$	$1,920x10^{-8}$	$1,682x10^{-8}$	$1,524x10^{-8}$	$1,416x10^{-8}$	$1,346x10^{-8}$
200	$4,810x10^{-9}$	$5,766x10^{-9}$	$5,960x10^{-9}$	$5,780x10^{-9}$	$5,620x10^{-9}$	$5,500x10^{-9}$	$5,420x10^{-9}$	$5,400x10^{-9}$
220	$6,180x10^{-10}$	$6,860x10^{-10}$	$7,340x10^{-10}$	$7,680x10^{-10}$	$8,020x10^{-10}$	$8,340x10^{-10}$	$8,700x10^{-10}$	$9,100x10^{-10}$
240	$2,396x10^{-10}$	$2,658x10^{-10}$	$2,920x10^{-10}$	$3,140x10^{-10}$	$3,340x10^{-10}$	$3,540x10^{-10}$	$3,780x10^{-10}$	$4,000x10^{-10}$
250	$1,920x10^{-10}$	$2,154x10^{-10}$	$2,358x10^{-10}$	$2,560x10^{-10}$	$2,760x10^{-10}$	$2,960x10^{-10}$	$3,140x10^{-10}$	$3,360x10^{-10}$

(c) The routine used to integrate the ion density equations. The simple linear segments algorithm used for the ion densities probably leads to inaccurate values of the chemical loss rate.

It should also be noted that since the temperatures and scale heights remain constant, the diffusion coefficients are unchanged. This leads to a slow decrease in electron density above the peak, since the diffusion terms increase with decreasing temperature and neutral density. The profiles thus obtained in Figure 6 are not truly representative of a nighttime ionosphere. The cost, however, in increased computer time that would result if a time-varying model were used, is prohibitive, and as order of magnitude effects only were sought, the night profile after 3000 seconds of integration was considered to be acceptable.

Table 3. Values of α

Ht(km)	$\alpha(cm^3s^{-1})$	Reference
125	$9x10^{-8}$	Jespersen et al., 1969
130	$1x10^{-7}$	Jespersen et al., 1969
135	$9,5x10^{-8}$	Jespersen et al., 1969
140	$6x10^{-8}$	Jespersen et al., 1969
140	$1,7x10^{-7}$ to $1,3x10^{-7}$	Arnoldy et al., 1975
225	$6,2x10^{-9}$ to $1,2x10^{-9}$	Arnoldy et al., 1975

CHAPTER 6

NIGHTTIME PRECIPITATION EFFECTS

6.1 Introduction

As has been noted in Chapter 5, precipitation effects are unlikely to be noticeable under normal daytime conditions, due to the large production by photoionization. At night, however, when there is no photoionization, precipitated electrons may well play some part in maintaining the nighttime ionosphere (Antonova and Ivanov-Kholodnyy, 1961), particularly in the E-region. If recombination rates are correct, and there is no alternative source of ionization, electron densities in the E-region should fall to below 10^{-2} cm^{-3} within some hours after sunset (Chen and Harris, 1971). Observations show, however, that the E-region density seldom falls below 10^{3} cm^{-3} at night, and can be as high as $10^{4} cm^{-3}$ (Strobel, 1974), which indicates a weak source of nighttime ionization or a change in rate coefficients (Yonezawa, 1968). This source of ionization could be due to scattered solar radiation (the H Lyman α and H Lyman β lines) or precipitating electrons (Morse and Rice, 1976). It is the latter which is of interest in this work.

From earlier calculations (Heighway, 1973; Huang, 1975), it seems that low energy ($E < 20$ keV) electrons would be most likely to produce ionization in the height range being considered. Although a significant correlation between high energy precipitation and E-region densities was found by Haschick and Gledhill (1974), the observations were of electrons with energies greater than 40 keV only. Thus the ionization in the E-region could well be due to the low-energy electrons not detected by the equipment. This is

confirmed by Arnoldy et al., (1975). In this study various fluxes of electrons with characteristic energies ranging from 0,5 keV to 5 keV were included as ionization sources in the continuity equation for a nighttime ionosphere. Finally, based on satellite data collected over the Anomaly, a flux of $1,1 \times 10^4$ els cm^{-2} s^{-1}, with characteristic energy 15 keV was included. (Gledhill, 1977).

Some considerable time was spent on developing the methods finally used in solving the equations, so as to produce stable results in as economical a way as possible. The program was adjusted until the results produced were reasonably reliable. This was considered to be important as it enabled us to distinguish between genuine physical effects and spurious ones generated by the computation. The program was then used to calculate some preliminary results for fluxes of interest.

6.2 Production Rates

The production rate for photoionization was calculated using program INIT. The solar zenith angle is 0°, i.e. a noon maximum production rate. The production due to precipitation was found using program IONS. The exospheric temperatures are all set to 700 K, and the characteristic energies were 0,5, 2,5, 5,0 and 15 keV. Figures 1-5 show the production rate profiles for photoionization and precipitation. The latter are shown for a unit integral IDH flux. It can be seen from Figures 2-5 that the profiles are strongly peaked, this effect becoming more marked as the energy increases. Thus one would expect that the effects of a low-energy electron flux would be seen

(a) relatively high in the atmosphere, since the peak production rate occurs higher than for a high-energy electron flux, and

(b) over a wider range of heights since the production is

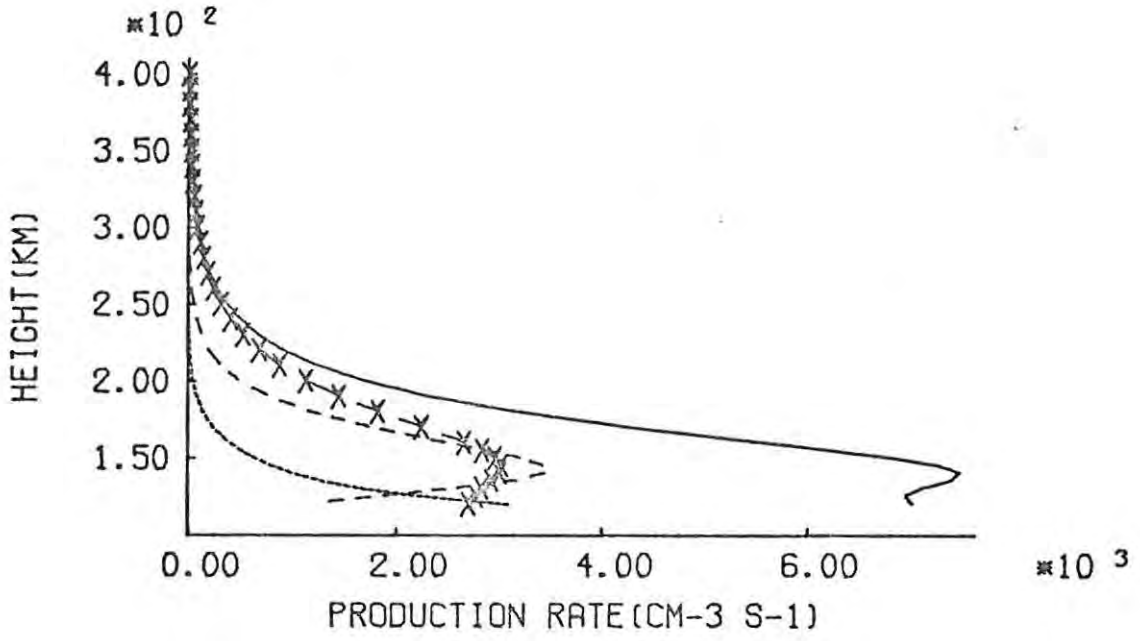

Figure 1. Production rate due to photoionization for solar zenith angle $\chi=0^{o}$.
(.....$Q(O_2^+)$; xxxxx$Q(O^+)$; -----$Q(N_2^+)$; ——— Q_{total})

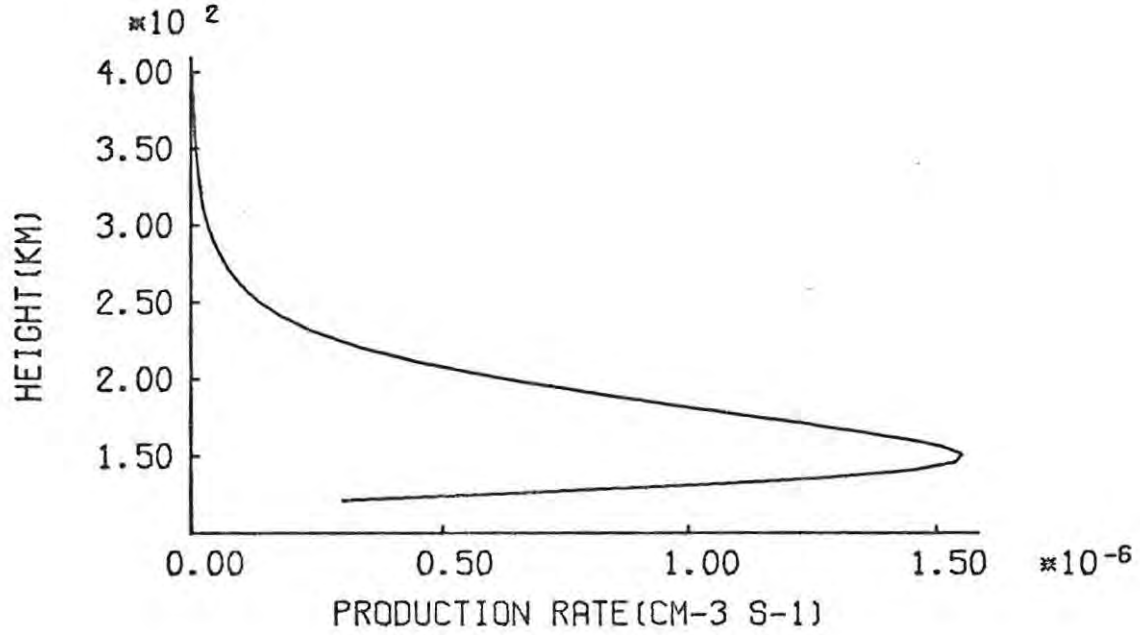

Figure 2. Production rate due to unit integral IDH flux of precipitated electrons.
E_o = 0,5 keV

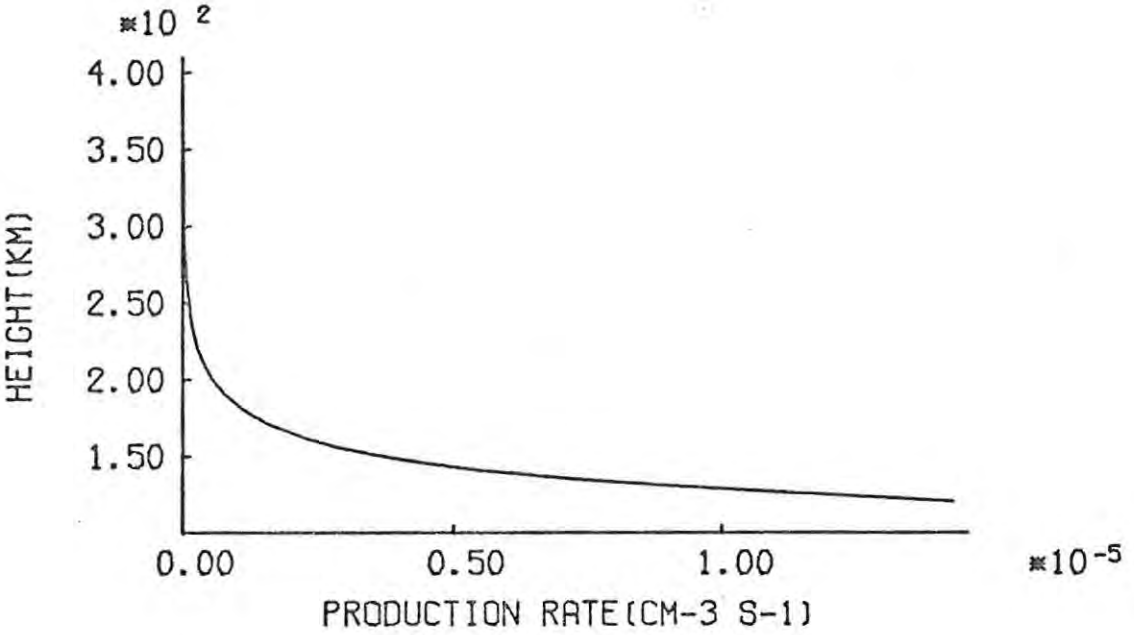

Figure 3. Production rate due to unit integral IDH flux of precipitated electrons.

E_o = 2,5 keV

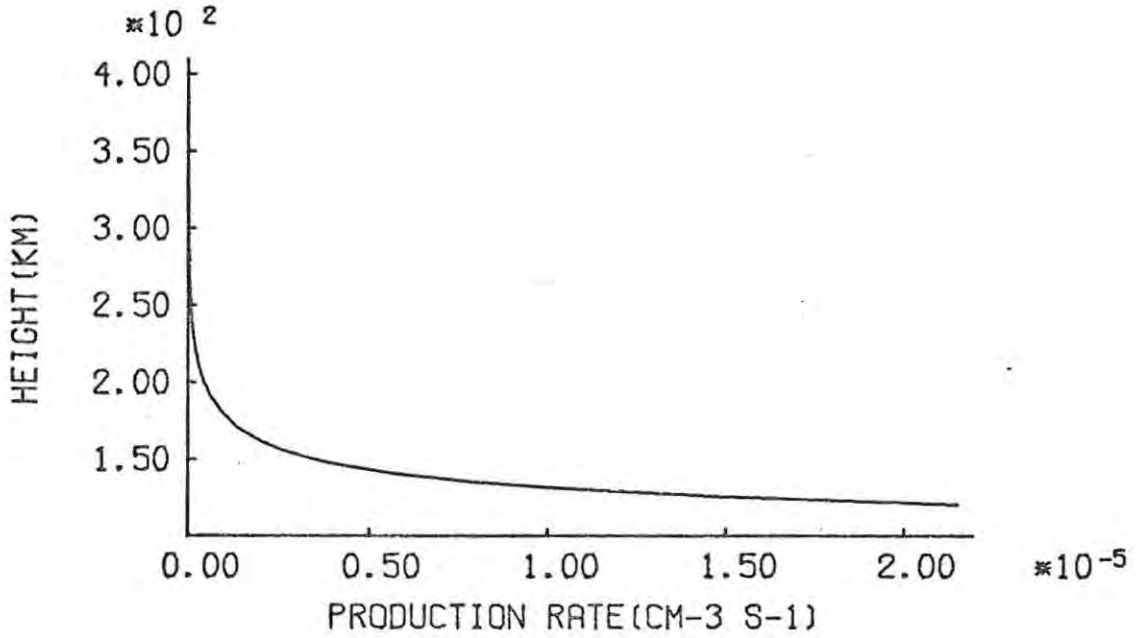

Figure 4. Production rate due to unit integral IDH flux of precipitated electrons.

E_o = 5,0 keV

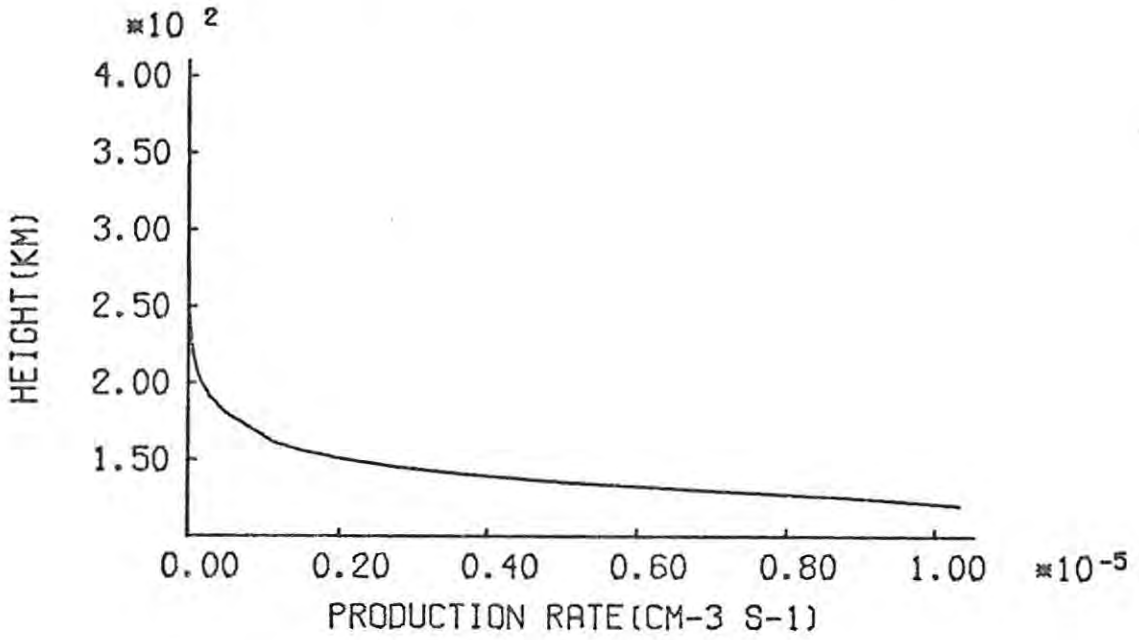

Figure 5. Production rate due to unit integral IDH flux of precipitated electrons.
E_o = 15,0 keV

more evenly spread over a range.

Thus a flux of low-energy electrons should produce a fairly thick layer of diffuse ionization relatively high in the ionosphere. High-energy fluxes would be expected to produce thin layers of dense ionization at lower altitudes.

The maximum production and the height at which this occurs are listed in Table 1.

It can be seen that with increasing energy, the Q(h) profile for precipitated electrons has a greater maximum value, and that this occurs lower down in the atmosphere. Even with the maximum flux used in these calculations,
3×10^8 els cm^{-2} s^{-1}, characteristic energy 0,5 keV,
the maximum production rate is $4{,}668 \times 10^2$ els cm^{-3} s^{-1},
only 6,23% of that by photoionization at noon. The densities

Table 1. Features of Q(h) profiles

Production Mechanism	Characteristic Energy (keV)	Height of maximum (km)	Max. Prod. Rate (els cm^{-3} s^{-1})
Photoionization	-	140	$7,484 \times 10^{3}$
Precipitated electrons	0,5	148,86	$1,556 \times 10^{-6}$
Precipitated electrons	2,5	115,05	$1,590 \times 10^{-5}$
Precipitated electrons	5,0	106,88	$4,032 \times 10^{-5}$
Precipitated electrons	15,0	96,57	$1,464 \times 10^{-4}$

in the lower part of the ionosphere at night, however, are so low that even a small production rate could be significant.

6.3 Precipitation Effects

The production rates due to fluxes of electrons with characteristic energy as shown in Figures 2-5 were included in the continuity equation. The starting profile was taken from those produced by the nighttime ionosphere simulation, as discussed in Chapter 5. The graphs below show the initial nighttime profile, with subsequent profiles after the production rate has been introduced. These are drawn at 500 second intervals, and are shown up to 600 km, and, on a larger scale, up to 200 km so that any change in electron density can be clearly seen.

6.4 Discussion of Results

The main features of Figures 6-12 are listed in Table 2.

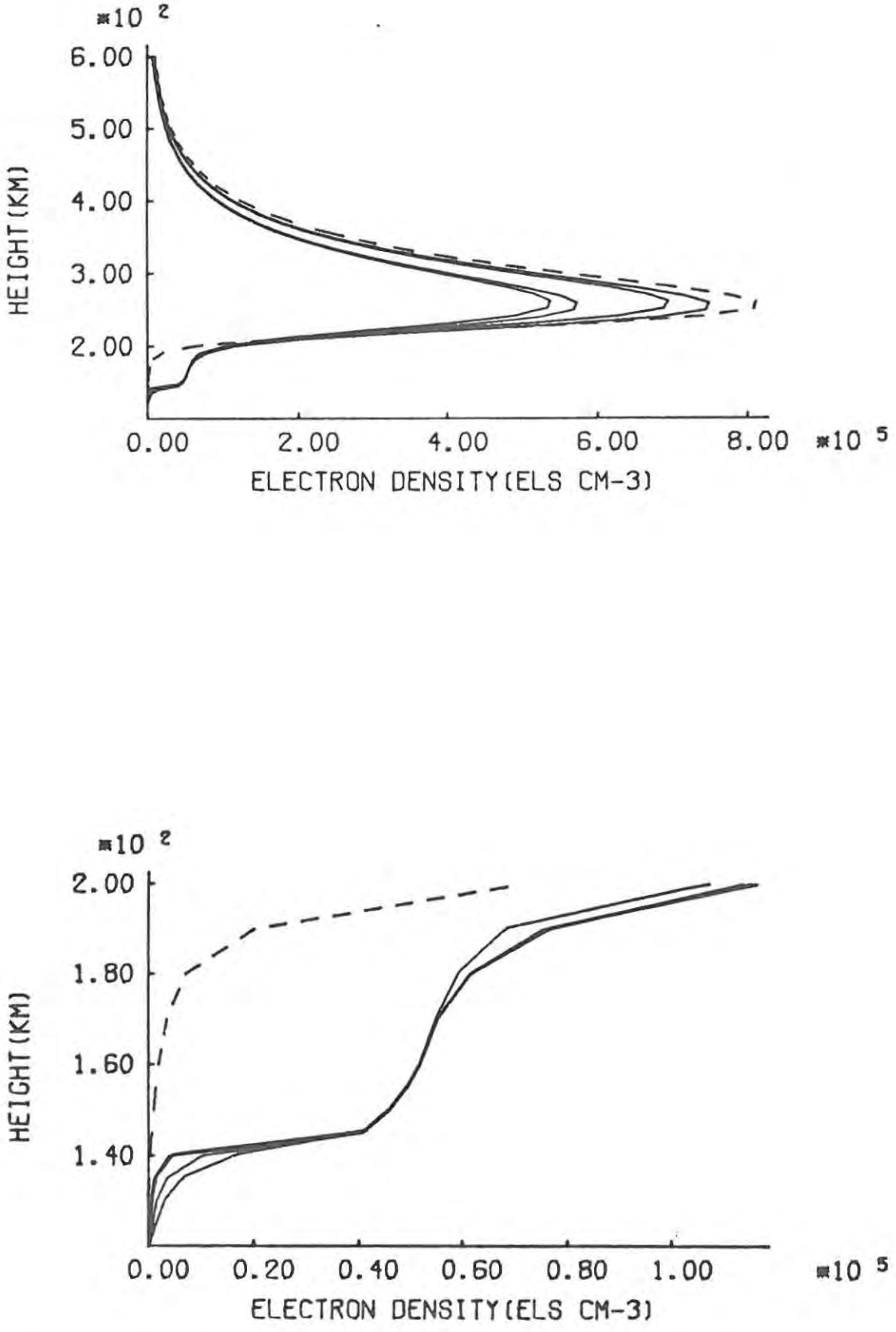

Figure 6. Resultant nighttime profiles. $J=3x10^{8}exp(-E/0,5)$ (----- original night profile; ——— subsequent profiles).

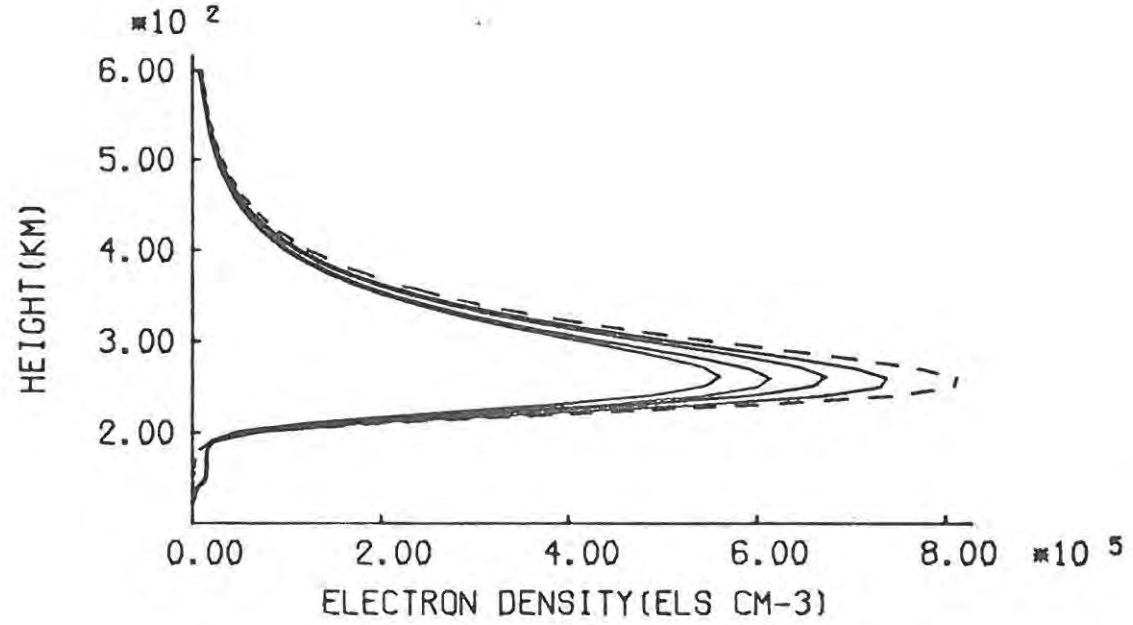

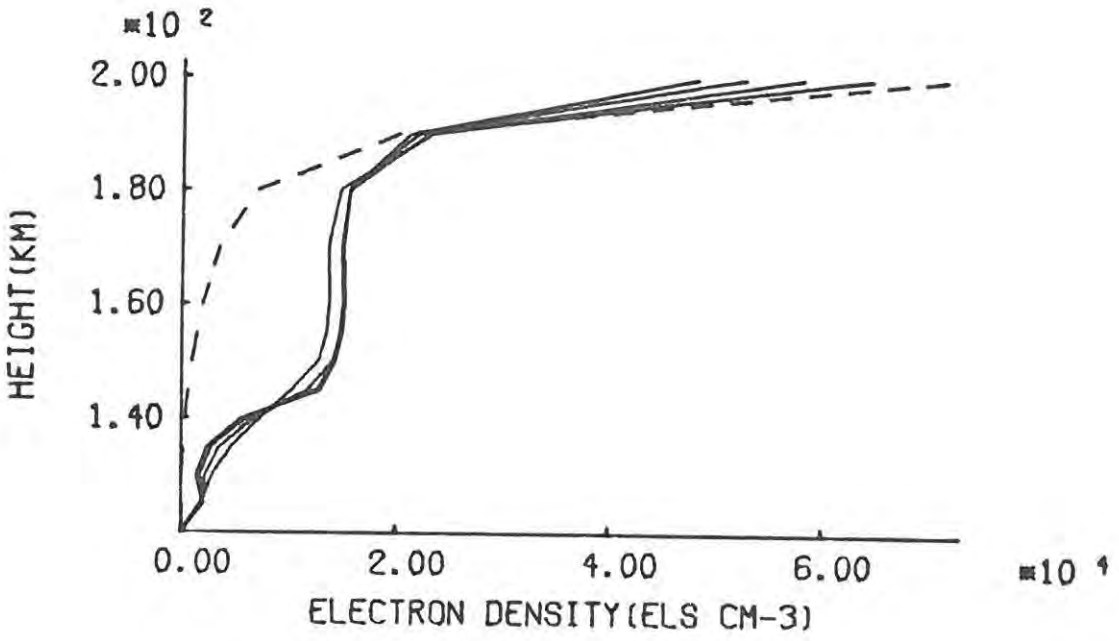

Figure 7. Resultant nighttime profiles. $J=3x10^{7}exp(-E/0,5)$ (----- original night profile; ——— subsequent profiles).

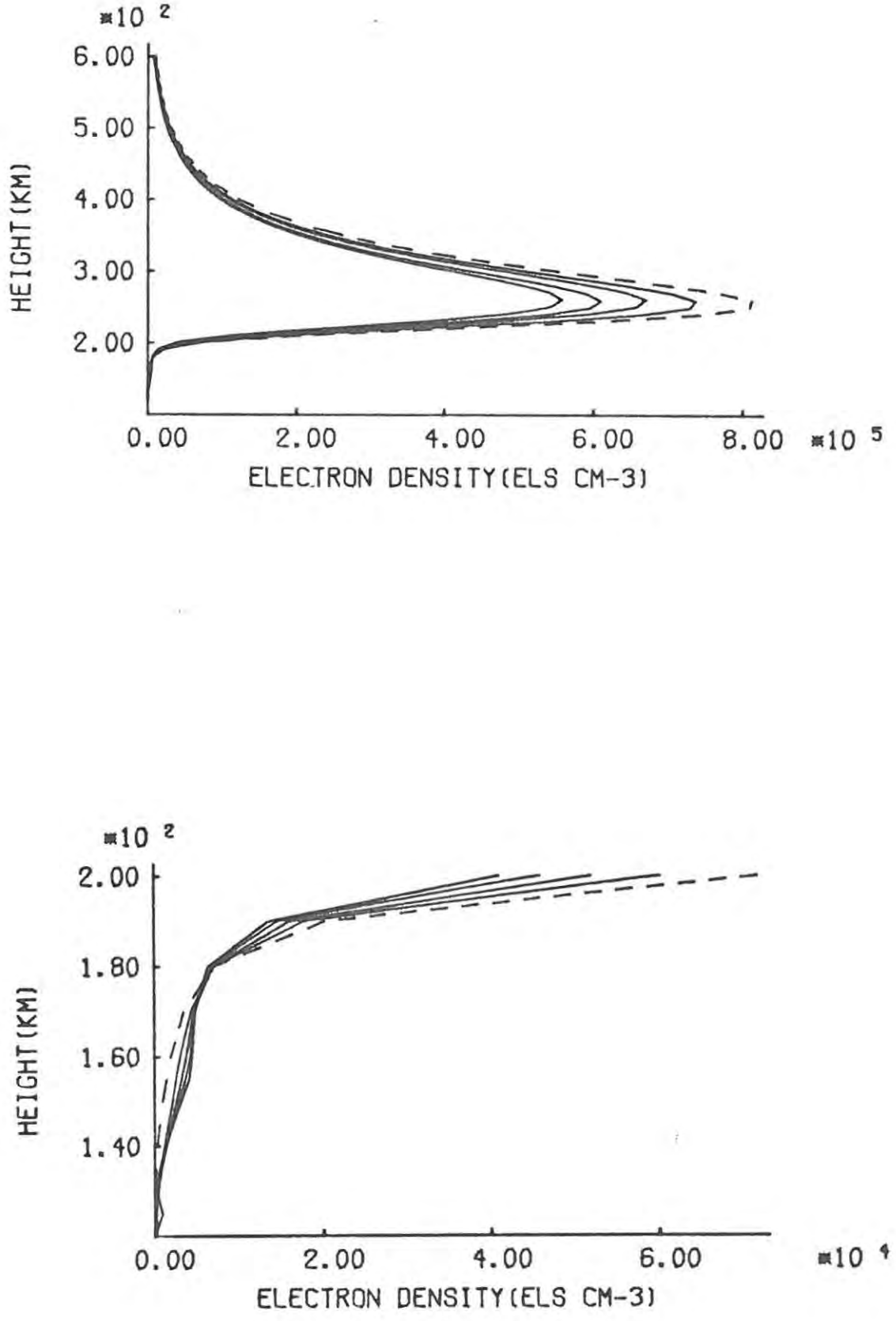

Figure 8. Resultant nighttime profiles. $J=3x10^{6}exp(-E/0,5)$ (----- original night profile; ——— subsequent profiles).

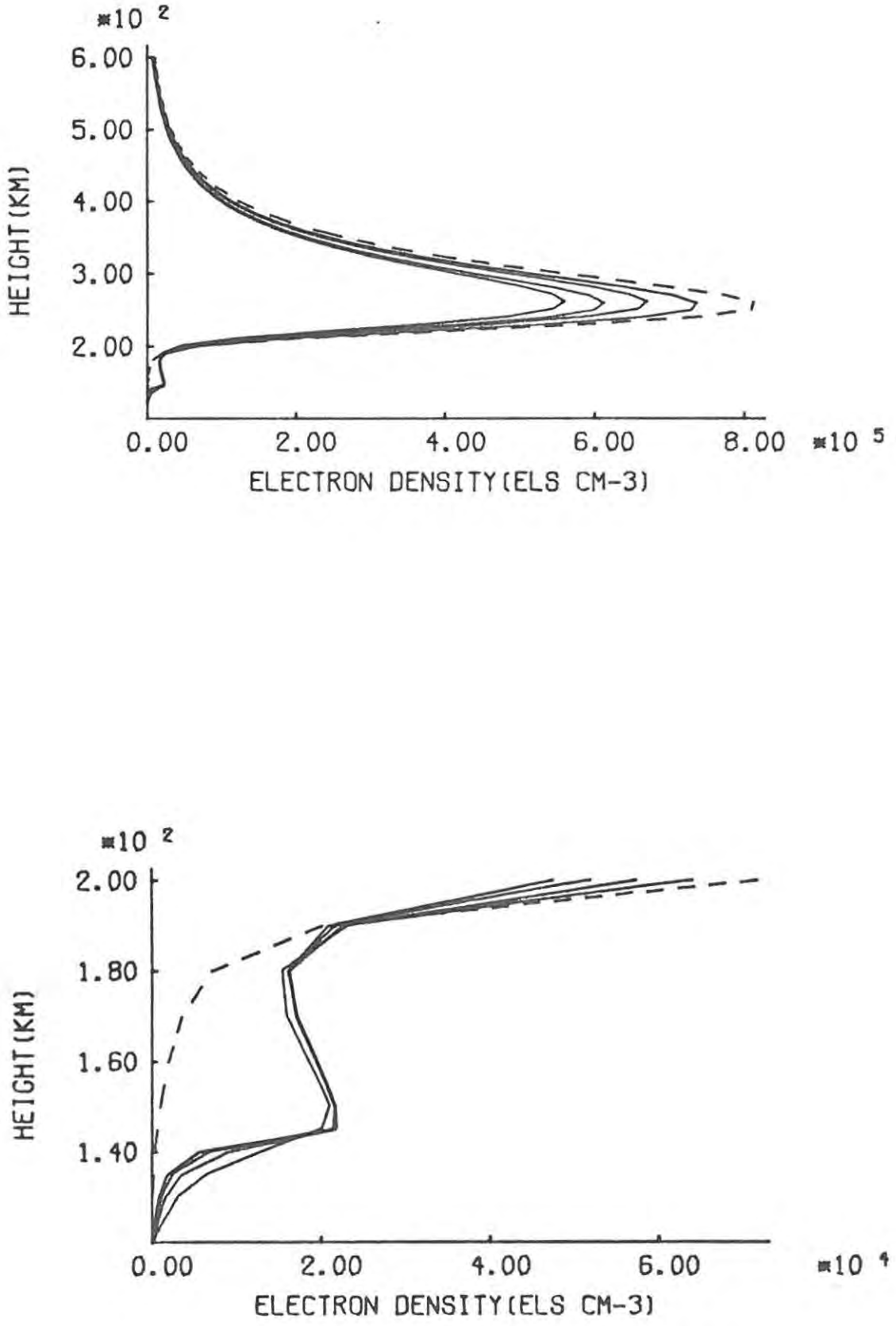

Figure 9. Resultant nighttime profiles. $J=3x10^{7}exp(-E/2,5)$. (----- original night profile; ——— subsequent profiles).

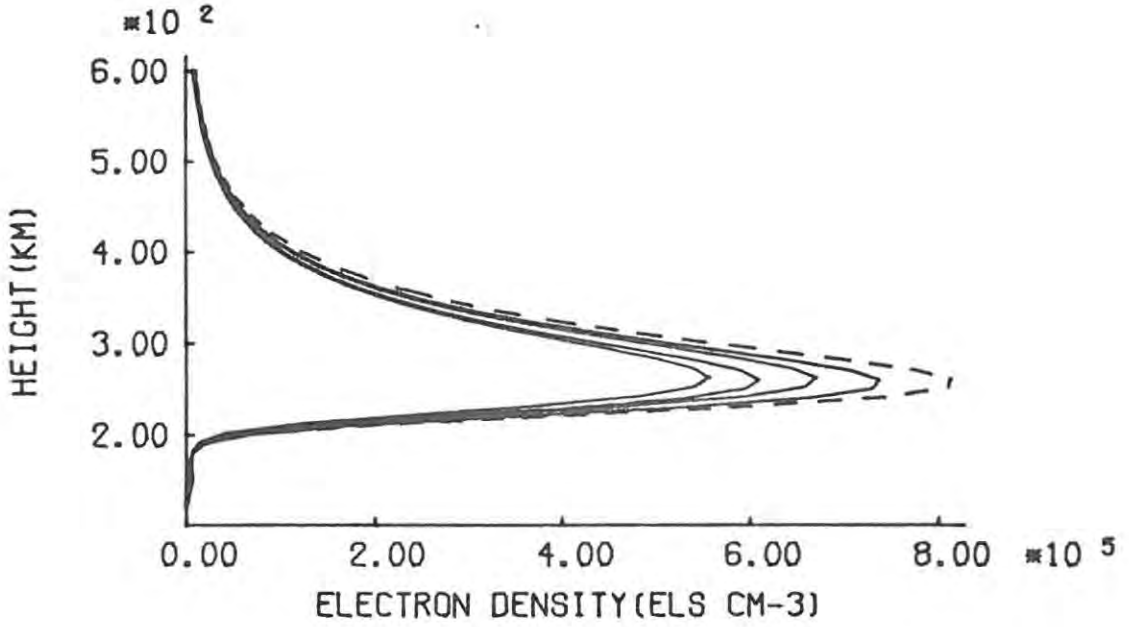

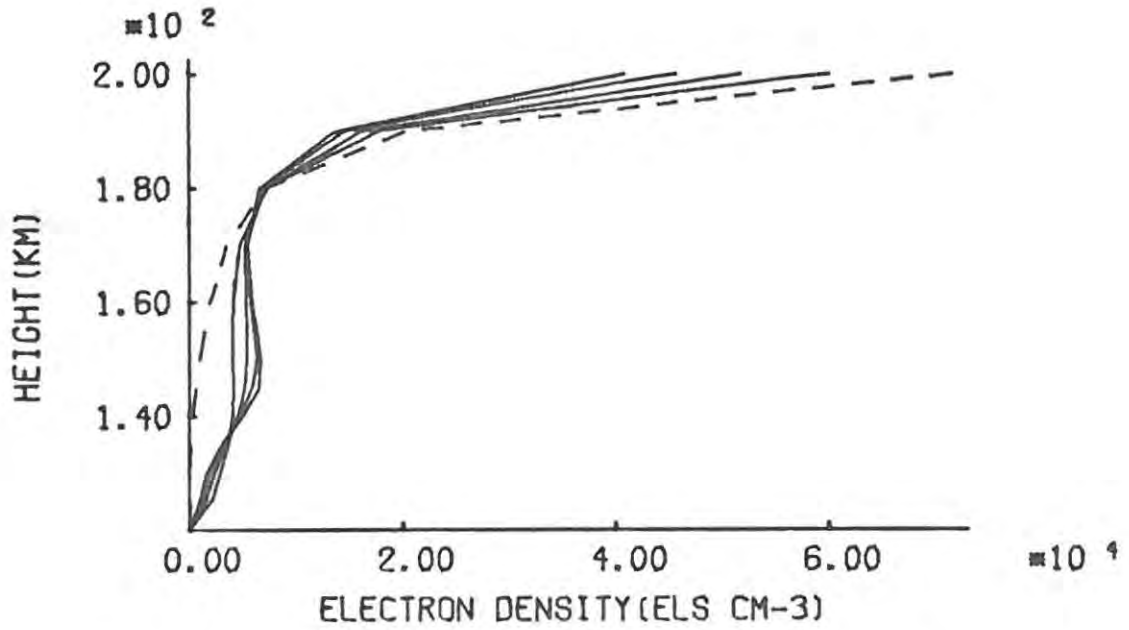

Figure 10. Resultant nighttime profiles. $J=3x10^{6}exp(-E/2,5)$ (----- original night profile; ——— subsequent profiles).

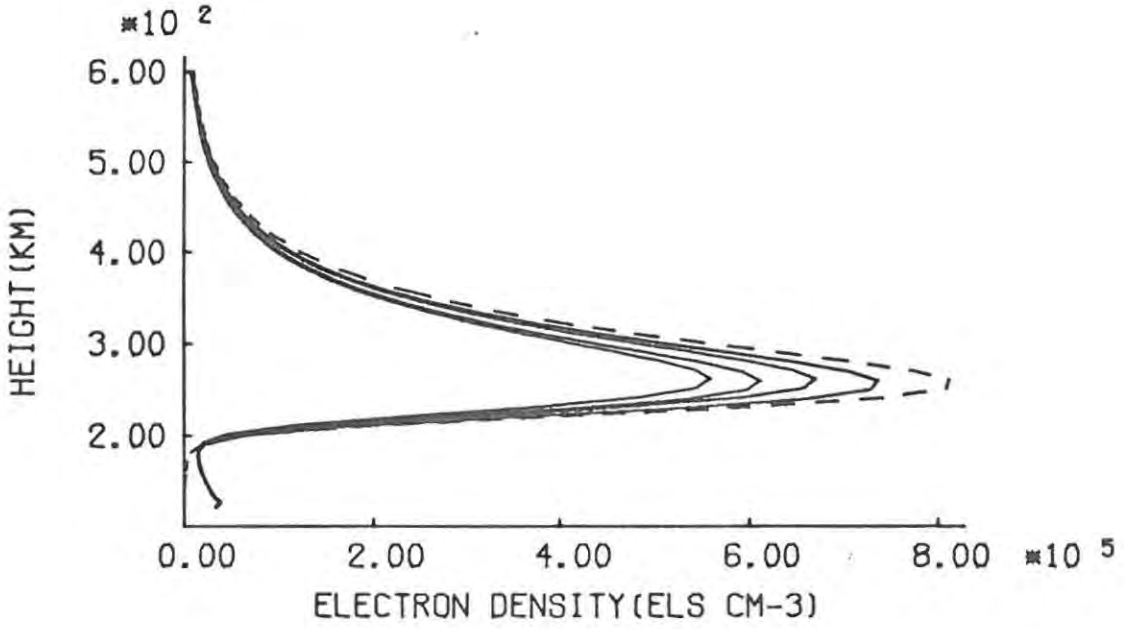

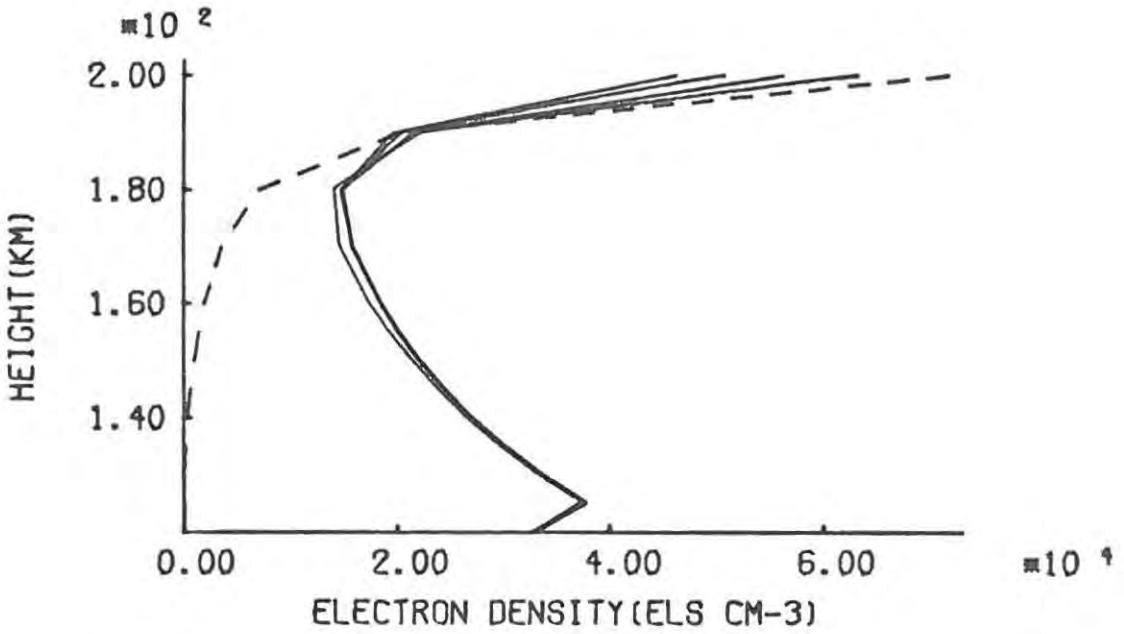

Figure 11. Resultant nighttime profiles. $J=3x10^{7}exp(-E/5,0)$. (----- original night profile; ——— subsequent profiles).

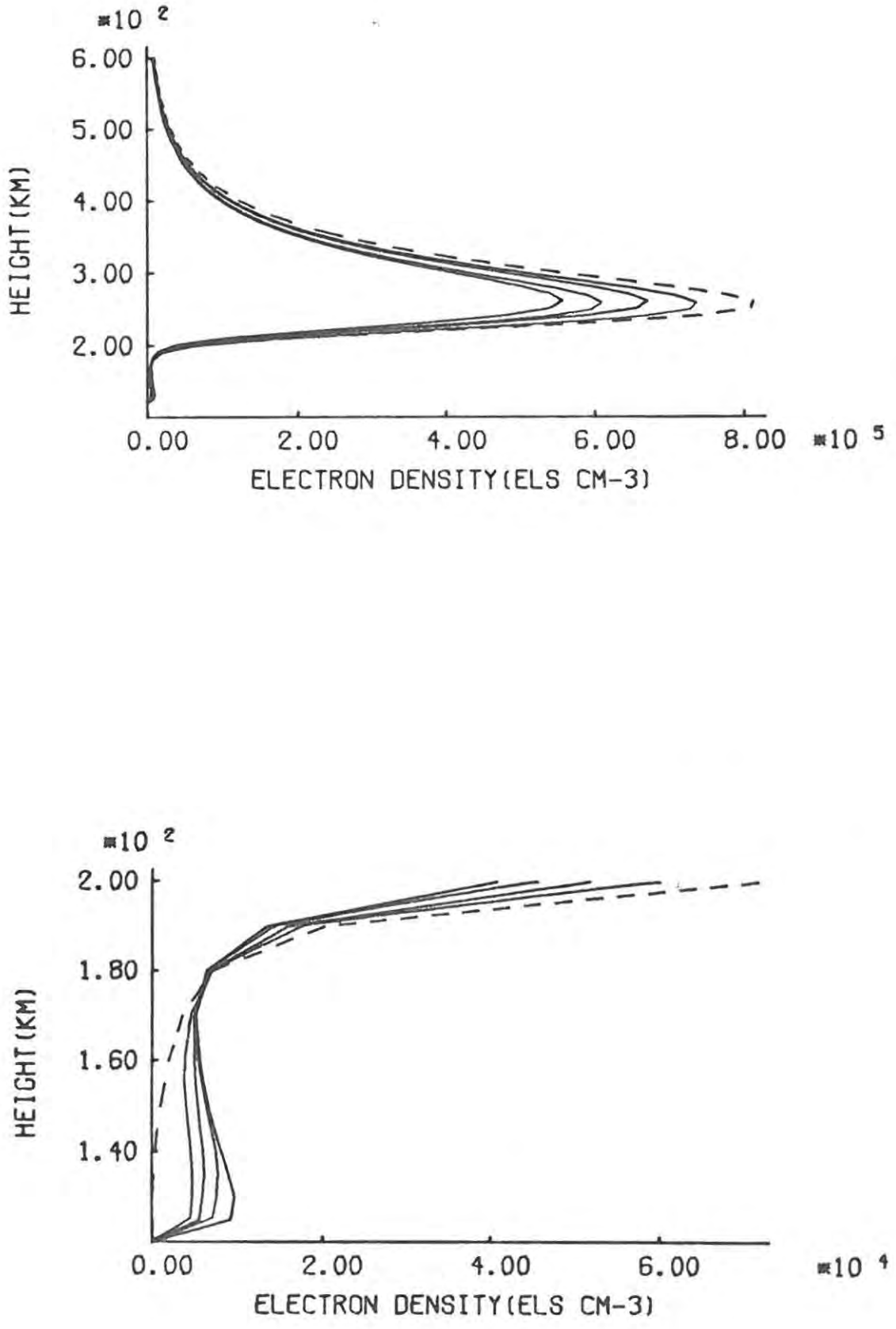

Figure 12. Resultant nighttime profiles. $J=3x10^{6}exp(-E/5,0)$. (----- original night profile; ——— subsequent profiles).

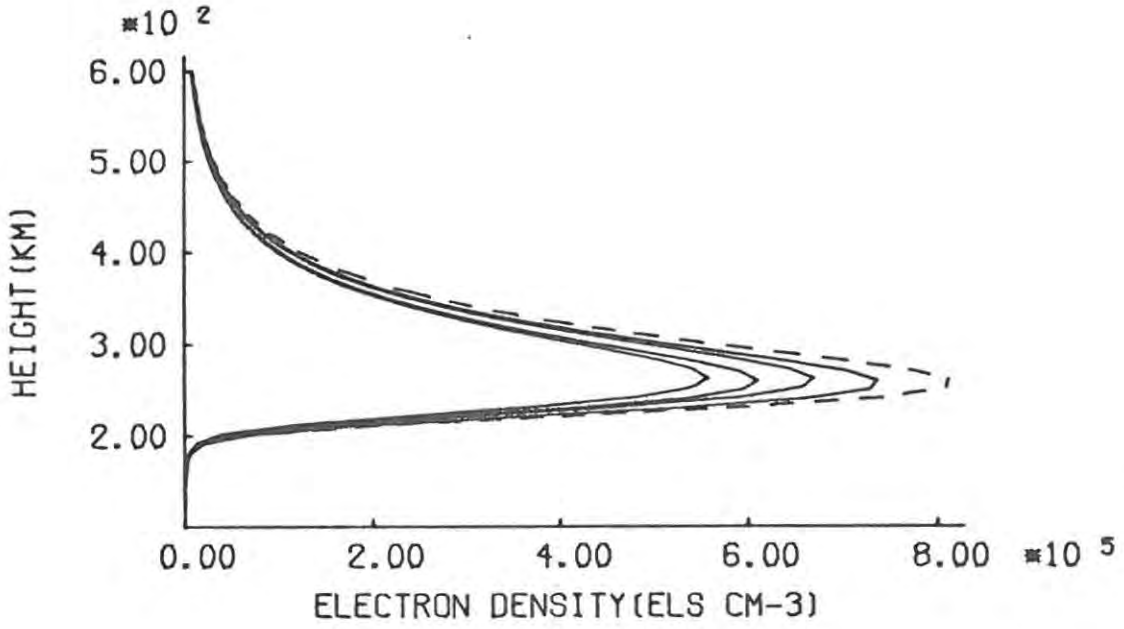

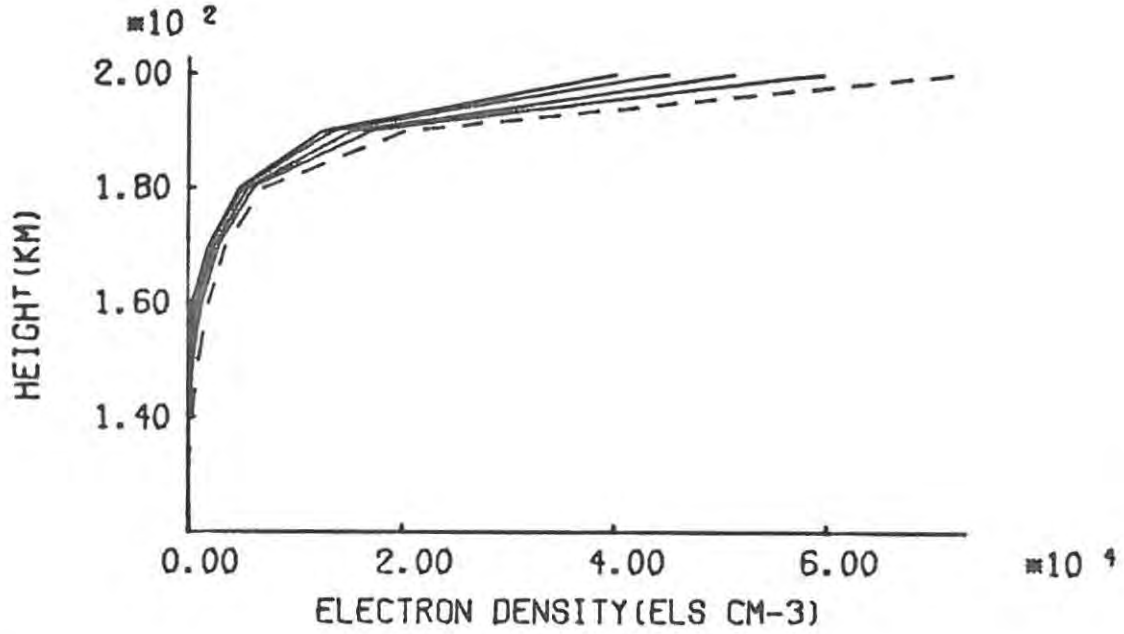

Figure 13. Resultant nighttime profiles. $J=1,1x10^{4}exp(-E/15,0)$. (----- original night profile; ——— subsequent profiles).

Table 2. Principal features of Figures 6-12

Figure	E_o (keV)	Flux (els $cm^{-2}s^{-1}$)	Feature	Height (km)	Electron Density (cm^{-3})
6	0,5	$3x10^8$	Point of inflection	145	$4,085x10^4$
7	0,5	$3x10^7$	Point of inflection	145	$1,295x10^4$
8	0,5	$3x10^6$	Point of inflection	155	$4,149x10^3$
9	2,5	$3x10^7$	Local maximum	145	$2,177x10^4$
10	2,5	$3x10^6$	Local maximum	150	$6,625x10^3$
11	5,0	$3x10^7$	Local maximum	125	$3,775x10^4$
12	5,0	$3x10^6$	Local maximum	130	$9,635x10^3$

From the above it can be seen that effects are visible in the lower atmosphere, as would be expected since the production rate profiles for the above spectra have maximum values below 150 km (see Table 1). The higher fluxes ($3x10^8$ els cm^{-2} s^{-1}) may be too high for the Anomaly (see later), but as reliable values are not available, the results are included.

The heights of the layers formed by the fluxes of electrons with energies less than 5 keV are somewhat higher than would be expected, values below 130 km for particle-E being usually observed (Chen and Harris, 1971). This may indicate that the characteristic energies chosen are too low, or that interactions between low energy electrons and the ionosphere are more complicated than has been assumed (Banks et al., 1974).

Even with the lowest fluxes used ($3x10^6$ els cm^{-2} s^{-1}), there

is some enhancement of electron density. In addition to the main features tabulated above, the additional ionization slows down the rate of decay of the nighttime profile, as can be seen from Figures 6-12. If such fluxes are present over the Anomaly, precipitation effects in the E-region may well be detectable.

It can be seen that the height of the local maximum or point of inflection depends on the flux as well as the characteristic energy. In general an increase in flux moves the layer downwards (see Table 1). An increase of an order of magnitude in the flux also produces an electron density maximum between three and four times greater than that with the lower flux value. If the loss rate is assumed to be proportional to N^2, then one would expect the increased electron density to be $\sqrt{10}$ times the lower value. The full range of energies and fluxes has still to be investigated, however, before conclusions may reliably be drawn.

The results of the inclusion of precipitation as detected by the Injun 5 satellite shows virtually no effect on electron density, beyond some slowing down of the rate of electron decay in the lower atmosphere (see Figure 13). The combination of a low flux value and high characteristic energy result in negligible ionization being produced in the height range under consideration. Thus, one would not expect to be able to detect evidence of such ionization, even at night, if this flux is representative. Further satellite data seem to indicate, however, that the values recorded by Injun 5 may be a lower limit to precipitation fluxes. The Atmospheric Explorer C satellite observed electron energy fluxes of the order of 10^{-3} ergs cm^{-2} s^{-1} over the Anomaly (Torr, 1977). If the characteristic energy is 10 keV, then the flux becomes 6×10^4 els cm^{-2} s^{-1}; similarly if an energy of 0,5 keV is considered, the flux is $1{,}2 \times 10^6$ els cm^{-2} s^{-1}, which is of the same order of magnitude as that used in Figure 8. Values observed by the DAPP satellite over the

great circle path between SANAE and Grahamstown indicate much higher fluxes of the order of 10^7 els cm^{-2} s^{-1} (Rash, 1977). It is uncertain whether these values have been corrected for background, so that they may be regarded as upper limits to actual precipitation. Until more data become available for the Anomaly, it is impossible to predict on purely theoretical grounds whether electron precipitation will be a significant source of ionization in this height range or not.

If further observations confirm the lower values as recorded by Injun 5, it may be necessary to revise the computational model used here. The lower boundary will in any case have to be extended down to 90 km in order to show the effects due to higher-energy electrons. From previous calculations (Wagstaff et al., 1976) the lower limit of 90 km would include peak ionization rates for electrons with energies up to 27 keV (height of maximum is 91,27 km). As has been noted earlier (Chapter 5, Table 1) the production by photoionization shows a slight increase at 120 km, which may indicate the presence of an E-layer below this level. The behaviour of this in a nighttime situation with a particle flux should prove interesting. The possibilities of this and further refinements of this preliminary treatment are discussed in the following chapter.

On the computational side, there appears to be a limit to the flux that can be introduced into the program. This is approximately 10^8 els cm^{-2} s^{-1}, and is probably due to the way in which the production rate is included since Q is simply set to the value due to precipitation. The resulting electron densities oscillate wildly, particularly in the region where production is high. It is most likely that, if the production rate were increased more gradually, in a fashion similar to the reduction of photoionization, these numerical difficulties could be removed. Much the same kind of instability is generated if the daytime production rate is

suddenly removed. In actual cases of electron precipitation the onset can be gradual or sudden, and both possibilities should be investigated. To see the permanent effect, however, only a steady-state solution is needed so that production could be gradually introduced as suggested above.

CHAPTER 7

CONCLUSION

7.1 Summary

The results of the work completed can be briefly summed up as follows:

(1) A fast and reliable method of solving the continuity equation for electrons and the more important of the ion density equations has been developed.

(2) This method has been used to find a daytime equilibrium electron density profile, which has proved to be stable and acceptable when compared with actual conditions.

(3) A large electron energy flux has been used as an additional source of daytime ionization, and there is little effect.

(4) A reasonable nighttime profile has been found by a simple reduction of photoionization to zero.

(5) Various fluxes of precipitated electrons have been used as nighttime ionization sources. The results are inconclusive in so far as this application to the Anomaly is concerned. If fluxes are sufficiently high (of the order of 10^6 els $cm^{-2}s^{-1}$), then there is a definite change in electron density which may be detectable. If further measurements show that actual fluxes are lower than has been assumed, there may be no significant effect in the higher parts of the E-region.

Before the argument regarding the importance of precipitation on the ambient nighttime densities can be concluded, more observations are needed. Values of fluxes and energies are

necessary, as well as the type of energy spectrum actually observed. The type assumed throughout this work has been of the form $J=J_o \exp(-E/E_o)$, but there seems to be evidence of a power-law spectrum $J=J_o E^{-\gamma}$ where γ is a constant, called the spectral index by many workers, characterising the particular spectrum. (Gledhill, 1977; Rash, 1977).

Various authors doubt the validity of particle fluxes as a significant factor when calculating N(h) profiles (e.g. Morse and Rice, 1976), preferring other possibilities such as wind shears (Chen and Harris, 1971), anomalous recombination (Yonezawa, 1968) or scattered solar radiation (Morse and Rice, 1976). In order to evaluate precipitation aginst these factors an accurate assessment of fluxes must be obtained. It will also be necessary to divide particle effects into two main groups: those that are caused by a continuous influx of precipitated electrons, e.g. maintenance of the nighttime ionosphere; and those that result from short high-intensity bursts of energetic electrons causing particle-E layers to form (Fisher et al., 1977). The relative importance of each can only be assessed when more information is available.

7.2 Possible Developments

There are many possibilities that should be considered if this work is to be continued. The major limitation of the program is the static model atmosphere used. More recent models have been published by Jacchia (1977) which indicate slight changes from earlier versions (Jacchia, 1971). What is needed is a time-varying model which would allow full diurnal cycles to be calculated. This would undoubtedly lead to a large increase in computer time and core, but would give more meaningful results. Two such time-varying models are available, by Hedin et al, (1974) and Hedin (1976). This latter allows for variations in

latitude and longitude as well as time of day, magnetic and solar activity in calculations of exospheric temperature, and densities of N_2, O_2, O, He, H, Ar, and temperature as functions of height. This program has been briefly run at Rhodes and first results seem to be promising.

The next step to take would be to extend the lower limit into the E- or even D-regions. There are complications arising from the high ion densities and complex chemistry involved. An attempt was made to solve the continuity equation down to 90 km. Equilibrium solutions are reasonably straightforward, but a nighttime profile was virtually impossible. This was because of the large instabilities in the ion density equations between 90 and 110 km, due to the change in production rate. Using a more sophisticated routine for solving "stiff" simultaneous ordinary differential equations due to Gear (1971) proved to be useless as the computer time needed was excessive. This difficulty may be caused by the simple reduction of photoionization. It is possible that with the full time-varying model atmosphere such complications will prove less troublesome.

It has been shown that neglect of ionospheric winds in the E-region at night leads to profiles lacking in the irregular features actually observed (Chen and Harris, 1971). Inclusion of wind-shear terms and ion-neutral collision frequencies (which in the current study are assumed to be negligible in comparison with gyrofrequencies) could give a more representative picture of the lower ionosphere, particularly at night. The importance of precipitation would be seen more clearly, and could be more directly related to the occurrence of sporadic-E layers on ionograms. Another difficulty arises with the inclusion of winds in the F-region, but this may prove to be necessary.

If work on the upper part of the atmosphere only is considered,

then inclusion of winds, and possibly of electric fields, will be the logical next step. Realistic T_e and T_i profiles should also be used. A discussion of boundary conditions can be found in Waldman (1973), and of computing techniques in Hastings and Roble (1977).

It is clear that there is a great deal of scope in this line of research. The present study has shown that precipitation effects may be a significant factor in understanding the behaviour of the ionosphere, particularly at night. Further work needs to be done to confirm this.

APPENDIX A

Appendix A

The Transport Term in the Continuity Equation

The transport of ionization in the continuity equation is expressed by $\nabla.(N\underline{V})$ where $\underline{V}$ is the velocity of electrons. Here an expression is derived for this term. The following is based on a treatment by Torr and Torr (1969).

The equations of motion for the electrons and ions are:

$$-Nm_e \frac{d\underline{V}}{dt} = \nabla(NkT_e) + \nu_{ei}\, Nm_e(\underline{V}-\underline{V}_i) + \nu_e\, Nm_e\, \underline{V}$$

$$- Nm_e\underline{g} + Ne(\underline{V} \times \underline{B} + \underline{E}) \qquad \text{-----} \qquad (1)$$

$$-Nm_i \frac{d\underline{V}_i}{dt} = \nabla(NkT_i) + \nu_{ei}\, Nm_e(\underline{V}_i-\underline{V}) + \nu_i Nm_i\, \underline{V}_i$$

$$- Nm_i\underline{g} - Ne(\underline{V}_i \times \underline{B} + \underline{E}) \qquad \text{-----} \qquad (2)$$

where $N_i = N_e = N$ = electron density

$\underline{V} = (u_e, v_e, w_e)$ is the velocity of the electrons

$\underline{V}_i = (u_i, v_i, w_i)$ is the velocity of the ions

m_e = mass of the electrons

m_i = mass of the ions

k = Boltzmann's constant

T_e = electron temperature

T_i = ion temperature

ν_{ei} = collision frequency between electrons and ions

ν_i or ν_e = collision frequency between ions or electrons and neutrals (note that since winds are ignored, the neutral gas is at rest)

$\underline{g}$ = (0,0,g) is the acceleration due to gravity

$\underline{B}$ = magnetic flux intensity = $B(-\cos|I|, 0, -\sin|I|)$ in the Southern Hemisphere

I = geomagnetic dip angle

$\underline{E}$ = electric field in the ionosphere

e = magnitude of the charge on the electron

The directions (x,y,z) are taken as pointing south, east and upwards respectively.

Assuming that terms in m_e are negligible and that accelerations are zero for large-scale motions, eqns (1) and (2) become:

$$0 = \frac{k}{N}\nabla(NT_e) + e(\underline{V} \times \underline{B} + \underline{E}) \quad \text{-----} \quad (3)$$

$$0 = \frac{k}{N}\nabla(NT_i) + m_i \nu_i \underline{V}_i - m_i \underline{g} - e(\underline{V}_i \times \underline{B} + \underline{E}) \text{-----} \quad (4)$$

Taking the scalar product of (3) with $\underline{B}$:

$$0 = \frac{k}{N}\nabla(NT_e).\underline{B} + e(\underline{E}.\underline{B})$$

Assuming that the atmosphere is horizontally stratified, so

that terms in $\frac{\partial}{\partial x}$ and $\frac{\partial}{\partial y}$ are zero, one obtains

$$0 = \left(\frac{k}{N}\frac{\partial(NT_e)}{\partial h}\right)(-B\sin I) + e(-E_x B\cos I - E_z B\sin I)$$

$$E_z = (-B\sin I.\frac{k}{N}\frac{\partial(NT_e)}{\partial h} - eE_x B\cos I)\frac{1}{eB\sin I}$$

$$E_z = -\frac{k}{Ne}\frac{\partial(NT_e)}{\partial h} - E_x \cot I \qquad \text{-----} \quad (5)$$

Taking components of (4):

$$0 = 0 + m_i \nu_i u_i - e(-B\sin I\ v_i + E_x) \qquad \text{-----} \quad (6)$$

$$0 = 0 + m_i \nu_i v_i - e(-B\cos I\ w_i + B\sin I\ u_i + E_y) \qquad \text{-----} \quad (7)$$

$$0 = \frac{k}{N}\frac{\partial(NT_i)}{\partial h} + m_i \nu_i w_i + m_i g - e(B\cos I\ v_i + E_z) \qquad \text{-----} \quad (8)$$

Substituting for E_z from (5) into (8) gives

$$0 = \frac{k}{N}\frac{\partial(NT_i)}{\partial h} + m_i \nu_i w_i + m_i g - eB\cos I\ v_i - e\left(-\frac{k}{Ne}\frac{\partial(NT_e)}{\partial h} - E_x \cot I\right)$$

$$0 = \frac{k}{N}\frac{\partial}{\partial h}\left[(T_i + T_e)N\right] + m_i \nu_i w_i + m_i g - eB\cos I\ v_i + eE_x \cot I \qquad \text{-----} \quad (9)$$

From eqn (6): $u_i = \frac{1}{m_i \nu_i}\left[-eB\sin I\ v_i + eE_x\right]$ ----- (10)

From eqn (7): $v_i = \frac{1}{m_i \nu_i}\left[-eB\cos I\ w_i + eB\sin I\ u_i + eE_y\right]$ ----- (11)

From eqn (8): $w_i = \frac{1}{m_i \nu_i} \left[- \frac{k}{N} \frac{\partial}{\partial h} \left[(T_i + T_e) N \right] - m_i g \right.$

$$\left. + eB\cos I \; v_i - eE_x \cot I \right] \qquad \text{-----} \quad (12)$$

Let $\frac{k}{N} \frac{\partial}{\partial h} \left[(T_i + T_e) N \right] + m_i g = V'$ ----- (13)

Then, from (12), $w_i = \frac{1}{m_i \nu_i} \left[-V' + eB\cos I \; v_i \right.$

$$\left. - eE_x \cot I \right] \qquad \text{-----} \quad (14)$$

Substituting for w_i from (14) into (11) gives

$$v_i = \frac{1}{m_i \nu_i} \left[-eB\cos I \left(\frac{1}{m_i \nu_i} \left[-V' + eB\cos I \; v_i - eE_x \cot I \right] \right) \right.$$

$$\left. + eB\sin I \left(\frac{1}{m_i \nu_i} \left[-eB\sin I \; v_i + eE_x \right] \right) + eE_y \right]$$

The horizontal components of the earth's electric field, E_x and E_y, are ignored due to the controversy surrounding theoretical and experimental values. According to measurements made by Haerendel et al.,(1967), the horizontal field has a value of the order of 10^{-3} Vm^{-1}. Theoretical calculations imply fields of 5 - 10 Vm^{-1} (Stubbe, 1968). The effects of electric fields on plasma transport is, in any case, thought to be rather small except during magnetic disturbances and about the geomagnetic equator (Banks and Kockarts, 1973b, p.186).

Thus:

$$v_i \left[1 + \frac{e^2 B^2 \cos^2 I}{m_i^2 \nu_i^2} + \frac{e^2 B^2 \sin^2 I}{m_i^2 \nu_i^2} \right] = \frac{1}{m_i \nu_i} \left[-eB\cos I \left(- \frac{V'}{m_i \nu_i} \right) \right]$$

$$v_i = \frac{m_i^2 \nu_i^2}{m_i^2 \nu_i^2 + e^2 B^2} \quad \frac{V' eB \cos I}{m_i^2 \nu_i^2} \qquad \text{-----} \quad (15)$$

Substituting for v_i into eqn (10), and omitting terms in E_x, E_y, one obtains:

$$u_i = \frac{1}{m_i \nu_i} \left[-eB \sin I \, \frac{V' eB \cos I}{m_i^2 \nu_i^2 + e^2 B^2} \right]$$

$$= \frac{-e^2 B^2 \sin I \cos I \, V'}{m_i \nu_i (m_i^2 \nu_i^2 + e^2 B^2)}$$

$$= \frac{-\sin I \cos I \, V'}{m_i \nu_i \left(\frac{m_i^2 \nu_i^2}{e^2 B^2} + 1 \right)}$$

$$= \frac{-\sin I \cos I \, V'}{m_i \nu_i \left(\frac{\nu_i^2}{w^2} + 1 \right)} \qquad \text{-----} \quad (16)$$

where $w^2 = \frac{e^2 B^2}{m_i^2}$ = (ion gyrofrequency)^2.

Thus, substituting for v_i into (14):

$$w_i = \frac{1}{m_i \nu_i} \left[-V' + eB \cos I \, \frac{V' eB \cos I}{m_i^2 \nu_i^2 + e^2 B^2} \right]$$

$$= \frac{-V'}{m_i \nu_i} + \frac{e^2 B^2 \cos^2 I \, V'}{m_i \nu_i (m_i^2 \nu_i^2 + e^2 B^2)}$$

$$= \frac{-V'}{m_i \nu_i} + \frac{\cos^2 I \; V'}{m_i \nu_i \left(\frac{\nu_i^2}{w^2} + 1\right)} \qquad \text{-----} \quad (17)$$

Assuming that the ion-neutral collision frequency $\ll$ ion gyrofrequency,

$$\text{i.e. } \frac{\nu_i}{w_i} \approx 0,$$

$$\text{then } v_i = \frac{V' \cos I}{\frac{m_i^2 \nu_i^2}{eB} + eB} \qquad \text{from (15)}$$

$$= \frac{V' \cos I}{\frac{m_i^2 \nu_i^2}{w} + eB}$$

$$\approx \frac{V' \cos I}{eB}$$

$$\text{and } u_i \approx \frac{-\sin I \cos I \; V'}{m_i \nu_i} \qquad \text{(from (16))}$$

$$\text{and } w_i \approx \frac{-V'}{m_i \nu_i} + \frac{V' \cos^2 I}{m_i \nu_i} \qquad \text{(from (17))}$$

$$= \frac{-V' \sin^2 I}{m_i \nu_i} \qquad \text{-----} \quad (18)$$

Taking components of (3):

$$0 = 0 + e(-B\sin I\ v_e + E_x) \qquad \text{-----} \qquad (19)$$

$$0 = 0 + e(-B\cos I\ w_e + B\sin I\ u_e + E_y) \qquad \text{-----} \qquad (20)$$

$$0 = \frac{k}{N}\frac{\partial(NT_e)}{\partial h} + e(B\cos I\ v_e + E_z)$$

Hence $v_e = 0$ (from (19), since $E_x = 0$)

$$u_e = \frac{\cos I}{\sin I} w_e \quad \text{(from (20), } E_y = 0)$$

$$= \cot I\ w_e$$

As there is no vertical current, $w_i = w_e$,

$$w_e = \frac{-V'\sin^2 I}{m_i \nu_i} \quad \text{(from (18))}$$

Thus $\underline{V} = (u_e, v_e, w_e) = \left(\frac{-V'\sin^2 I\cot I}{m_i\nu_i}, 0, \frac{-V'\sin^2 I}{m_i\nu_i}\right)$

$$\text{-----} \qquad (21)$$

The transport term is $\nabla.(N\underline{V}) = \nabla.N\left(\frac{-V'\sin^2 I\cot I}{m_i\nu_i}, 0, \frac{-V'\sin^2 I}{m_i\nu_i}\right)$

As only $\frac{\partial}{\partial z}$ terms are included, this becomes

$$\nabla.(N\underline{V}) = \nabla.N\ \left(\frac{-V'\sin^2 I}{m_i \nu_i}\right)$$

$$= -\nabla.N\ \left(\frac{\sin^2 I}{m_i \nu_i}\right)\left(\frac{k}{N}\frac{\partial}{\partial h}\left[(T_i + T_e)N\right] + m_i g\right) \quad \text{from (13)}$$

$$= -\nabla.(NV_D)$$

where $V_D \equiv$ diffusion velocity $= \frac{\sin^2 I}{m_i \nu_i}\left[\frac{k}{N}\frac{\partial}{\partial h}[(T_i + T_e)N] + m_i g\right]$

$$\frac{V_D}{kT} = \frac{\sin^2 I}{m_i \nu_i}\left[\frac{1}{NT}\frac{\partial}{\partial h}\left[(T_i + T_e)N\right] + \frac{1}{H(O)}\right]$$

where H(O) = scale height of atomic oxygen, the principal ionic constituent over most of the upper atmosphere.

Let $T_i = T_e = T$, the temperature of the neutral gas.

Then, $\frac{V_D}{kT} = \frac{\sin^2 I}{m_i \nu_i}\left[\frac{2}{NT}\frac{\partial}{\partial h}(NT) + \frac{1}{H(O)}\right]$

$$V_D = \frac{kT}{m_i \nu_i}\sin^2 I\left[\frac{2}{NT}\frac{\partial}{\partial h}(NT) + \frac{1}{H(O)}\right]$$

$$= D\sin^2 I\left[\frac{2}{NT}\frac{\partial}{\partial n}(NT) + \frac{1}{H(O)}\right] \qquad \text{-----} \qquad (22)$$

where $D = \frac{kT}{m_i \nu_i} \equiv$ ambipolar diffusion coefficient

The above expression for V_D may be compared with that for

ambipolar diffusion derived by Schunk and Walker (1973). The expression for D is that derived by Chapman and Cowling (1960)

$$D = \frac{3}{8\rho^2 n(O)} \left(\frac{kT}{\pi m(O)}\right)^{\frac{1}{2}}$$

where ρ = collision diamter = 6×10^{-8} cm

$n(O)$ = number density of atomic oxygen

$m(O)$ = mass of atomic oxygen

Hence $\nabla.(N\underline{V}) = -\nabla.(NV_D) = -\nabla.\left[D\sin^2 I \left(\frac{2N}{T}\frac{\partial T}{\partial h} + 2\frac{\partial N}{\partial h} + \frac{N}{H}\right)\right]$

(writing H(O) as H)

$$= -D\sin^2 I \left(\frac{3}{2T}\frac{\partial T}{\partial h} + \frac{1}{H}\right)\left(\frac{2N}{T}\frac{\partial T}{\partial h} + 2\frac{\partial N}{\partial h} + \frac{N}{H}\right)$$

$$-D\sin^2 I \left(\frac{2}{T}\frac{\partial T}{\partial h}\frac{\partial N}{\partial h} - \frac{2N}{T^2}\left(\frac{\partial T}{\partial h}\right)^2 + \frac{2N}{T}\frac{\partial^2 T}{\partial h^2}\right.$$

$$\left. + 2\frac{\partial^2 N}{\partial h^2} + \frac{1}{H}\frac{\partial N}{\partial h} - \frac{N}{H^2}\frac{\partial H}{\partial h}\right)$$

$$= -2D\sin^2 I \frac{\partial^2 N}{\partial h^2} - D\sin^2 I \left(\frac{5}{T}\frac{\partial T}{\partial h} + \frac{3}{H}\right)\frac{\partial N}{\partial h}$$

$$- D\sin^2 I \left(\frac{7}{2HT}\frac{\partial T}{\partial h} + \frac{1}{T^2}\left(\frac{\partial T}{\partial h}\right)^2 + \frac{2}{T}\frac{\partial^2 T}{\partial h^2} - \frac{1}{H^2}\frac{\partial H}{\partial h} + \frac{1}{H^2}\right)N$$

----- (23)

This is the expression used in the continuity equation for the transport of electrons due to diffusion.

APPENDIX B

FLOW-CHART FOR PROGRAM INIT

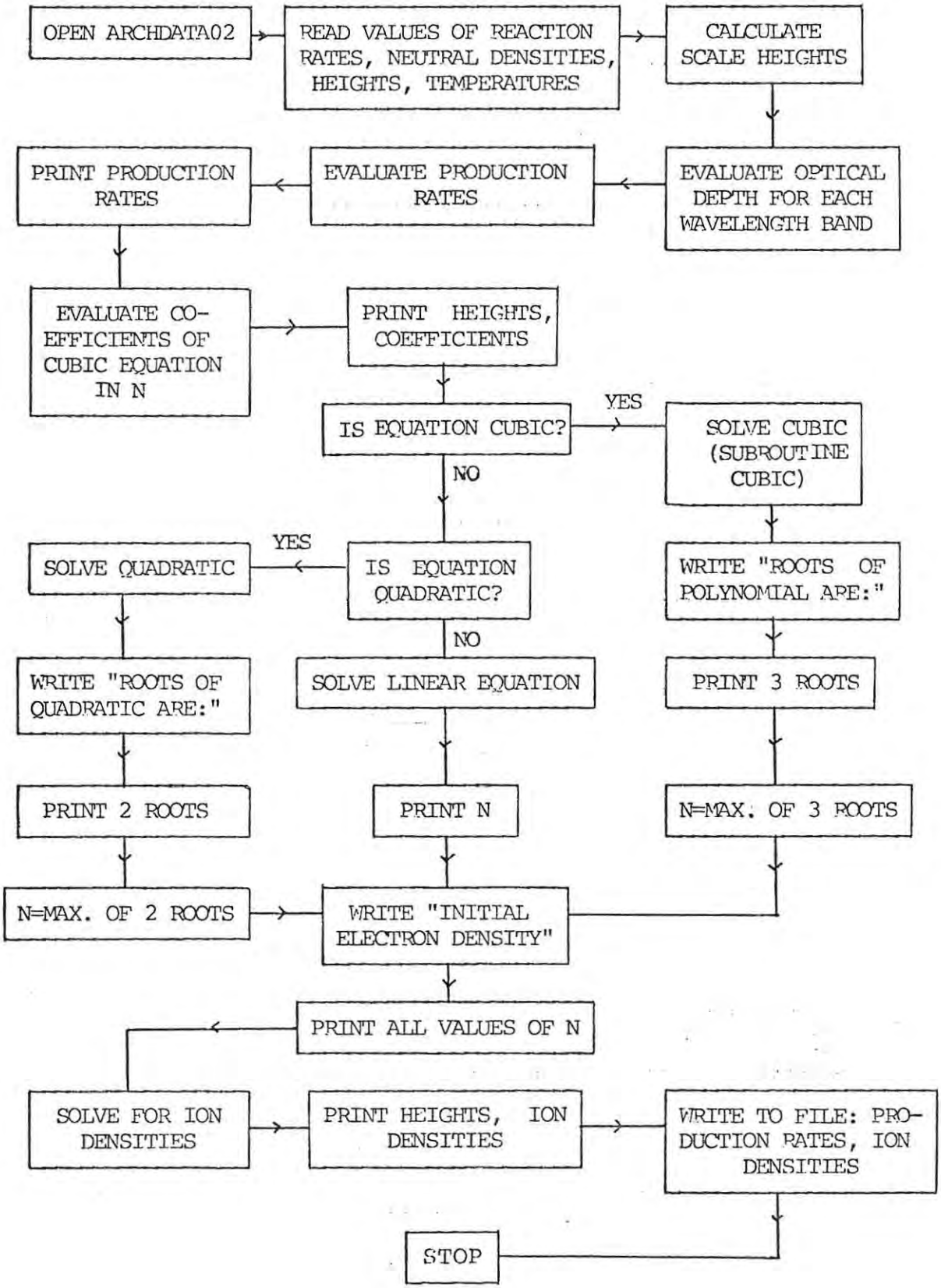

```
      SHORTLIST
      LIBRARY (AMPTROUTINES)
      PROGRAM(INIT)
      COMPRESS INTEGER AND LOGICAL
      COMPACT
      INPUT 5=CRO
      OUTPUT 6=LPO
      USE 4=ED1/UNFORMATTED (ARCHDATA04  )/256
      END

C
C     ESTIMATES Q VALUES, INITIAL ELECTRON DENSITY(WITHOUT
C     . DIFFUSION), ION DENSITIES
C

      MASTER INITIALVALUE
      REAL K1(53),K2(53),K3(53)
      COMPLEX COEF(4),ELECT(3),FLEC(2),X(3),COEFF(5),ROOT(4)
      DIMENSION F(53),EROOT(4),A(53),B(53),C(53),E(53),
     *D(53),ALOGDEN(53),EL(2),ED(3)
      COMMON/B1/DO(53),DN2(53),DO2(53),HT(53),DN21(53),DO21(53)
      COMMON/B2/DNOI(53),EDEN(53),QO2(53),QO(53),QN2(53),Q(53)
      COMMON/B3/SCALED(53),K1,K2,K3,AL1(53),AL2(53),AL3(53)
      COMMON/B5/TEMP(53)
      CALL USEFILE(7,2HED,12HARCHDATA02  ,-1,0)
      N=10318
      CALL GETARRAY(7,N,K1)
      CALL GETARRAY(7,N,K2)
      CALL GETARRAY(7,N,K3)
      CALL GETARRAY(7,N,AL1)
      CALL GETARRAY(7,N,AL2)
      CALL GETARRAY(7,N,AL3)
      N=10901
      CALL GETARRAY(7,N,HT)
      CALL GETARRAY(7,N,DN2)
      CALL GETARRAY(7,N,DO2)
      CALL GETARRAY(7,N,DO)
      N=2634
      CALL GETARRAY(7,N,TEMP)
C
C     SET UP COEFFICIENTS IN CUBIC EQUATION
C
      CALL PHOTOION
      DO 1 J=1,53
      A(J)=-AL1(J)*AL2(J)*AL3(J)*(K1(J)*DN2(J)+K2(J)*DO2(J))
      B(J)=AL1(J)*AL2(J)*AL3(J)*QO(J)-AL1(J)*AL2(J)*K3(J)*
     * DO(J)*(K1(J)*DN2(J)+K2(J)*DO2(J))
      C(J)=Q(J)*(AL1(J)*AL3(J)*K2(J)*DO2(J)+AL2(J)*AL3(J)*
     * K1(J)*DN2(J)+AL1(J)*AL2(J)*K3(J)*DO(J))
     *-QN2(J)*(AL1(J)*AL3(J)*K2(J)*DO2(J)+AL2(J)*AL3(J)*K1(J)*DN2(J)+
     * AL1(J)*AL2(J)*K3(J)*DO(J))
     *-QO2(J)*(AL2(J)*AL3(J)*K1(J)*DN2(J)+AL1(J)*AL2(J)*K3(J)*DO(J)-
     * AL1(J)*AL3(J)*K1(J)*DN2(J))
      E(J)=AL1(J)*K3(J)*DO(J)*K2(J)*DO2(J)*Q(J)+AL2(J)*K3(J)*DO(J)
     *  *K1(J)*DN2(J)*Q(J)-AL1(J)*K3(J)*DO(J)*K2(J)*DO2(J)*QN2(J)
     *+AL1(J)*K3(J)*DO(J)*K1(J)*DN2(J)*QO2(J)+AL2(J)*K3(J)*DO(J)
     **K2(J)*DO2(J)*QN2(J)-AL2(J)*K3(J)*DO(J)*K1(J)*DN2(J)*QO2(J)
 1    CONTINUE
      WRITE(6,6008)(HT(J),A(J),B(J),C(J),E(J),J=1,53)
6008  FORMAT(1H ,F5.1,4E20.4)
```

```
      DO 4 M=1,53
      EDEN(M)=0.0
 4    CONTINUE
C
C     TEST TO SEE IF EQUATION IS TRUE CUBIC,
C     I.E. WHETHER COEFFICIENTS ARE OF COMPARABLE MAGNITUDE
C
      DO 2 J=1,53
      E(J)=E(J)/A(J)
      C(J)=C(J)/A(J)
      B(J)=B(J)/A(J)
      A(J)=A(J)/A(J)
      IF((B(J)/A(J)).GT.1.E6.AND.(C(J)/B(J)).GT.1.E6) GO TO 6
      IF((B(J)/A(J)).GT.1.E6) GO TO 5
      COEF(1)=CMPLX(E(J),0.0)
      COEF(2)=CMPLX(C(J),0.0)
      COEF(3)=CMPLX(B(J),0.0)
      COEF(4)=CMPLX(A(J),0.0)
C
C     SOLVE CUBIC EQUATION
C
      CALL CUBIC(COEF,ELECT)
      WRITE (6,6000) (ELECT(I),I=1,3)
 6000 FORMAT(1H0,24HROOTS OF POLYNOMIAL ARE:,6E16.2)
      ED(1)=REAL(ELECT(1))
      ED(2)=REAL(ELECT(2))
      ED(3)=REAL(ELECT(3))
      EDEN(J)=AMAX1(ED(1),ED(2),ED(3))
      DO 3 L=1,3
      ELECT(L)=(0.0,0.0)
      DO 3 M=1,4
      COEF(M) = (0.0,0.0)
 3    CONTINUE
      GO TO 2
 5    X(1)=CMPLX(B(J),0.0)
      X(2)=CMPLX(C(J),0.0)
      X(3)=CMPLX(E(J),0.0)
C
C
C     SOLVE QUADRATIC EQUATION
C
      IF((X(2)*X(2)).GE.(4*X(1)*X(3)))ELEC(1)=(-X(2)+SQRT(X(2)*X(2)-4*X(
     11)*X(3)))/(2*X(1))
      IF((X(2)*X(2)).LT.(4*X(1)*X(3)))ELEC(1)=CMPLX(-X(2)/(2*X(1)),
     1SQRT(4*X(1)*X(3)-X(2)*X(2))/(2*X(1)))
      ELEC(2)=X(3)/(X(1)*ELEC(1))
      WRITE(6,6005) (ELEC(I),I=1,2)
 6005 FORMAT(1H0,23HROOTS OF QUADRATIC ARE:,4E16.4)
      EL(1)=REAL(ELEC(1))
      EL(2)=REAL(ELEC(2))
      EDEN(J)=AMAX1(EL(1),EL(2))
      GO TO 2
 6    EDEN(J)=-E(J)/C(J)
C
C     SOLVE LINEAR EQUATION
C
      WRITE(6,6006)(EDEN(J))
 6006 FORMAT(1H0,26HSOLUTION TO LINEAR EQN IS:,E16.4)
 2    CONTINUE
      WRITE (6,6001)
 6001 FORMAT(1H1,38X,25HINITIAL ELECTRON DENSITY//)
```

```
      WRITE(6,6002) (HT(J),EDEN(J),J=1,53)
 6002 FORMAT(1H ,35X,F6.1,20X,E12.4)
      CALL IONDENSITY
      WRITE (6,6004) (HT(J),DN2I(J),DO2I(J),DNOI(J),J=1,53)
 6004 FORMAT(1H ,F6.1,11X,E12.4,9X,E12.4,9X,E12.4)
C
C     STORE VALUES ON DISC
C
      N=14000
      CALL PUTARRAY(7,N,QO2)
      CALL PUTARRAY(7,N,QN2)
      CALL PUTARRAY(7,N,QO)
      CALL PUTARRAY(7,N,Q)
      CALL PUTARRAY(7,N,DO2I)
      CALL PUTARRAY(7,N,DNOI)
      CALL PUTARRAY(7,N,DN2I)
      STOP OK
      END

      SUBROUTINE IONDENSITY
      REAL K1(53),K2(53),K3(53)
      DIMENSION C1(53),C2(53)
      DIMENSION A1(53),A2(53),A3(53),B1(53),B3(53),D(2,2),C(2),B2(53)
      COMMON/B1/DO(53),DN2(53),DO2(53),HT(53),DN2I(53),DO2I(53)
      COMMON/B2/DNOI(53),EDEN(53),QO2(53),QO(53),QN2(53),Q(53)
      COMMON/B3/SCALEO(53),K1,K2,K3,AL1(53),AL2(53),AL3(53)
      COMMON/B5/TEMP(53)
      DO 4 J=1,53
      DN2I(J)=0.0
      DO2I(J)=0.0
      DNOI(J)=0.0
 4    CONTINUE
      DO 1 J=1,53
      IF(EDEN(J).LE.1.E-59) GO TO 1
      IF(Q(J).LE.1.E-59)GO TO 1
C
C     SOLVE FOR DN2I FIRST
C
      DN2I(J)=QN2(J)/(K3(J)*DO(J)+AL3(J)*EDEN(J))
C
C     SOLVE SIMULTANEOUS EQUATIONS IN DO2I,DNOI
C
C     AL2*EDEN*DO2I + K2*DO2*DO2I + K2*DO2*DNOI=QO2 + K2*EDEN*DO2
C     - K2*DO2*DN2I
C     K1*DN2*DO2I + K1*DN2*DNOI + AL1*EDEN*DNOI = K3*DN2I*DO + K1*EDEN*DN2
C     - K1*DN2*DN2I
C
      A1(J) = AL2(J)*EDEN(J)
      A2(J) = K2(J)*DO2(J)
      B1(J) = K2(J)*DO2(J)
      C1(J) = QO2(J)+K2(J)*EDEN(J)*DO2(J)-K2(J)*DO2(J)*DN2I(J)
      A3(J) = K1(J)*DN2(J)
      B2(J) = K1(J)*DN2(J)
      B3(J) = AL1(J)*EDEN(J)
      C2(J) =K3(J)*DN2I(J)*DO(J)+K1(J)*EDEN(J)*DN2(J)-
     * K1(J)*DN2(J)*DN2I(J)
C       SOLVE:  (A1 + A2)*DO2I + B1*DNOI = C1
C       A3*DO2I + (B2 + B3)*DNOI = C2
      D(1,1)=A1(J)+A2(J)
      D(1,2)=B1(J)
      D(2,1) = A3(J)
```

```
      D(2,2)=B2(J)+B3(J)
      C(1)=C1(J)
      C(2)=C2(J)
      CALL LINALG(D,C,2,1,0,2,1,IER)
      IF(IER.NE.0) GO TO 2
      DO2I(J)=C(1)
      DNOI(J)=C(2)
      GO TO 1
2     WRITE(6,6000) J
6000  FORMAT(1H0,18HSINGULAR MATRIX AT,I4,7H  HEIGHT)
1     CONTINUE
      RETURN
      END

      SUBROUTINE PHOTOION
      REAL K1(53),K2(53),K3(53)
      DIMENSION SCALEN2(53),SCALEO2(53),TAU1(53),TAU2(53),TAU3
     * (53),TAU4(53),TAU5(53),TAU6(53),TAU7(53),TAU8(53),TAU9(53),
     * TAU10(53),TAU11(53),TAU12(53)
      DIMENSION G(53),FACTOR(53)
      COMMON/B1/DO(53),DN2(53),DO2(53),HT(53),DN2I(53),DO2I(53)
      COMMON/B2/DNOI(53),EDEN(53),QO2(53),QO(53),QN2(53),Q(53)
      COMMON/B3/SCALEO(53),K1,K2,K3,AL1(53),AL2(53),AL3(53)
      COMMON/B5/TEMP(53)
C
C     EVALUATE SCALE HEIGHTS
C
      DO 1 J=1,53
      G(J)=980.655/((1+(1.573*HT(J)*1.E-4))*(1+(1.573*HT(J)*1.E-4)))
      FACTOR(J)=1.3804E-16/(1.6604E-24*G(J))
      SCALEO(J)=FACTOR(J)*TEMP(J)/16.
      SCALEO2(J)=FACTOR(J)*TEMP(J)/32.
      SCALEN2(J)=FACTOR(J)*TEMP(J)/28.
1     CONTINUE
      WRITE(6,7000)(HT(I),TEMP(I),I=1,53)
      WRITE(6,7001)(HT(I),SCALEO(I),SCALEO2(I),SCALEN2(I),I=1,53)
7000  FORMAT(1H ,F6.1,E20.4)
7001  FORMAT(1H ,F6.1,3E20.4)
C
C     CALCULATE OPTICAL DEPTHS, HENCE PRODUCTION RATES
C
      DO 4 J=1,53
      TAU1(J)=DO2(J)*SCALEO2(J)*1.55E-18
      TAU2(J)=DO2(J)*SCALEO2(J)*4.E-18
      TAU3(J)=(DO2(J)*SCALEO2(J)*7.5E-18)+(DO(J)*SCALEO(J)*3.E-18)
      TAU4(J)=(DN2(J)*SCALEN2(J)*2.E-17)+(DO2(J)*SCALEO2(J)*2.E-17)+
     * (DO(J)*SCALEO(J)*3.E-18)
      TAU5(J)=(DN2(J)*SCALEN2(J)*2.3E-17)+(DO2(J)*SCALEO2(J)*2.E-17)+
     * (DO(J)*SCALEO(J)*8.E-18)
      TAU6(J)=(DN2(J)*SCALEN2(J)*2.3E-17)+(DO2(J)*SCALEO2(J)*2.5E-17)+
     * (DO(J)*SCALEO(J)*1.2E-17)
      TAU7(J)=(DN2(J)*SCALEN2(J)*1.4E-17)+(DO2(J)*SCALEO2(J)*1.7E-17)+
     * (DO(J)*SCALEO(J)*8.E-18)
      TAU8(J)=(DN2(J)*SCALEN2(J)*5.E-18)+(DO2(J)*SCALEO2(J)*7.5E-18)+
     * (DO(J)*SCALEO(J)*7.5E-18)
      TAU9(J)=(DN2(J)*SCALEN2(J)*2.2E-18)+(DO2(J)*SCALEO2(J)*3.5E-18)+
     * (DO(J)*SCALEO(J)*1.8E-18)
      TAU10(J)=(DN2(J)*SCALEN2(J)*9.28E-19)+DO2(J)*SCALEO2(J)*5.45E-19+
     * DO(J)*SCALEO(J)*4.64E-19
      TAU11(J)=DN2(J)*SCALEN2(J)*4.4E-19+DO2(J)*SCALEO2(J)*2.35E-19+
     * DO(J)*SCALEO(J)*2.E-19
```

```
      TAU12(J)=DN2(J)*SCALEN2(J)*1.64E-19+DO2(J)*SCALEO2(J)*9.67E-20+
     * DO(J)*SCALEO(J)*0.82E-19
      QO(J)=DO(J)*(4.5E-8*EXP(-TAU3(J))+1.5E-8*EXP(-TAU4(J))+1.5E-8*EXP
     * (-TAU5(J))+8.7E-8*EXP(-TAU6(J))+1.1E-7*EXP(-TAU7(J))+5.2E-8*EXP(-
     * TAU8(J))+4.4E-9*EXP(-TAU9(J))+2.44E-10*EXP(-TAU10(J))+1.E-10*EXP(
     * -TAU11(J))+1.E-11*EXP(-TAU12(J)))
      QO2(J)=DO2(J)*(5.E-9*EXP(-TAU1(J))+1.1E-8*EXP(-TAU2(J))+5.7E-8*
     * EXP(-TAU3(J))+1.5E-8*EXP(-TAU4(J))+1.5E-8*EXP(-TAU5(J))+2.E-7*
     * EXP(-TAU6(J))+2.3E-7*EXP(-TAU7(J))+1.E-7*EXP(-TAU8(J))+9.E-8*
     * EXP(-TAU9(J))+4.87E-10*EXP(-TAU10(J))+2.2E-10*EXP(-TAU11(J))+
     *2.E-11*EXP(-TAU12(J)))
      QN2(J)=DN2(J)*(1.5E-8*EXP(-TAU4(J))+1.6E-8*EXP(-TAU5(J))+1.9E-7*
     * EXP(-TAU6(J))+1.9E-7*EXP(-TAU7(J))+7.E-8*EXP(-TAU8(J))+5.5E-9*
     * EXP(-TAU9(J))+2.86E-10*EXP(-TAU10(J))+1.2E-10*EXP(-TAU11(J))+1.1
     * E-11*EXP(-TAU12(J)))
      Q(J)=QO2(J)+QO(J)+QN2(J)
4     CONTINUE
      WRITE(6,6003)(HT(I),QO(I),QO2(I),QN2(I),Q(I),I=1,53)
6003  FORMAT(1H ,3X,F6.1,4X,E10.4,3X,E10.4,4X,E10.4,4X,E10.4)
      RETURN
      END

      SUBROUTINE CUBIC (A,Z3)

C SOLVES CUBIC EQUATION A(J+1).X**J, J=0,3 WITH COMPLEX COEFFICIENTS.
C ROOTS (COMPLEX) APPEAR IN Z3(I) I=1,3

      COMPLEX A,Z3,G,H,P,Q,A1,A2,W1,W2
      DIMENSION Z3(3),A(4)
      IF (CABS(A(4)).LE.1.E-40) GO TO 50
      H=A(4)*A(2)/3.0-A(3)*A(3)/9.0
      G=A(4)*A(4)*A(1)-A(4)*A(3)*A(2)/3.0+2.0*A(3)*A(3)*A(3)/27.0
      Q=CSQRT(G*G+4.*H*H*H)
      P=.5*(-G+Q)
      Q=.5*(-G-Q)
      A1=(0.,0.)
      A2=(0.,0.)
      IF (CABS(P).EQ.0.0) GO TO 10
      A1=CEXP(CLOG(P)/3.0)
      GO TO 20
10    IF (CABS(Q).EQ.0.0) GO TO 30
      A1=CEXP(CLOG(Q)/3.0)
20    A2=-H/A1
30    W1=(-.5,.8660254038)
      W2=(-.5,-.8660254038)
      Z3(1)=A1+A2
      Z3(2)=A1*W1+A2*W2
      Z3(3)=A1*W2+A2*W1
      DO 40 I=1,3
40    Z3(I)=(Z3(I)-A(3)/3.0)/A(4)
      RETURN
50    DO 60 I=1,3
60    Z3(I)=(0.,0.)
      RETURN
      END

      SUBROUTINE LINALG (A,B,M,N,MODE,IA,IB,IER)

C SOLVES LINEAR EQUATIONS AND/OR INVERTS MATRIX BY PIVOTAL CONDENSATION
C MATRIX OF ORDER  M  IN  A,  N RIGHT HAND SIDES IN  B.
C IA DEFINES NUMBER OF ROWS IN  A  AND  B  AND NUMBER OF COLS
```

```
C OF  A.     IB  DEFINES NUMBER OF COLUMNS OF  B
C IF N=0, MODE>0  CARRY OUT INVERSION ONLY (INVERSE OVERWRITES A)
C IF N>0, MODE=0  SOLVE EQUATIONS ONLY (SOLUTION OVERWRITES  B)
C IF N>0, MODE>0  INVERT AND SOLVE
C IER RETURNED AS 0 IF SUCCESSFUL, AND AS 1 IF UNSUCCESSFUL (SINGULAR)

      DIMENSION A(IA,IA),B(IA,IB),C(100),IND(100)
      IER=0
      MM=M-1
1     AMAX=0.0
      DO 3 I=1,M
      IND(I)=I
      IF (ABS(A(I,1))-AMAX) 3,3,2
2     AMAX=ABS(A(I,1))
      I4=I
3     CONTINUE
      DO 16 J=1,MM
      IF (I4-J) 8,8,4
4     ISTO=IND(J)
      IND(J)=IND(I4)
      IND(I4)=ISTO
      DO 5 K=1,M
      STO=A(I4,K)
      A(I4,K)=A(J,K)
      A(J,K)=STO
5     CONTINUE
      IF (N) 8,8,6
6     DO 7 K=1,N
      STO=B(I4,K)
      B(I4,K)=B(J,K)
      B(J,K)=STO
7     CONTINUE
8     AMAX=0.0
      J1=J+1
      DO 15 I=J1,M
      IF (A(J,J).EQ.0.) GO TO 46
      A(I,J)=A(I,J)/A(J,J)
      DO 11 K=J1,M
      A(I,K)=A(I,K)-A(I,J)*A(J,K)
      IF (K-J1) 9,9,11
9     IF (ABS(A(I,K))-AMAX) 11,11,10
10    AMAX=ABS(A(I,K))
      I4=I
11    CONTINUE
12    IF (N) 15,15,13
13    DO 14 K=1,N
      B(I,K)=B(I,K)-A(I,J)*B(J,K)
14    CONTINUE
15    CONTINUE
16    CONTINUE
      IF (N) 23,23,17
17    DO 22 I1=1,M
      I=M+1-I1
      DO 21 J=1,N
      IF (M-1) 20,20,18
18    I2=I+1
      DO 19 K=I2,M
      B(I,J)=B(I,J)-A(I,K)*B(K,J)
19    CONTINUE
20    IF (A(I,I).EQ.0.) GO TO 46
      B(I,J)=B(I,J)/A(I,I)
```

```
21      CONTINUE
22      CONTINUE
23      IF (MODE) 45,45,24
24      DO 30 I1=1,MM
        I=M+1-I1
        I2=I-1
        DO 28 J1=1,I2
        J=I2+1-J1
        J2=J+1
        W1=-A(I,J)
        IF (I2-J2) 27,25,25
25      DO 26 K=J2,I2
        W1=W1-A(K,J)*C(K)
26      CONTINUE
27      C(J)=W1
28      CONTINUE
        DO 29 K=1,I2
        A(I,K)=C(K)
29      CONTINUE
30      CONTINUE
        I=M+1-I1
        I2=I+1
        W=A(I,I)
        DO 38 J=1,M
        IF (I-J) 31,32,33
31      W1=0.
        GO TO 34
32      W1=1.
        GO TO 34
33      W1=A(I,J)
34      IF (I1-1) 37,37,35
35      DO 36 K=I2,M
        W1=W1-A(I,K)*A(K,J)
36      CONTINUE
37      C(J)=W1
38      CONTINUE
        DO 39 J=1,M
        IF (W.EQ.0.) GO TO 46
        A(I,J)=C(J)/W
39      CONTINUE
40      CONTINUE
        DO 44 I=1,M
41      IF (IND(I)-I) 42,44,42
42      J=IND(I)
        DO 43 K=1,M
        STO=A(K,I)
        A(K,I)=A(K,J)
        A(K,J)=STO
43      CONTINUE
        ISTO=IND(J)
        IND(J)=J
        IND(I)=ISTO
        GO TO 41
44      CONTINUE
45      RETURN
46      IER=1
        DO 47 I=1,M
        DO 47 J=1,M
47      B(I,J)=0.
        RETURN
        END
```

FINISH

FLOW-CHART FOR PROGRAM NEQM

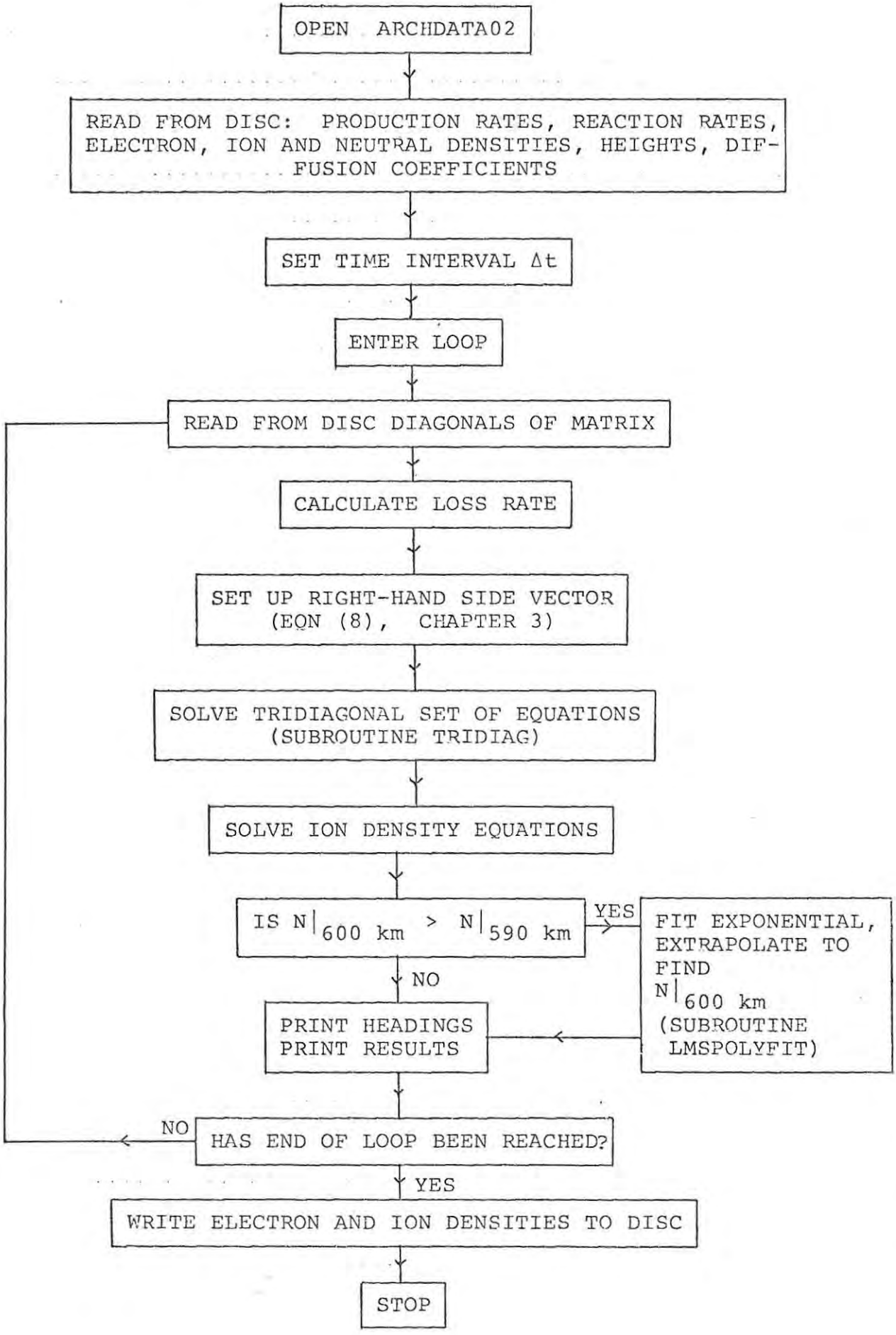

```
      SHORTLIST
      LIBRARY(AMPTROUTINES)
      PROGRAM(DEQN)
      INPUT 5=CRO
      OUTPUT 6=LPO
      COMPRESS INTEGER AND LOGICAL
      END

C
C     EQUILIBRIUM VALUE
C     USES BOUNDARY CONDITION DN/DT=-DIV(NV),
C     FLUX AT UPPER BOUNDARY = 3.E8
C     INTERPOLATES AT 10 KM INTERVALS BETWEEN 400-600 KM
C     TAKES ACCOUNT OF STEP CHANGE AT 160 KM
C     RESULTS DUMPED AT N=19000 ON DISC
C

      MASTER CONTINUITY
      REAL K1(53),K2(53),K3(53)
      DIMENSION HT(53),X(53),Y(53),Z(53),EL(53),DH(53),A(52),
     *B(52),D(52),R(52),P(53),Q(53),S(53),Q1(53),Q2(53),Q3(53)
      COMMON/B1/AL1(53),AL2(53),AL3(53),M,DO(53),DN2(53),DO2(53),E(53)
      COMMON/B3/K1,K2,K3,DOI(53),DO2I(53),DNOI(53),DN2I(53),TM,NO
      COMMON/B2/QO2(53),QN2(53),QO(53)
      COMMON/B4/HT,CON,SCALE
      CALL USEFILE(7,2HED,12HARCHDATA02  ,-1,0)
      N=14000
      CALL GETARRAY(7,N,QO2)
      CALL GETARRAY(7,N,QN2)
      CALL GETARRAY(7,N,QO)
      N=10318
      CALL GETARRAY(7,N,K1)
      CALL GETARRAY(7,N,K2)
      CALL GETARRAY(7,N,K3)
      CALL GETARRAY(7,N,AL1)
      CALL GETARRAY(7,N,AL2)
      CALL GETARRAY(7,N,AL3)
      N=19000
      CALL GETARRAY(7,N,E)
      CALL GETARRAY(7,N,DO2I)
      CALL GETARRAY(7,N,DNOI)
      CALL GETARRAY(7,N,DN2I)
      CALL GETARRAY(7,N,DOI)
      N=10901
      CALL GETARRAY(7,N,HT)
      CALL GETARRAY(7,N,DN2)
      CALL GETARRAY(7,N,DO2)
      CALL GETARRAY(7,N,DO)
C
C     CALL UP COEFFICIENTS IN TRANSPORT TERM
C
      N=13000
      CALL GETARRAY(7,N,X)
      CALL GETARRAY(7,N,Y)
      CALL GETARRAY(7,N,Z)
      DO 12 N=1,8
      DH(N)=5.E5
12    CONTINUE
      DO 13 N=9,53
```

```
      DH(N)=10.E5
13    CONTINUE
C
C     SET TIME INTERVAL, TM
C
      TM=1.0
      DO 6 NO=1,1000
C
C     CALL UP DIAGONALS OF MATRIX
C
      KK=28000
      CALL GETARRAY(7,KK,A)
      CALL GETARRAY(7,KK,B)
      CALL GETARRAY(7,KK,D)
C
C     CALCULATE LOSS RATE
C
      DO 2 N=1,53
      EL(N)=(AL1(N)*DNOI(N)+AL2(N)*DO2I(N)+AL3(N)*DN2I(N))*E(N)
2     CONTINUE
C
C     SET UP RIGHT-HAND SIDE COLUMN VECTOR
C
      DO 16 N=1,51
      R(N)=E(N+1)/TM+X(N+1)*(E(N+2)-2.*E(N+1)+E(N))/
     *(2.*DH(N)*DH(N))+Y(N+1)*(E(N+2)-E(N))/(2.*DH(N))
     *+Z(N+1)*E(N+1)+QO2(N+1)+QN2(N+1)+QO(N+1)-EL(N+1)
16    CONTINUE
      R(1)=R(1)+E(1)*X(2)/(2.*DH(1)*DH(1))
      R(8)=E(9)/TM+X(9)*(5*(E(10)-E(8))-15*(E(9)-E(6)))
     */750.E10+Y(9)*(E(10)-E(8))/15.E5+Z(9)*E(9)-EL(9)+
     *QO2(9)+QN2(9)+QO(9)
      R(52)=E(53)*.765184E7-3.E8-E(53)*6.5730E12*(1.54E-7/
     *699.5+1/.582592E7)-6.5730E12*(E(53)-E(52))/5.E5
C
C     SOLVE SET OF EQUATIONS
C
      CALL TRIDIAG(E,D,A,F,52,IER)
C
C     SOLVE ION DENSITY EQUATIONS
C
      DO 10 M=1,53
      DNOI(M)=DNOI(M)+TM*(K1(M)*DN2(M)*DOI(M)+K3(M)*DO(M)*DN2I(M)-
     * AL1(M)*DNOI(M)*E(M))
      DO2I(M)=DO2I(M)+TM*(QO2(M)+DOI(M)*K2(M)*DO2(M)-AL2(M)*
     * E(M)*DO2I(M))
      DN2I(M)=QN2(M)/(K3(M)*DO(M)+AL3(M)*E(M))
      DOI(M)=E(M)-DO2I(M)-DNOI(M)-DN2I(M)
10    CONTINUE
      DO 21 M=2,13
      DOI(M)=DOI(M)+TM*(QO(M)-DOI(M)*(K1(M)*DN2(M)+K2(M)*DO2(M)))
21    CONTINUE
      DO 20 N=1,53
      IF(DO2I(N).LE.0.0)DO2I(N)=1.0
      IF(DNOI(N).LE.0.0)DNOI(N)=1.0
      IF(DN2I(N).LE.0.0)DN2I(N)=1.0
20    CONTINUE
      DO 4 N=1,52
      E(N+1)=R(N)
4     CONTINUE
      IF(E(53).GE.E(52))CALL LEASTSQ
```

```
      IF(NO.NE.100.AND.NO.NE.200.AND.NO.NE.300.AND.NO.NE.400.
     * AND.NO.NE.500.AND.NO.NE.600.AND.NO.NE.700.AND.NO.NE.800.
     * AND.NO.NE.900.AND.NO.NE.1000)GO TO 6
9     WRITE(6,6001)
6001  FORMAT(1H1,45X,18HELECTRON DENSITIES///20X,6HHEIGHT,45X,
     *16HELECTRON DENSITY/21X,4H(KM),50X,6H(/CMS)//)
      WRITE(6,6002)(HT(N),E(N),N=1,53)
6002  FORMAT(1H ,19X,F6.1,43X,E16.4)
      WRITE(6,6000)
6000  FORMAT(1H1,42X,13HION DENSITIES//)
      WRITE(6,6003)(HT(N),DO2I(N),DNOI(N),DN2I(N),DOI(N),N=1,53)
6003  FORMAT(F6.1,4E25.4)
6     CONTINUE
      N=19000
      CALL PUTARRAY(7,N,E)
      CALL PUTARRAY(7,N,DO2I)
      CALL PUTARRAY(7,N,DNOI)
      CALL PUTARRAY(7,N,DN2I)
      CALL PUTARRAY(7,N,DOI)
      STOP OK
      END

      SUBROUTINE LEASTSQ
      REAL K1(53),K2(53),K3(53)
      DIMENSION X(3),F(3),W(3),ERROR(3),FITTED(3),COEFFS(2),
     *HT(65),WORK(3)
      COMMON/B1/AL1(53),AL2(53),AL3(53),H,DO(53),DN2(53),DO2(53),E(53)
      COMMON/B3/K1,K2,K3,DOI(53),DO2I(53),DNOI(53),DN2I(53),TM,NO
      COMMON/B2/QO2(53),QN2(53),QO(53)
      COMMON/B4/HT,CON,SCALE
C
C     FIT EXPONENTIAL TO PREVIOUS THREE POINTS
C
      DO 1 N=50,52
      F(N-49)=ALOG(E(N))
      X(N-49)=HT(N)*1.E5
      W(N-49)=E(N)*E(N)/1.E10
1     CONTINUE
      IDEG=1
      CALL LMSPOLYFIT(COEFFS,X,F,W,ERROR,FITTED,WORK,IDEG,3)
      ELEC=EXP(COEFFS(1)+COEFFS(2)*600.E5)
      WRITE(6,6000)(ELEC,E(53))
6000  FORMAT(1H0,2E20.4)
      E(53)=ELEC
      RETURN
      END
      SUBROUTINE LMSPOLYFIT (A,X,F,W,ERROR,PJM1,PJ,N,M)

C ORTHOGONAL POLYNOMIAL LEAST SQUARES FITTING TO  M  POINTS, ABSCISSAE
C IN  X , ORDINATES IN  F , WEIGHT FACTORS IN  W, POLYNOMIAL OF DEGREE N
C ON EXIT, A  CONTAINS COEFFICIENTS IN STANDARD FORM (A(J+1) IS COEFF
C OF X**J )  PJM1  AND PJ  ARE WORKING ARRAYS OF DIMENSION M
C ERROR  CONTAINS RESIDUALS  (SUPPLIED - FITTED VALUES)
C PJM1 CONTAINS FITTED VALUES

      REAL LAMDA,LAMDA1
      DIMENSION A(M),X(M),F(M),W(M),ERROR(M),PJM1(M),PJ(M),E(31),G(31)
      COMMON /FITCOMMON/ RMSERR,AMAXERR,JMAX,VARIANCE,CORR,ORTCOEF(31)
      M1=N+1
C CHECK INPUT CONDITIONS MET
      IF (N.GT.30.OR.N.GT.M-1) GO TO 80
```

```
C CLEAR INNER PRODUCT TOTALS
      LAMDA=0.0
      B=0.0
      D=0.0
C FORM FIRST ORTHOGONAL POLYNOMIAL INNER PRODUCTS
      DO 10 I=1,M
      PJ(I)=1.0
      D=D+F(I)*W(I)
      B=B+X(I)*W(I)
10    LAMDA=LAMDA+W(I)
      B=B/LAMDA
      C=0.0
      D=D/LAMDA
      ORTCOEF(1)=D
      A(1)=D
C STORE LAMDA FOR LATER USE
      SW=LAMDA
      DO 20 I=1,M
20    ERROR(I)=F(I)-D
      IF (N1.EQ.1) RETURN
C INITIALISE TERMS IN RECURRENCE RELATION FOR USUAL POLYNOMIAL
C COEFFICIENT CALCULATIONS
      G(N1)=1.0
      E(N1)=0.0
C START MAIN LOOP TO GENERATE ORTHOGONAL POLYNOMIALS
      DO 60 J=2,N1
      J1=J-1
      LAMDA1=LAMDA
      B1=B
      C1=C
C CLEAR INNER PRODUCT TOTALS
      LAMDA=0.0
      B=0.0
      D=0.0
C USE RECURRENCE RELATION TO COMPUTE NEXT POLYNOMIAL
      DO 30 I=1,M
      P=PJ(I)
      PJ(I)=(X(I)-B1)*PJ(I)-C1*PJM1(I)
      PJM1(I)=P
      P=PJ(I)*W(I)
      D=D+ERROR(I)*P
      P=P*PJ(I)
      B=B+X(I)*P
30    LAMDA=LAMDA+P
C COMPUTE COEFFICIENTS IN RECURRENCE RELATION
      B=B/LAMDA
      C=LAMDA/LAMDA1
C COMPUTE COEFFICIENT IN LEAST SQUARES EXPANSION
      D=D/LAMDA
      ORTCOEF(J)=D
C EVALUATE COEFFICIENTS OF LEAST SQUARES POLY IN USUAL FORM
      NJ=N-J1+1
      A(J)=0.0
      G(NJ)=0.0
      DO 40 JK=NJ,N
      G(JK)=G(JK)-G(JK+1)*B1-E(JK+1)*C1
40    E(JK)=G(JK+1)
      DO 50 JK=1,J
50    A(JK)=D*G(JK+N-J1)+A(JK)
C COMPUTE RESIDUALS
      DO 60 I=1,M
```

```
60      ERROR(I)=ERROR(I)-D*PJ(I)
C CLEAR TOTALS FOR CORRELATION COMPUTATION
        SY=0.0
        SZ=0.0
        SY2=0.0
        SZ2=0.0
        SYZ=0.0
        RMSERR=0.0
        AMAXERR=0.0
C ACCUMULATE TOTALS FOR CORRELATION COMPUTATION
        DO 70 I=1,M
        PJM1(I)=F(I)-ERROR(I)
        SY=SY+W(I)*F(I)
        SZ=SZ+W(I)*PJM1(I)
        SY2=SY2+W(I)*F(I)*F(I)
        SZ2=SZ2+W(I)*PJM1(I)*PJM1(I)
        SYZ=SYZ+W(I)*F(I)*PJM1(I)
        P=ERROR(I)*ERROR(I)
        RMSERR=RMSERR+W(I)*P
C DETERMINE GREATEST RESIDUAL
        IF (AMAXERR.GE.P) GO TO 70
        AMAXERR=P
        JMAX=I
70      CONTINUE
C COMPUTE VARIANCE AND CORRELATION COEFFICIENT
        VARIANCE=RMSERR/(SW-FLOAT(N1))
        RMSERR=SQRT(RMSERR/SW)
        AMAXERR=SQRT(AMAXERR)
        CORR=(SW*SYZ-SY*SZ)/SQRT((SW*SY2-SY*SY)*(SW*SZ2-SZ*SZ))
        RETURN
C ERROR EXIT POINT
80      DO 90 I=1,N1
90      A(I)=0.0
        K=-1
        RETURN
        END

      SUBROUTINE TRIDIAG (B,D,A,C,N,IER)

C SOLVES TRIDIAGONAL SYSTEM BY ELIMINATION. COEFFICIENTS ARRANGED AS FOL
C D1  A1   0   0   ...0   0    =C1
C B2  D2  A2   0   ...0   0    =C2
C  0  B3  D3  A3   ...0   0    =C3
C ..............................
C  0   0   0   0   ..BN  DN    =CN
C SOLUTION APPEARS IN C(I), I=1,N.  D IS ALSO DESTROYED.
C REFERENCE... GERALD PAGE 164

        DIMENSION B(N),A(N),D(N),C(N)
        IER=0
        DO 10 I=2,N
        IF (D(I-1).EQ.0.0) GO TO 30
        R=B(I)/D(I-1)
        D(I)=D(I)-R*A(I-1)
10      C(I)=C(I)-R*C(I-1)
        IF (D(N).EQ.0.0) GO TO 30
        C(N)=C(N)/D(N)
        DO 20 I=2,N
        J=N-I+1
        IF (D(J).EQ.0.0) GO TO 30
20      C(J)=(C(J)-A(J)*C(J+1))/D(J)
```

```
      RETURN
30    IER=1
      DO 40 I=1,N
40    C(I)=0.0
      RETURN
      END
      FINISH
```

ELECTRON DENSITIES

HEIGHT (KM)	ELECTRON DENSITY (/CM3)
120.0	0.1664E 06
125.0	0.1293E 06
130.0	0.1448E 06
135.0	0.1609E 06
140.0	0.1754E 06
145.0	0.1879E 06
150.0	0.1996E 06
155.0	0.2207E 06
160.0	0.2339E 06
170.0	0.2761E 06
180.0	0.3533E 06
190.0	0.4822E 06
200.0	0.6790E 06
210.0	0.9326E 06
220.0	0.1186E 07
230.0	0.1373E 07
240.0	0.1462E 07
250.0	0.1456E 07
260.0	0.1380E 07
270.0	0.1263E 07
280.0	0.1126E 07
290.0	0.9864E 06
300.0	0.8533E 06
310.0	0.7325E 06
320.0	0.6255E 06
330.0	0.5326E 06
340.0	0.4530E 06
350.0	0.3854E 06
360.0	0.3281E 06
370.0	0.2798E 06
380.0	0.2392E 06
390.0	0.2049E 06
400.0	0.1760E 06
410.0	0.1516E 06
420.0	0.1308E 06
430.0	0.1133E 06
440.0	0.9831E 05
450.0	0.8552E 05
460.0	0.7458E 05
470.0	0.6518E 05
480.0	0.5709E 05
490.0	0.5009E 05
500.0	0.4402E 05
510.0	0.3874E 05
520.0	0.3414E 05
530.0	0.3014E 05
540.0	0.2664E 05
550.0	0.2356E 05
560.0	0.2087E 05
570.0	0.1859E 05
580.0	0.1642E 05
590.0	0.1458E 05
600.0	0.1277E 05

FLOW-CHART FOR PROGRAM IONS

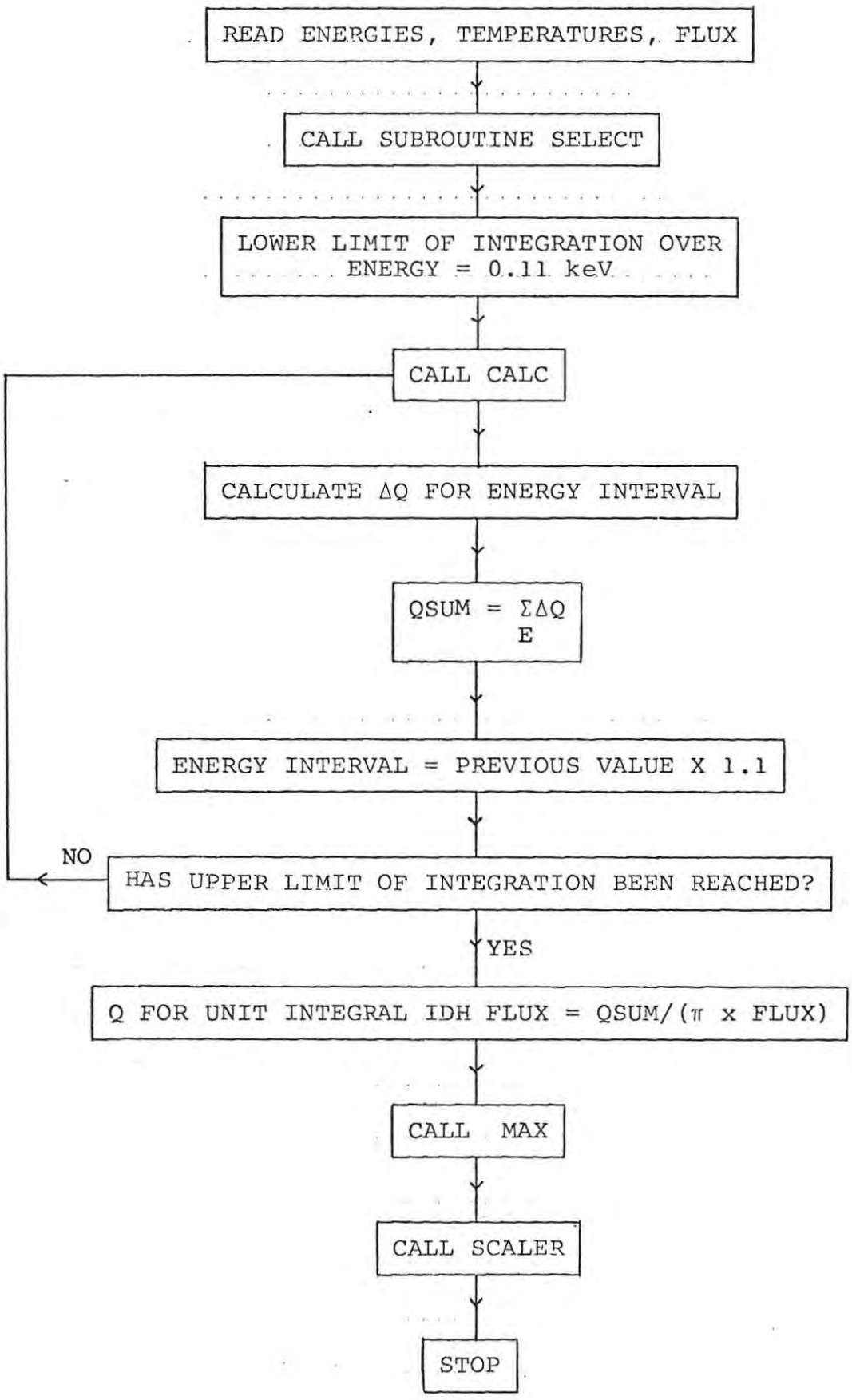

Subroutine MAX

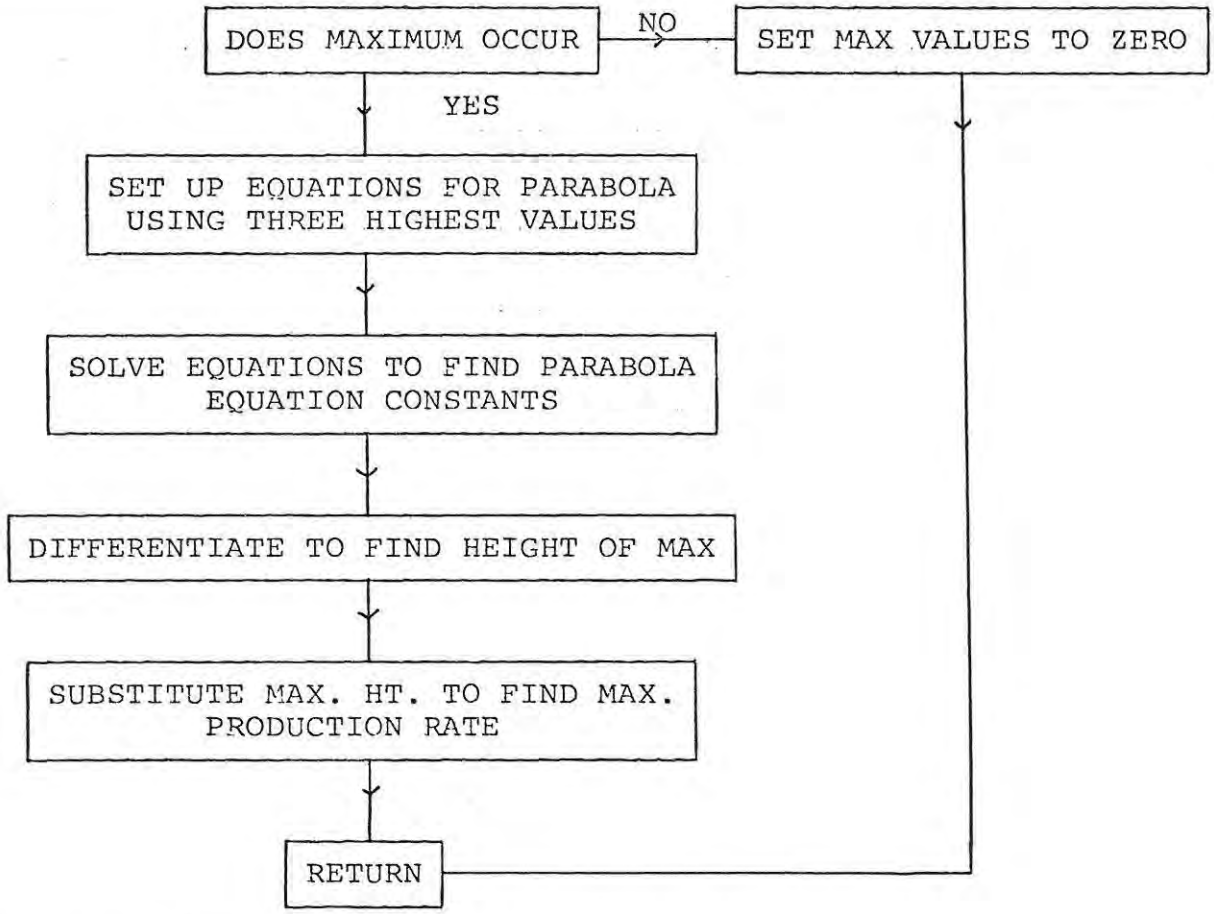

Subroutine SCALER

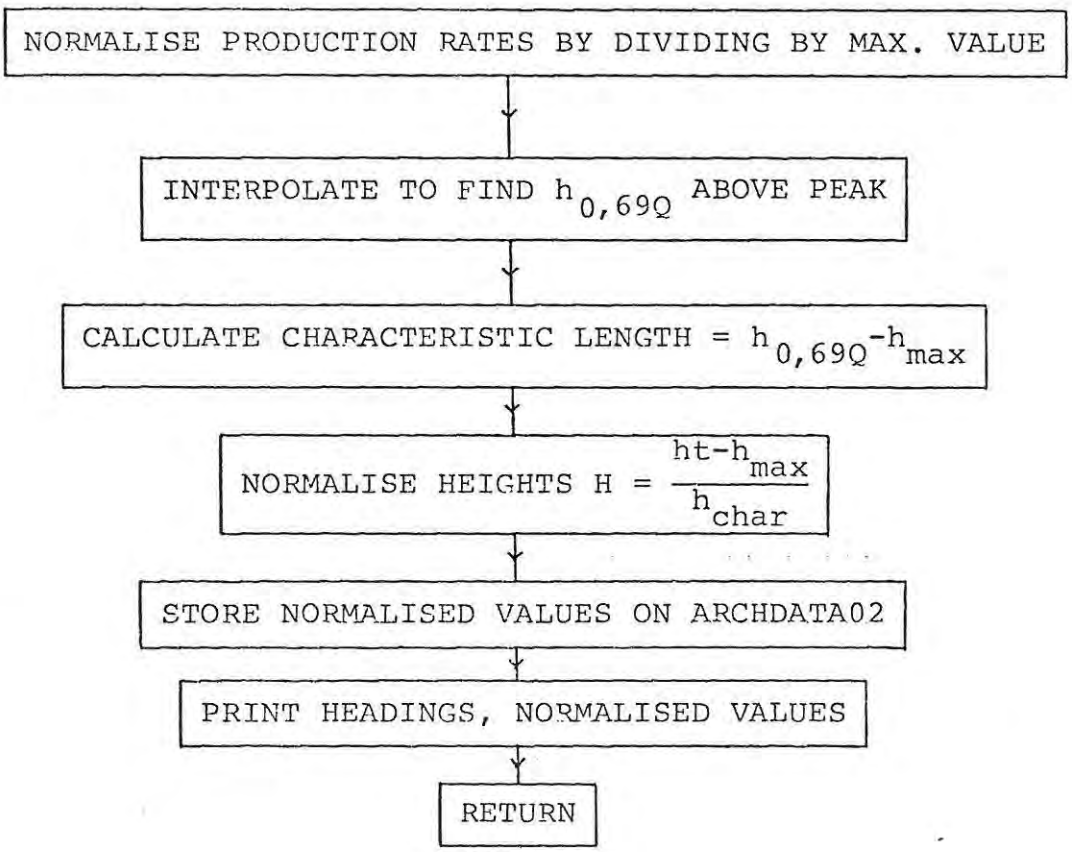

Subroutine SELECT

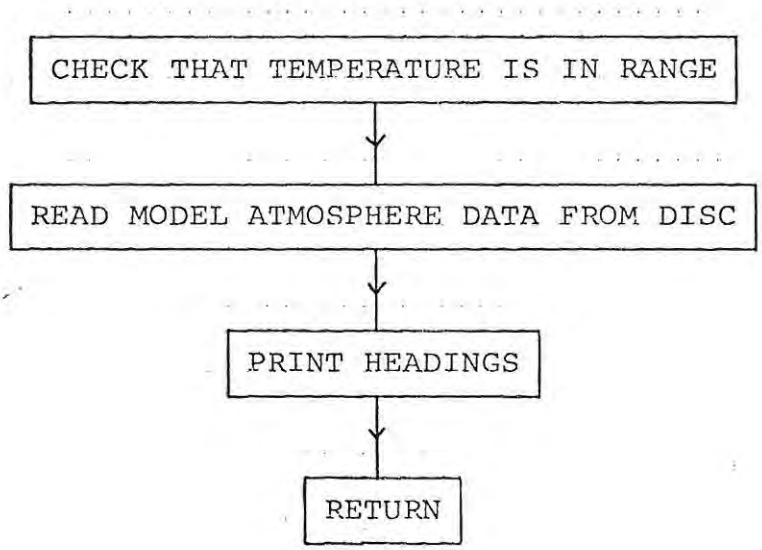

Subroutine CALC

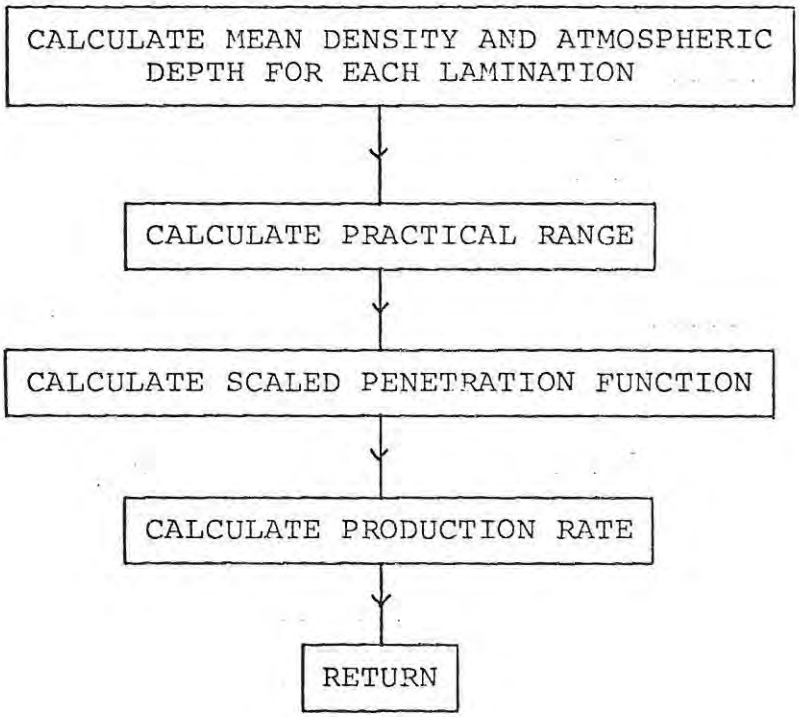

```
      LIST
      PROGRAM(IONS)
      INPUT 1,5=CRO
      USE 4=ED2/UNFORMATTED (ARCHDATA04  )/512
      OUTPUT 2,6=LPO
      COMPRESS INTEGER AND LOGICAL
      TRACE 0
      END

      BLOCK DATA
      INTEGER H(8)
      COMMON/B1/H
      DATA H(1)/20HE-FOLDING ENERGY IS /
      END

      SUBROUTINE SELECT
      DIMENSION IHIGH(45),Q(45),ALOGDEN(45),D(45),YRP(45),E(10),IT(10)
      DIMENSION HCH(10,10),HTOP(10,10),QTOP(10,10),QSUM(45)
      INTEGER H(8)
      COMMON IHIGH,Q,ALOGDEN,D,YRP,HCH,HTOP,QTOP,E,IT,ITHETA,ENERGY
      COMMON QMAX,HTMAX,NO,NN,HCHAR,QSUM
      COMMON/B1/H
      IF (ITHETA - 500) 3,8,1
    1 IF (ITHETA - 1900) 8,8,3
    2 RETURN
    3 WRITE (6,4) ITHETA
    4 FORMAT (1H1,10X,14HTEMPERATURE OF,I4,36H IS OUT OF RANGE. PROGRAM
     1TERMINATED)
    8 READ (4) (ITEMP,(ALOGDEN(J),J=1,45),(D(J),J=1,45))
      IF (ITHETA - ITEMP) 8,9,8
    9 WRITE (6,5) ITEMP,H,ENERGY
    5 FORMAT (1H1,35X,24HJACCHIA MODEL ATMOSPHERE/36X,24H----------------
     1---------/20X,26HEXOSPHERIC TEMPERATURE IS ,I4,15H DEGREES KELVIN/
     220X,8A4,F5.1,4H KEV/)
      RETURN
      END

      SUBROUTINE CALC
      DIMENSION IHIGH(45),Q(45),ALOGDEN(45),D(45),YRP(45),E(10),IT(10)
      DIMENSION HCH(10,10),HTOP(10,10),QTOP(10,10),QSUM(45)
      DIMENSION Z(45),ATMOS(45),ARP(45)
      COMMON IHIGH,Q,ALOGDEN,D,YRP,HCH,HTOP,QTOP,E,IT,ITHETA,ENERGY
      COMMON QMAX,HTMAX,NO,NN,HCHAR,QSUM
      DO 3 N = 1,45
    3 Z(N) = 0.0
C
C     MEAN DENSITY AND ATMOSPHERIC DEPTH FOR EACH LAMINATION
C
      DO 2 K = 1,44
      N = 45-K
      IF (ALOGDEN(N+1) - ALOGDEN(N)) 5,1,5
    5 DMEAN = (D(N+1) - D(N))/(ALOGDEN(N+1) - ALOGDEN(N))
      ATMOS(N) = DMEAN * (IHIGH(N+1) - IHIGH(N)) * 100000
      DO 1 J = N,44
      Z(N) = Z(N) + ATMOS(J)
    1 CONTINUE
    2 CONTINUE
C
C     PENETRATION FUNCTION
```

```
C
      X = ALOG10(ENERGY)
      RPLOG = -5.100 + x*(1.358 + x*(0.215 - x*0.043))
      RP = EXP10(RPLOG)
      IF (RP) 6,7,6
    7 WRITE (2,8)
    8 FORMAT(1H1,23HPRACTICAL RANGE IS ZERO)
      RETURN
C
C     SCALED PENETRATION FUNCTION
C
    6 DO 4 J = 1,44
      N = 45-J
      ZRP = Z(N)/RP
      YRP(N)=1.212*EXP(-2.228*ZRP*ZRP*ZRP)+0.0776*EXP(-57.83*ZRP*ZRP)
C
C     PRODUCTION RATE PER UNIT FLUX
C
      ARP(N) = YRP(N)*ENERGY/RP
      Q(N) = (D(N)*ARP(N))/0.035
C
C     0.035 KEV IS THE ASSUMED ENERGY LOSS PER ION PAIR PRODUCED
C
    4 CONTINUE
      RETURN
      END

      SUBROUTINE MAX
      DIMENSION IHIGH(45),Q(45),ALOGDEN(45),D(45),YRP(45),E(10),IT(10)
      DIMENSION HCH(10,10),HTOP(10,10),QTOP(10,10),QSUM(45)
      DIMENSION AX(3,3),AY(3)
      COMMON IHIGH,Q,ALOGDEN,D,YRP,HCH,HTOP,QTOP,E,IT,ITHETA,ENERGY
      COMMON QMAX,HTMAX,NO,NN,HCHAR,QSUM
      DO 6 N = 2,44
      IF (Q(N) - Q(N-1)) 7,6,6
    6 CONTINUE
    2 HTMAX = 0.0
      QMAX = 0.0
   15 WRITE (6,16)
   16 FORMAT (1H ,19X,50HMAXIMUM PRODUCTION RATE OCCURS BELOW 90 KILOMET
     1RES/)
      RETURN
C
C     LOCATE MAXIMUM PRODUCTION RATE
C
    7 IF (N-2) 2,2,1
    1 DO 8 J = 1,3
      AX(J,1) = 1.0
      AX(J,2) = IHIGH(N-3+J)
      AX(J,3)=IHIGH(N-3+J)*IHIGH(N-3+J)
      AY(J) = ALOG10(Q(N-3+J))
    8 CONTINUE
      DO 9 N = 1,3
      STO1 = AX(N,N)
      IF(AX(N,N)) 4,9,4
      DO 10 K = 1,3
   10 AX(N,K) = AX(N,K)/STO1
      DO 5 K = 1,3
      STO2 =AX(K,N)
      IF (N-K) 11,5,11
   11 AY(K) = AY(K) - AY(N)*STO2
```

```
      DO 12 J = 1,5
   12 AX(K,J) = AX(K,J) - AX(M,J)*STO2
    5 CONTINUE
    9 CONTINUE
      HTMAX = -AY(2)/(2.0*AY(3))
      QMAX=EXP10(HTMAX*(AY(3)*HTMAX+AY(2)) + AY(1))
   14 WRITE (6,13) QMAX,HTMAX
   13 FORMAT (1H ,19X,20HMAXIMUM PRODUCTION RATE OF,E11.4,30H (ION PAIRS
     1/EL.CM.) OCCURS AT ,F6.2,11H KILOMETRES//)
      RETURN
      END

      SUBROUTINE SCALER
      DIMENSION IHIGH(45),Q(45),ALOGDEN(45),D(45),YRP(45),E(10),IT(10)
      DIMENSION HCH(10,10),HTOP(10,10),QTOP(10,10),QSUM(45)
      DIMENSION X(45),QNORM(45)
      COMMON IHIGH,Q,ALOGDEN,D,YRP,HCH,HTOP,QTOP,E,IT,ITHETA,ENERGY
      COMMON QMAX,HTMAX,NO,NN,HCHAR,QSUM,KK,X,QNORM
      H69 = 0.0
C
C     NORMALISE HEIGHT AND PRODUCTION RATE
C
      DO 10 J = 1,44
   10 QNORM(J) = Q(J)/QMAX
      DO 1 N = 1,44
      J = 45-N
      IF (H69) 6,5,6
    5 IF (QNORM(J) - 0.69) 1,2,2
    2 H69 = (IHIGH(J+1)-IHIGH(J))*(0.69-QNORM(J+1))/
     1(QNORM(J)-QNORM(J+1))
    3 H69 = IHIGH(J+1) - H69
    4 HCHAR = H69 - HTMAX
      GO TO 6
    1 CONTINUE
    6 DO 9 J = 1,44
      X(J) = (IHIGH(J) - HTMAX)/HCHAR
    9 CONTINUE
      CALL PUTARRAY(7,KK,X)
      CALL PUTARRAY(7,KK,QNORM)
      WRITE (6,7)
    7 FORMAT (1H ,25X,45HNORMALISED HEIGHT (X) AND PRODUCTION RATE (Q)//
     135X,1HX,35X,1HQ//)
      WRITE (6,8) (X(J),QNORM(J),J = 1,44)
    8 FORMAT (1H ,28X,F8.4,29X,F8.4)
      WRITE (6,11) HCHAR
   11 FORMAT (1H0,20X,25HCHARACTERISTIC LENGTH IS  ,F7.3,11H KILOMETRES)
      RETURN
      END

      MASTER PREC ELECTRONS
      DIMENSION IHIGH(45),Q(45),ALOGDEN(45),D(45),YRP(45),E(10),IT(10)
      DIMENSION HCH(10,10),HTOP(10,10),QTOP(10,10),QSUM(45)
      DIMENSION X(45),QNORM(45)
      INTEGER N(3)
      REAL JO
      COMMON IHIGH,Q,ALOGDEN,D,YRP,HCH,HTOP,QTOP,E,IT,ITHETA,ENERGY
      COMMON QMAX,HTMAX,NO,NN,HCHAR,QSUM,KK,X,QNORM
      COMMON/B1/N,I
      PI = 3.14159
      IVX = 0
C
```

```
C       PARAMETERS
C       ----------
C
C       NO = NO. OF ENERGY VALUES
C       NN = NO. OF TEMPERATURE VALUES
C       E = ENERGIES
C       IT = TEMPERATURES
C
        DO 10 L = 1,44
   10   QSUM(L) = 0.0
C
C       OPEN BACKING STORAGE FILE ARCHDATA01
        CALL USEFILE(7,2HED,12HARCHDATA01  ,-1,9000)
C       INTEGRATION OVER ENERGY UP TO E-FOLDING ENERGY
C       ----------------------------------------------
C
        READ (5,28) NO,NN,FLUX
   28   FORMAT (2I3,E8.2)
        READ (4)(IHIGH(J),J = 1,45)
        READ (5,29) (E(K),K=1,NO)
   29   FORMAT (10F5.2)
        READ (5,50) (IT(J),J=1,NN)
   50   FORMAT (10I4)
        KK=2881
C       KK=FILE ELEMENT NO. IN ARRAY TO BE STORED
        DO 51 K=1,NO
        DO 35 J=1,NN
        DO 42 L = 1,44
   42   QSUM(L) = 0.0
        ENERGY = E(K)
        ITHETA = IT(J)
        CALL SELECT
        ENERGY = 0.11
   31   CALL CALC
        DO 34 L = 1,44
        DELTAQ=Q(L)*ENERGY*EXP(-ENERGY/E(K))*PI*FLUX/(11.0*E(K))
   34   QSUM(L) = QSUM(L) + DELTAQ
        ENERGY = ENERGY*1.10
        IF (ENERGY - 10.0*E(K)) 31,31,32
   32   DO 33 M = 1,44
   33   Q(M) = QSUM(M)/(PI*FLUX)
        CALL MAX
        IF (QMAX) 39,40,39
   40   HCHAR = 0.0
        IVX = IVX+1
        GO TO 41
   39   CALL SCALER
   41   HTOP(I,J) = HTMAX
        HCH(I,J) = HCHAR
        QTOP(I,J) = QMAX
   35   CONTINUE
        REWIND 4
   51   CONTINUE
        STOP
        END
        FINISH
```

REFERENCES

Antonova, L.A. and Ivanov-Kholodnyy, G.S. "Corpuscular hypothesis for the ionization of the night ionosphere." Geomagn.Aeron., 1, 149, 1961.

Arnoldy, R.L., Hendrickson, R.A. and Winckler, J.R. "A determination of F-region effective recombination coefficients from the Echo 2 sounding rocket plasma wave and particle measurements." J.Geophys.Res., 80, 4307, 1975.

Banks, P.M., Chappell, C.R. and Nagy, A.F. "A new model for the interaction of auroral electrons with the atmosphere: spectral degradation, backscatter, optical emission and ionization." J.Geophys.Res., 79, 1459, 1974.

Banks, P.M. and Kockarts, G. "Aeronomy." Part A. Academic Press, 1973(a).

Banks, P.M. and Kockarts, G. "Aeronomy." Part B. Academic Press, 1973(b).

Berger, M.J., Seltzer, S.M. and Maeda, K. "Energy deposition by auroral electrons in the atmosphere." J.Atmos.Terr. Phys., 32, 1015, 1970.

Biondi, M.A. "Laboratory measurements of electron-ion recombination coefficients." Space Res., 7, 154, 1967.

Biondi, M.A. "Atmospheric electron-ion and ion-ion recombination processes." Can.J.Chem., 47, 1711, 1969.

Briggs, B.H. and Rishbeth, H. "An analogue solution of the continuity equation of the ionospheric F-region." Proc. Phys.Soc., 78, 409, 1961.

Chapman, S. and Cowling, T.G. "The mathematical theory of non-uniform gases." Cambridge University Press, 1960.

Chen, W.M. and Harris, R.D. "An ionospheric E-region nighttime model. "J.Atmos.Terr.Phys., 33, 1193, 1971.

Crank, J. "The mathematics of diffusion." Oxford University Press, 1956.

Dalgarno, A. and Griffing, G.W. "Energy per ion pair for electron and proton beams in atomic hydrogen." Proc.Roy. Soc.Series A, 248, 415, 1958.

Dixon, A.F. and Forsyth, P.A. "Measurements of the shape of ionospheric irregularities using satellite transmissions." Can.J.Phys., 48, 2097, 1970.

Donahue, T.M. "Ionospheric reaction rates in light of recent measurements in the ionosphere and the laboratory." Planet Space.Sci., 14, 33, 1966.

Dyson, P.L. "Direct measurements of the size and amplitude of irregularities in the topside ionosphere." J.Geophys. Res., 74, 6291, 1969.

Eccles, D., King, J.W., Rüster, R. and Slater, A. "The maintenance of the ionosphere at high latitudes in winter." J.Atmos.Terr.Phys., 35, 1285, 1973.

Evans, J.V. "A study of F2-region daytime vertical ionization fluxes at Millstone Hill during 1969." Planet.Space Sci., 23, 1461, 1975.

Fehsenfeld, F.C., Dunkin, D.B. and Ferguson, E.E. "Rate constants for the reaction of CO_2^+ with 0, 0_2 and NO; N_2^+ with 0 and NO; and 0_2^+ with NO." Planet. Space Sci., 18, 1267, 1970.

Ferguson, E.E., Fehsenfeld, F.C., Goldan, P.D. and Schmeltekopf, A.L. "Positive ion-neutral reactions in the ionosphere." J.Geophys.Res., 70, 4323, 1965.

Fisher, J.S., Taylor D.K. and Gledhill, J.A. "Some upper atmospheric events observed at SANAE." Read at SAIP Conference, 1977.

Frihagen, J. and Jacobsen, T. "In situ observations of high latitude F-region irregularities." J.Atmos.Terr.Phys., 33, 519, 1971.

Gear, C.W. "Numerical initial-value problems in ordinary differential equations." Prentice-Hall, 1971.

Gerald, C.F. "Applied numerical analysis." Addison-Wesley, 1970.

Gledhill, J.A. "The range-energy relation for 0,1-600 keV electrons." Journal of Physics, A, 6, 1420, 1973.

Gledhill, J.A. "The International Magnetospheric Study (IMS) and the Antarctic and Southern Hemisphere Aeronomy Year (ASHAY)." South African Journal of Antarctic Research, No. 5, 1975.

Gledhill, J.A. "Aeronomic effects of the South Atlantic Anomaly." Rev.Geophys.Space Phys., 14, 173, 1976.

Gledhill, J.A. "Injun 5 satellite data." Private discussion, 1977.

Grün, A.E. "Lumineszeug-photometrische messungen der energieabsorption im strahlungsfeld von electroneuguellen. Eindimensienaber fall in luft." Z.Naturf., 12a, 89, 1957.

Haerendel, G., Lüst, R. and Rieger, E. "Motion of artificial ion clouds in the upper atmosphere." Planet. Space Sci., 15, 1967.

Haschick, A.D. and Gledhill, J.A. "Ionization of the E-region of the ionosphere by precipitated electrons." South African Journal of Antarctic Research, No. 4, 1974.

Hastings, J.T. and Roble, R.G. "An automatic technique for solving coupled vector systems of non-linear parabolic partial differential equations in one space dimension." Planet.Space Sci., 25, 209, 1977.

Hedin, A.E., Mayr, A.G., Reber, C.A. and Spencer, N.W. "Empirical model of global thermospheric temperature and composition based on data from the OGO-6 quadrupole mass spectrometer." J.Geophys.Res., 79, 215, 1974.

Hedin, A.E. "MSIS neutral thermospheric model." Unpublished, 1976.

Heighway, R.H. "Atmospheric ionization by precipitated electrons." Honours project, Rhodes University, 1973.

Heroux, L., Cohen, M. and Higgin, J.E. "Improved calculations of electron densities between 110 and 300 km derived from solar EUV fluxes of August 23, 1972." J.Geophys.Res., 80, 4732, 1975.

Hess, W.N., Mead, G.D. and Nakada, M.P. "Advances in particles and field research in the satellite era." Rev.Geophys., 3, 521, 1965.

Huang, C.Y. "Normalized ionization profiles for electron precipitation." Honours project, Rhodes University, 1975.

ICL 1900 Series. "FORTRAN: Compiler libraries." International Computers, 1976.

Jacchia, L.G. "Revised static models of the thermosphere and exosphere with empirical temperature profiles." Smithsonian Astrophysical Observatory, Special Report 332, 1971.

Jacchia, L.G. "Thermospheric temperature, density and composition:new models." Smithsonian Astrophysical Observatory, Special Report 375, 1977.

Jespersen, M., Landmark, B. and Måseide, K. "Comparison of auroral light emission and electron density." J.Atmos. Terr.Phys., 31, 1251, 1969.

Jones, K.L. and Rishbeth, H. "The origin of storm increases of mid-latitude F-layer electron concentration." J.Atmos. Terr.Phys., 33, 391, 1971.

Kraut, E.A. "Fundamentals of mathematical physics." McGraw-Hill, 1967.

McFarland, M., Albritton, D.L., Fehsenfeld, F.C., Ferguson, E.E. and Schmeltekopf, A.L. "Flow-drift technique for ion mobility and ion-molecule reaction rate constant measurements. Positive ion reactions of N^+, O^+ and N_2^+ with O_2 and O^+ with N_2 from thermal to ~ 2 keV." J.Chem.Phys. 59, 6620, 1973.

McFarland, M., Albritton, D.L., Fehsenfeld, F.C., Schmeltekopf, A.L. and Ferguson, E.E. "Energy dependence of the rate constant for the reaction $O^+ + NO \rightarrow NO^+ + O$." J.Geophys. Res., 79, 2005, 1974a.

McFarland, M., Albritton, D.L., Fehsenfeld, F.C., Ferguson, E.E. and Schmeltekopf, A.L. "Energy dependence and branching ratio of the $N_2^+ + O$ reaction." J.Geophys. Res., 79, 2925, 1974b.

Morse, F.A. and Rice, C.J. "Mid-latitude E-region: An examination of the existence of a corpuscular source." J.Geophys.Res., 81, 2795, 1976.

Rash, J.P.S. "Dapp satellite data." Private discussion, 1977.

Rees, M.H. "Auroral ionization and excitation by incident energetic electrons." Planet.Space Sci., 11, 1209, 1963.

Rishbeth, H. and Garriott, O.K. "Introduction to ionospheric physics." Academic Press, 1969.

Rüster, R. "Solution of the coupled ionospheric equations and the equations of motion for the ions, electrons and neutral particles." J.Atmos.Terr.Phys., 33, 137, 1971.

Schunk, R.W. and Walker, J.C.G. "Minor ion diffusion in the F2-region of the ionosphere." Planet.Space Sci., 18, 1334, 1970.

Schunk, R.W. and Walker, J.C.G. "Ambipolar diffusion in the F1-region of the ionosphere." Planet.Space Sci., 21, 526, 1973.

Stolarski, R.S. "Calculation of auroral emission rates and heating effects." Planet.Space Sci., 16, 1265, 1968.

Strobel, D.F. "Physics and chemistry of the E-region: a review." Radio Sci., 9, 159, 1974.

Stubbe, P. "Theory of the nighttime F-layer." J.Atmos. Terr.Phys., 30, 243, 1968.

Stubbe, P. "Simultaneous solution of the time dependent coupled continuity equations, heat conduction equations, and equations of motion for a system consisting of a neutral gas, an electron gas, and a four component gas." J. Atmos.Terr.Phys., 32, 865, 1970.

Terry, P.D. "Special Mathematical Routines on the 1901 T." Rhodes University Applied Mathematics Department, 1976.

Thuillier, G., Falin, J.L. and Wachtel, C. "Experimental global model of the exospheric temperature based on measurements from the Fabry-Perot interferometer on board the OGO-6 satellite - discussion of the data and properties of the model." J.Atmos.Terr.Phys., 39, 399, 1977.

Titheridge, J.E. "The characteristics of large ionospheric irregularities." J.Atmos.Terr.Phys., 30, 73, 1968.

Titheridge, J.E. "The diffraction of satellite signals by isolated ionospheric irregularities." J.Atmos.Terr.Phys., 33, 47, 1971.

Torr, D.G., Torr, M.R., Walker, J.C.G. and Hoffman, R.A. "Particle precipitation in the South Atlantic Geomagnetic Anomaly." Planet.Space Sci., 23, 15, 1975.

Torr, D.G. "Boundary conditions at 600 km for the continuity equation." Private discussion, 1976.

Torr, D.G. "Atmospheric Explorer C satellite data." Private correspondence with J.A. Gledhill, 1977.

Torr, M.R. and Torr, D.G. "A theoretical investigation of the F-region of the ionosphere." CSIR Research Report 271, 1969.

Van Allen, J.A. and Frank, L.A. "Radiation around the earth to a radial distance of 107400 km." Nature, 183, 430, 1959.

Wagstaff, R.H., Gledhill, J.A. and Huang, C.Y. "Energy loss in the atmosphere by electrons with exponential energy spectra." Read at SAIP Conference, 1976.

Waldman, H. "The specification of distributed boundary conditions in numerical simulation of the ionosphere." J.Atmos.Terr.Phys., 35, 2205, 1973.

Wulff, A. "Atmospheric ionization by precipitated electrons." M.Sc. thesis, Rhodes University, 1972.

Wulff, A. and Gledhill, J.A. "Atmospheric ionization by precipitated electrons." J.Atmos.Terr.Phys., 36, 79, 1974.

Yonezawa, T. "A consideration of the effective recombination coefficient in the E-region of the ionosphere." J.Atmos. Terr.Phys., 30, 473, 1968.